Erosion Tests with the Annular Flume

Jirat Laksanalamai

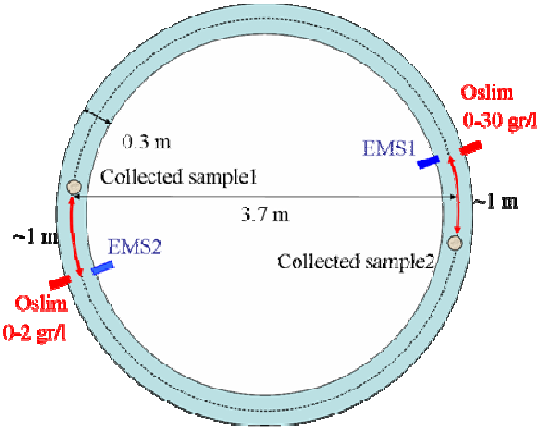

TU Delft
Delft University of Technology

Erosion Tests with the Annular Flume

M.Sc. Thesis
Jirat Laksanalamai

December 2007

Committee:
Prof.dr.ir. H.J. de Vriend
Ir. W. G. M. van Kesteren
Dr.ir. J.C. Winterwerp
Dr. M. van der Vegt
Ir. W. Jacobs

Abstract

To predict the changes of natural systems like estuaries and tidal lagoons as a consequence of human interferences often numerical models are applied. An important aspect is the erosion and transport of sediment. Therefore, these models require formulations that describe the erosion of the sediment bed consisting of sand, mud and organic matter. A physically founded and validated process-based description of these mixed sediments is still missing. Recently, a theoretically derived formulation for erosion of mixed sediments has been proposed. However, a proper validation of this new formula is lacking. Therefore, a systematic study has been undertaken. First, studies have been executed to investigate the individually physical properties in this formula. Next, erosion tests have been executed on a large number of varying sample compositions using a straight, re-circulating flume. The effect of sediment structures and cohesiveness of the sediment bed has been investigated, from which the new formulations could be qualified. However, this experimental set-up was relatively small, with possible large influences of e.g. boundary effects. Therefore, another set of erosion experiments had to be carried out to supplement the results of the mentioned tests.

The objective of this study was to quantify the newly defined theorem for the erosion behavior of sand-mud mixtures. The experiments were carried out on three different artificially generated sand-silt-clay mixtures, using a large annular flume. The mixtures were homogeneously mixed and 100% saturated and, subsequently, placed in the flume. A unidirectional flow was generated by rotating the top-lid and the flume in opposite directions. The flow-induced shear stresses near the bottom were varied by increasing the rotational speeds step by step. An observation on the erosion behavior of the beds was carried out, as well as the measurement of the concentration of suspended fines over the vertical. Due to the occurring secondary currents, the eroded sand accumulated along the outer bend of the flume. By collecting this the amount of eroded sand was quantified. The shear stresses near the bottom were not measured directly, but were determined by means of a large eddy simulation model.

The results show two parts regarding the erosion behavior of the mixtures. Before the complete failure of the bed (part 2), different modes of erosion were identified in which only small amounts of material were eroded (part 1). Mainly due to the placement of the bed, the bed strength was slightly varying in the upper part of the sediment bed concerning both the horizontal as the vertical direction. In this first part floc erosion occurred for the fines. Sand was transported as bed load as well as in the sheet flow regime. For this part, the concentration of eroded fines showed a typically non-linear increase as usually occurred for erosion tests with deposited beds. Several possible explanations for this unexpected behavior are discussed.

For part 2, surface erosion was observed, during which the concentration was increasing linearly with time. The erosion rate as function of bed shear stresses revealed that the threshold of erosion for samples with a sand-silt skeleton was relatively high, while the threshold for the sample with the clay-water matrix was lower. A transition in erosion behavior was observed when regarding the erosion parameters for both fines and

sand. This transition occurred for a plasticity index of around seven, which agrees well with the transition in mechanical behavior for sand-dominated to clay-dominated sediment as found in previous empirical geotechnical studies.

Acknowledgment

This report would not be possible without help and support from the following persons: Prof.dr.ir. H.J. de Vriend, Dr.ir. J.C. Winterwerp, Ir. W. G. M. van Kesteren and Dr. M. van der Vegt. I would like to express my gratitude towards all of my thesis committees for their constructive comments and valuable suggestions. More especially, I would like to thank Walter Jacobs for his help and guidance throughout the whole process of the work. His daily supervision and enormous effort during both the experimental and writing processes are very significant for the accomplishment of this work. I would also like to thank all the people who work at stevinlab III, faculty of Civil Engineering, TU Delft for their hospitality and friendship. A special thank goes to A.M. den Toom, J.A. Duin, S. de Vree, A.D. Schuit and R.P. Andeweg who helped me dealing with the technical aspects during the experiments. I also want to express my gratitude towards the Royal Thai Government for the financial support throughout the entire period of my stay in the Netherlands. Lastly, I thank my family for their constant support and encouragement.

Jirat Laksanalamai
Delft
Decemebr 15, 2007

Table of contents

List of symbols

A	Activity of a clay mineral
A'	Projected area of a sand grain
$Area(t)$	Surface area as function of time
$Area_{total}$	Total surface area of sediment beds
b	Width of the water column
C	Concentration of eroded fines
C_u	Uniformity coefficient (1) and undrained shear strength (2)
c_v	Consolidation coefficient
d	Grain size
$10d_{50}$	Median floc size
d_m	Mean diameter
d_i	Grain size of fraction i
D	Deposition rate
E	Erosion rate
E_h	Redox potential
F_D	Drag force
F_L	Vertical lifting force
F_F	Frictional force
F_S	Shear force
g	Gravitational force
h	Height of the water column (1) and height of accumulated sand (2)
k_s	Sediment roughness
M_{sand}	Mass of eroded sand
M_{fine}	Total amount of eroded fines
M, M_E	Erosion parameter
M_f	Floc erosion parameter
n	Porosity
n_{sa}	Porosity of the sand fraction
$n_{sa,\,max}$	Maximum porosity of a 100% sand skeleton
n_{si}	Porosity of the silt fraction
$n_{si,max}$	Maximum porosity of a 100% silt skeleton
n_{max}	Maximum porosity
n_{sasi}	Porosity of sand-mud mixtures
R	Radius of the annular flume
R_e	Particle Reynolds-number
r	Radius of sediment grains
t	time
U	Streamlines of the water flow
U_{av}	Average flow velocity within the flume
U_*	Frictional velocity
V_{sand}	Volume of accumulated sand

V_{pores}	Volume of pores
$V_{total,wet}$	Total volume of sediment beds
W	Submerged weight of the sand grain (1) and width of accumulated sand (2)
$W(t)$	Width of accumulated sand as function of time
W_{LL}	Liquid limit
W_{PI}	Plasticity index
W_{PL}	Plastic limit
W_{rel}	Relative water content
W_s	Settling velocity
x	Horizontal (main) axis of water flow within the flume
z	Vertical axis of water flow within the flume
τ_b	Bed shear stress
τ_e	Threshold of erosion
τ_s	Shear strength of sediment beds
θ_{cr}	Shields parameter
ν_w	Kinematic viscosity of water
n_w	Dynamic viscosity of water
α_{fl} and β_{fl}	Material dependent parameters
σ	Normal stress
σ_d	Standard deviation
ξ_{sa}	Sand content by dry weight
ξ_{cl}	Clay content by dry weight
$\xi_{cl,0}$	Offset of clay content (dry weight) for cohesive behavior
ρ_{dry}	Dry density of sediment
ρ_{sed}	Density of sediment
ρ_{wet}	Bulk density of sediment
ρ_w	Density of water
ϕ_{sed}	Solid volume concentration
ϕ_{cl}	Volume concentration of clay
ϕ_{sa}	Volume concentration of sand
ϕ_{si}	Volume concentration of silt
ψ_{sa}	Sand fraction
ψ_{cl}	Clay fraction
ψ_{si}	Silt fraction
ω_t	Rotational speed of the top-lid
ω_b	Rotational speed of the flume

List of figures

List of tables

1. Introduction

1.1 Background

Marine wetlands as encountered in estuaries and tidal lagoons are valuable ecosystems. The use and management of these wetlands are restricted by national and international law and regulation. Human activities which have an impact on these areas, therefore, require measures to compensation. Examples of such human activities are gas mining in the Wadden Sea or the deepening of the fairway towards Antwerp (Westerschelde). To design required compensating measures, it is essential to predict the consequences of such interferences at a sufficient level of confidence. This is difficult, as these systems are characterized by complicated interactions between hydrodynamics, morphology and biology. For this reason, large-scale numerical models are applied to predict the behavior of these systems. These models require detailed formulations to describe determining processes. An ongoing research is, therefore, executed to improve the accuracy of such formulations in relation with these small-scale processes. An example is the formulation describing the erosion behavior of mixed sediments.

1.2 Problem description

In estuaries and lagoons often a mixture of sand and mud is found. Therefore, the understanding of the erosion behavior of these mixtures is important. Most of existing erosion formulations deals with sand and mud as separate fractions. For sand the dominant stabilizing force results from the weight of the individual particles. For cohesive beds, the stabilizing force is predominantly determined by the cohesiveness of the mud fraction. The relevant properties for the cohesiveness of mud are e.g. chemical composition of the pore water and the structural composition of the bed. As sand and mud influence erosion behavior differently, it is not properly to combine the individual formulations for sand and mud to determine a formulation for the erosion of a mixture.

Most commonly used erosion formulations for mixed sediments have limited physical background and are highly empirical. For this reason, a physically founded erosion formulation for sand-mud mixtures has been developed by van Kesteren (Winterwerp and van Kesteren, 2004). This formulation has to be validated experimentally. First, the occurring physical parameters in these new formulations have been studied for varying mixtures of sand and mud (Jacobs et al., 2005, 2006). The next step in validating this formulation was to study the erosion behavior of mixed sediments. The Erodimetre erosion device at Ifremer was applied to test a large variety of compositions. However, the erosion surface of the sample in this flume was relatively small, which might influence the accuracy of the measurement e.g. due to boundary effects. Therefore, in this study an annular flume is used for erosion tests as this type of flume enables large quantity of sediment sample to be tested. Moreover, an annular flume has an advantage for an infinite length of sediment sample, which means that no boundary effects would occur.

1.3 Objective

The main aim of this study is to perform erosion tests with the annular flume in order to attain a result which can be used to validate the erosion formula. During the erosion tests, different sand-silt-clay samples are artificially generated and placed in the flume. Using different sediment compositions, the effect of the dominating structure on the erosion behavior can be studied. A tangential flow is generated and increased step-by-step to enhance erosion of the bed. By measuring the amount of eroded sediment in time it is possible to determine the critical bed shear stress for erosion as well as the erosion rate.

1.4 Outline of the thesis

In Chapter 2 a general description of the composition, structure and geotechnical parameters of mixed sediment beds is given. Existing formulations for sand, mud and sand-mud mixtures, as well as the newly proposed erosion formulation are presented as well. Chapter 3 deals with the methods as applied in this study. Chapter 4 presents the results of all erosion tests. The measured velocity as well as simulated velocity is also presented. Chapter 5 discusses the results of the erosion tests. In Chapter 6 the conclusions and recommendations for further study are discussed.

2 Literature study

2.1 General description of sand-mud mixtures

Sediments originate from the weathering of rocks. They exhibit a variety of sizes, shapes and materials. In general, there are several methods to classify sediments, for example based on the physical appearance and/or the mineralogy. The physical appearance varies between large, round boulders to small sheet-like colloidal fragments, while on the mineralogy can be referred to two important mineral types; quartz and clay.

Different mineralogy as well as its quantity determines whether the sediments exhibit (non) cohesive behavior. This is important for the understanding of erosion, transport and deposition. A granular structure is dominant for non-cohesive sediments and do not form a coherent mass, whereas cohesive sediments stick together as a coherent mass due to both electro-chemical interactions and the undrained behavior. Sediment dominated by quartz has no cohesive properties, whereas sediments with sufficient clay content exhibit cohesive behavior. Apart from the physical appearance and mineralogy, the organic component is another important factor influencing the cohesive properties of sediments.

The structure of sediments is treated as a criterion determining the cohesive properties of sediment mixtures. This classification is very important for the understanding of erosion of sediments. In principle, sand-mud mixtures can exhibit two sediment structures; (1) sand-silt skeleton (2) clay-water matrix. These two sediment structures are used to classify the cohesive properties of sediment mixtures. For non-cohesive sediments, a granular structure is present. Erosion depends on the grain size, permeability and density of sediments. For cohesive sediments, a clay-water matrix is dominant. Its behavior is dominated by the cohesiveness of the clay fraction.

2.1.1 Composition of sediments

As mentioned, natural sediments exist of a variety of sizes, shapes and materials. One of the simplest ways to classify sediments is by considering the specific particle size. For this reason, the diameter (d) is used (see Table 2.1).

	Min. d (mm)	Max. d (mm)
Colloidal	-	0.0001
Clay	-	0.002
Silt	0.002	0.063
Mud	-	0.063
Sand	0.063	2.0
Gravel	2.0	63.0
Cobble	63.0	-

Table 2.1 Variety of sizes of sediments, as present in nature, is classified firstly by the metric scale.

As sediment is in general not unimodal but a mixture, it can be characterized by a density function of the grain size or by a cumulative curve. Figure 2.1 shows an example

of a density function and cumulative distribution. In this way one can define the mean, median and standard deviation:

Median diameter (d_{50}): the size at which 50% of the sediments is finer by weight.

Mean diameter (d_m): the weighted average of the dry weight of several fractions with grain size (d_i)

Standard deviation (σ_d): the length on the x-axis of the frequency distribution curve between the d_5 and the d_{95}. Low σ_d indicates uniform and well sorted sediments, whereas high σ_d indicates that the grains are scattered over a range of different size classes.

Uniformity coefficient (C_u): a non-statistical measure which is used for sediments that do not follow a normal distribution curve.

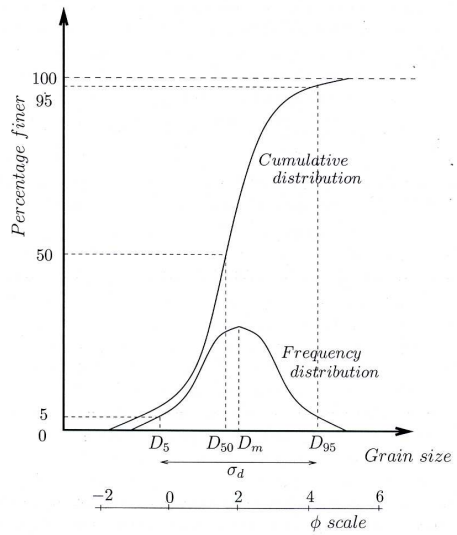

Figure 2.1: Cumulative distribution and frequency distribution (Raudkivi, 1990).

In sedimentology the sand-silt-clay triangles are commonly used for a classification based on the grain size distribution. Although many triangles are only qualitative, an improved triangle (see Figure 2.2), which enables the classification in a more quantitative way, was proposed by Van Ledden *et al.* (2003).

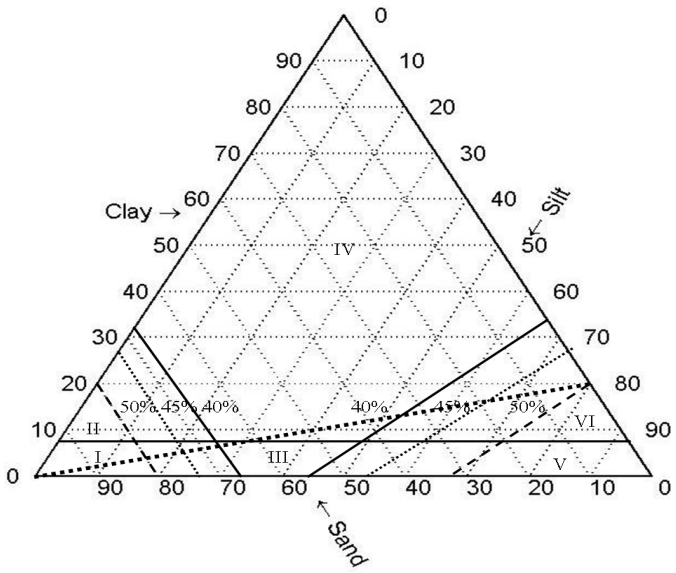

Figure 2.2: Classification of sediment based on a grain size distribution, the so-called sand-silt-clay diagram, after Van Ledden (2003).

Concerning the organic composition, especially in mud, they consist of particulate or dissolved organic matter. Neutral (non-ionic) particles or poly-saccharides play an important role in adsorbing to clay particles (Winterwerp and Van Kesteren, 2004). The absorption of organic material is a result of the following intermolecular bonding: Van der Waals forces (dispersion forces and dipole-dipole interactions) and hydrogen bonding. Large flocs, which bind water molecules, may be generated due to dipole-dipole interactions between electro negatively charged clay minerals and polymer strings. Hydrogen bonding is less significant in estuaries due to the presence of numerous ions (salt water). This reduces the influence of the pairs of electrons of the oxygen in the water molecules.

Cohesion of sediments can be characterized in two types; first the cohesion due to organic matter and next the cohesion due to the physico-chemical interactions between clay particles. The latter type is also defined as 'real' cohesion. The cohesion between clay particles is a result of substitution within the sheets of clay particles. Positively charged cations in the pores are attracted by negatively charged cations at the surface of the particles. On the contrary, these positive cations also tend to diffuse away from the particles to the lower concentration in the pore water. This process results in the formation of a cloud of cations around clay particles, so called the diffusive double layer. The attraction of sediment particles depends on the thickness of this diffusive double layer and the concentration of the clay particles. In addition, (clay) particles can also behave cohesive when the time scale of re-locating particles is short related to the time scale of the replacement by water. Vacuum is generated when this replacement is slow. The resistance against the occurrence of the vacuum yields cohesive behavior. This type of cohesion is called 'apparent' cohesion, and can be seen in i.e. silty sediments.

Sediment behavior can be characterized using a basic geotechnical measure, so called the Atterberg limits. First, the liquid limit (W_{LL}) defines the transition from plastic to liquid behavior, and then the plastic limit (W_{PL}) defines the transition from solid to

plastic behavior. Obviously, these two parameters are defined in terms of water content of the sediment. The difference between these two terms is defined as the plasticity index (W_{PI})

$$W_{PI} = W_{LL} - W_{PL} \tag{2.1}$$

Mitchell (1976) proposed a correlation between this plasticity index and several parameters of clay (see equation (2.2);

$$W_{PI} = A(\xi_{cl} - \xi_{cl,0}) \tag{2.2}$$

where A is the activity of the clay mineral, ξ_{cl} the clay content by dry weight and $\xi_{cl,0}$ the so-called offset of the clay content (dry weight) for cohesive behavior. It was found that this offset for sand-mud mixtures is about 5 – 10 % clay content in natural sediments (Mitchell, 1976). This range of offset was also found by Dyer (1986) and Raudkivi (1990) as the minimum clay content required for a natural bed to have cohesive properties.

Regarding equation (2.2), for a sample with clay content lower than $\xi_{cl,0}$, no cohesive behavior occurs; water is bounded by clay particles and thus permeability is reduced, but sand/silt skeleton still dominates, thus exhibits non-cohesive behavior. Despite the same density, samples may have different mechanical behavior, i.e. erosion, permeability or shear strength due to the different relations between free and bonded water. It is then clear that sediment density alone cannot classify sediment mixtures. The solution in soil mechanics is to relate the Atterberg limit to the water content, resulting in dimensionless water content, so-called the liquidity index (Mitchell, 1976);

$$W_{LI} = \frac{W - W_{PL}}{W_{LL} - W_{PL}} \tag{2.3}$$

where W_{LI} is the liquidity index. This term is used to compare samples with different clay contents, clay minerals and water contents. However, the determination requires some extrapolation which makes it inaccurate. For this reason, the relative water content (W_{rel}) is applied;

$$W_{rel} = \frac{W}{W_{PI}} \tag{2.4}$$

This relative water content reflects the relation between the water content of the clay fraction and water in the pores. According to Jacobs (2006), the determination of a grain size distribution is not straightforward. Thus, this makes the relative water content as a more appropriate term to be used to classify sediment samples as ξ_{cl} is not required.

2.1.2 Structural classification

In sand-mud mixtures, the properties such as the cohesiveness and sediment structures are determined by inter-particle forces and pore size distribution. For the sediment highly dominated by large fractions such as sand and silts, non-cohesive behavior is found despite some clay content in the sediments. The inter-particle forces are unable to generate a net effect (cohesion) within sediments when the concentration of

cohesive materials is low. This condition can be classified for its structure as a sand-or silt-dominated skeleton. The condition for this sediment structure is illustrated in Figure 2.3 (a). In comparison with cohesive sediment, sediment with this sand-or silt-dominated skeleton is stiffer due to its mutual contact. When there is no contact between these large fractions, the stiffness becomes zero (see Figure 2.3c). Another sediment structure, so-called a clay-water matrix, is formed when there is sufficient amount of clay content. The sediment with this structure has cohesive behavior. The cohesive condition is induced by the attractive forces between clay particles and the chemical properties of the pore water.

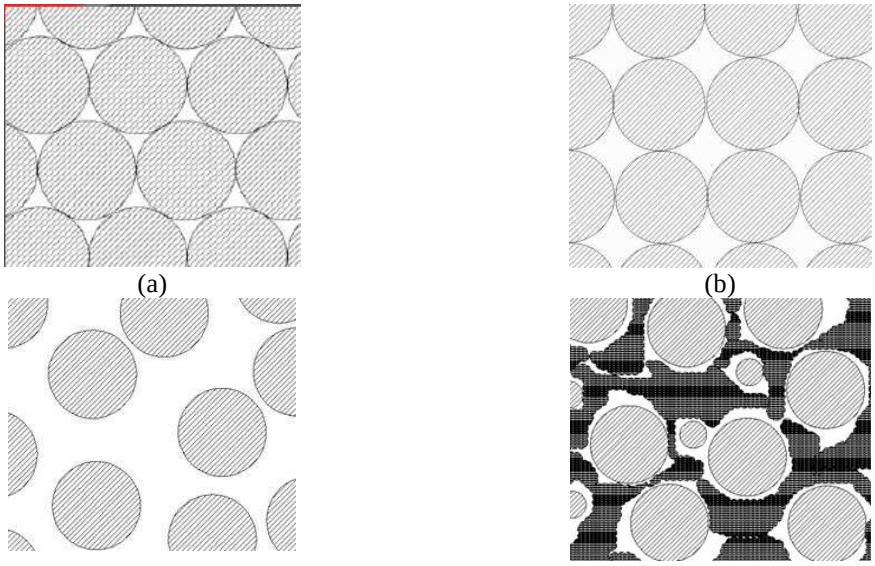

Figure 2.3: Different network structures for sand-mud mixtures. The sediment highly dominated by large fractions like sand has a sand-or silt-dominated skeletons with minimum porosity (a) and maximum porosity (b). Quick sand occurs in (c) as there is no mutual contact between grains. For high concentration of cohesive materials, the sediment has a clay-water matrix (d) as the inter-particle forces generate a net effect (cohesion).

In principle, density depends on the concentration of the sediments. For non-cohesive sediments, the density is determined by the way the sediment grains are packed. For example, maximum pore volume indicates a loosely packed sediment bed, whereas minimum pore volume indicates a densely packed sediment bed. This relation between density and porosity of sediments is derived and results in the following formula.

The dry density [kg/m^3] of a sediment bed is denoted as follows;

$$\rho_{dry} = (1-n)\rho_{sed} = \phi_{sed}\rho_{sed} \tag{2.5}$$

Where ρ_{sed} is the bulk density of sediment, ϕ_{sed} the solid volume concentration and n [-] the porosity is defined as:

$$n = \frac{V_{pores}}{V_{total,wet}} = \frac{\rho_{sed} - \rho_{wet}}{\rho_{sed} - \rho_{w}} \tag{2.6}$$

The bulk density ρ_{wet} of sediment is defined as follows, provided that the sediment is fully saturated.

$$\rho_{wet} = n\rho_w + (1-n)\rho_{sed} = \rho_w + \left(\frac{\rho_{sed} - \rho_w}{\rho_{sed}}\right)\rho_{dry} \tag{2.7}$$

where ρ_w is 1000 kg/m^3 for fresh water and 1030 kg/m^3 for salt water.

As porosity depends on the relation between the sand, silt and clay concentration, each fraction has its own specific porosity. For this reason, the porosity equations for sand, silts and sand-mud mixtures are determined differently. For the case of a sand skeleton, i.e. the silt and clay particles are situated in the pores of the sand fraction, the overall porosity (n_{sa}) can be defined as;

$$n_{sa} = \frac{n + \phi_{cl} + \phi_{si}}{n + \phi_{cl} + \phi_{si} + \phi_{sa}} = 1 - \psi_{sa}(1-n) \tag{2.8}$$

where ϕ_{cl}, ϕ_{si} and ϕ_{sa} are the volume concentrations of clay, silt and sand, respectively. ψ_{sa} defines the sand fraction;

$$\psi_{sa} = \frac{\phi_{sa}}{\phi_{sed}} \tag{2.9}$$

For a silt skeleton, the overall porosity can be denoted as;

$$n_{si} = \frac{n + \phi_{cl}}{n + \phi_{cl} + \phi_{si}} = \frac{n + \psi_{cl}(1-n)}{1 - \psi_{sa}(1-n)} \tag{2.10}$$

where ψ_{cl} is the clay fraction, which is defined as;

$$\psi_{cl} = \frac{\phi_{cl}}{\phi_{sed}} \tag{2.11}$$

The overall porosities for sand and silt above (Equation (2.8) and (2.10)) are applicable only for lower percentage of sand and silt in sediment mixtures (Jacobs, 2006). . A purely sand or a purely silt dominated skeleton can be affected once the percentages of sand and silt in sediment mixtures are higher than 30% and 15% (by weight), respectively. In such case, the following two equations are applied to determine the porosity.

$$n_{\max} = \frac{n_{si,\max}(100 - (100 - n_{si,\max})\psi_{sa}) - \psi_{cl}}{100 - \psi_{cl}} \text{ for } \psi_{sa} = 0 - 86\ \% \tag{2.12}$$

$$n_{\max} = n_{si,\max} - (100 - n_{sa,\max})(100 - \psi_{sa}) \text{ for } \psi_{sa} = 86 - 100\ \% \tag{2.13}$$

As a result of these equations, the minimum and maximum porosity of sand-silt mixtures (see Figure 2.4) are established (Winterwerp and van Kesteren, 2004). The maximum porosity $(n_{\max})$ can be used as a discriminator between sand- or silt-dominated skeletons and clay-water-dominated skeletons. For the area above the maximum porosity line, sediment fractions are either floating within the pore water as quick sand or bounded within a clay-water matrix. For the area in between the maximum and minimum porosity line, sand and silt are in mutual contact, reflecting to a sand-silt-dominated skeleton.

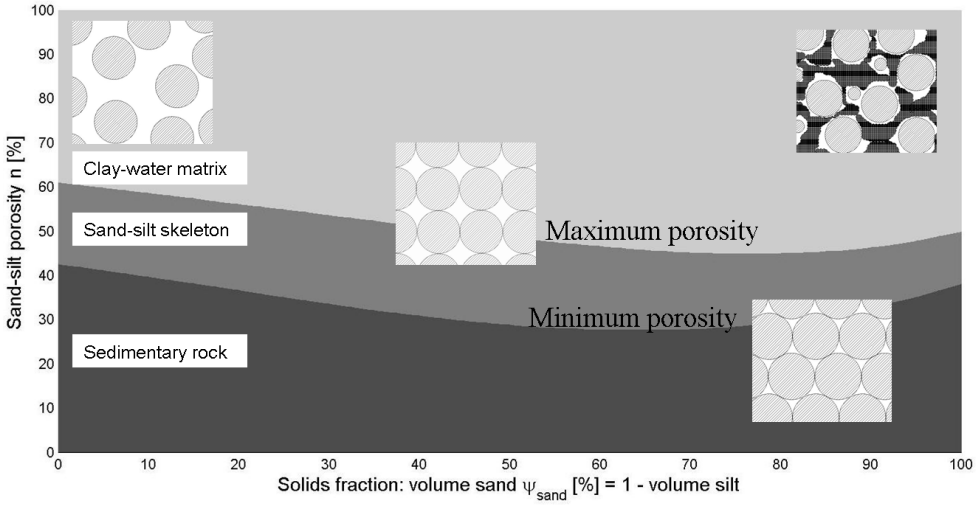

Figure 2.4: Minimum and maximum porosity of sand-silt mixtures (Winterwerp and Van Kesteren, 2004 and Jacobs, 2006)

The cohesive properties and sediment network structures can also be classified with the sand-silt-clay triangle proposed by Van Ledden (2003), as shown in Figure 2.2. In this figure the horizontal line indicates a minimal amount of clay as required for plastic or cohesive behavior (Mitchell, 1976). An average value of 7.5 % is used here. The network structure for a sand and silt dominated structure is separated from a clay-water matrix dominated structure by means of the parallel lines in the lower-left and lower-right corner of the triangle. The location of these parallel lines depends on the water content. For example, a triangle with a water content of 50 % requires ξ_{sa} of 80 % instead of 67 % for a water content of 40 %. Another important aspect in this triangle is the dotted diagonal line, indicating a constant clay-silt ratio. Such a ratio is found for a specific estuary or tidal lagoon. Here, a ratio of 0.25 represents samples as found in the Western Scheldt estuary in the Netherlands. The possible explanation for a constant clay-silt ratio is that clay particles entrap silt particles while settling. Six textural bed types as indicated in the triangle by the Roman numbers are explained in table 2.2.

Number	Cohesion	Network structure
I	No	Sand
II	Yes	Sand
III	No	Mixed
IV	Yes	Clay
V	No	Silt
VI	Yes	Silt

Table 2.2: Overview of various bed types.

2.2 Erosion of sand-mud mixtures

Erosion describes the entrainment of grains or aggregates from the bed surface as a result of bed shear stress. In order to study the erosion behavior of sand-mud mixtures in estuaries and tidal lagoon, it is important to understand the mechanisms of erosion for different sediment compositions. According to Van Ledden et al. (2003) sand erosion is determined assuming a specific equilibrium situation. This means that sand deposition and erosion balances over sediment beds. This equilibrium depends on the flow conditions and the sediment characteristics. On the contrary, with limitation of mud this equilibrium only occurs in highly concentrated mud suspensions. Therefore, the erosion formulations for mud beds do not include an equilibrium condition, but depend on the flow conditions and the bed properties.

2.2.1 Erosion of sand

Erosion of non-cohesive beds (sand and/or silt) depends on the flow-induced force and bed properties, i.e. gravity, density and grain size of sand. The flow-induced force can act upon sand grains in several manners. First, for curved streamlines, a lower pressure above a particle is generated. This induces a vertical lifting force. Second, the force as a result of flow by means of viscous skin friction and a low pressure behind a grain generate a drag force. This force usually acts horizontally on a grain. The last but important force is shear stress. This force is commonly called a bed shear stress (τ_b). It is induced as a result of the frictional flow. The resisting force for erosion in case of non-cohesive sediments is gravity. This means that the submerged weight, which is a function of density and size, is the dominant factor.

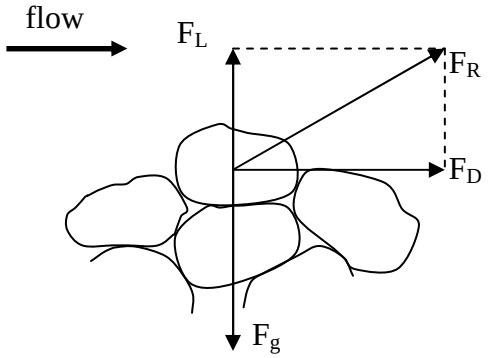

Figure 2.5: Schematic illustration showing both the stabilizing and de-stabilizing forces on sediment grains. F_D the drag force, F_L the vertical lifting force and F_g the gravity force. (Dohmen-janssen, 1999)

A number of erosion formulations for sand exist. For instance, an initiation of motion for sand is proposed by Shields (1936). He developed a theory of the so-called Shields parameter θ_{cr} which is defined as a function of the particle Reynolds-number R_{e^*}. In principle, this θ_{cr} is based on a force balance as shown in Figure 2.5. The formulation of Shields is given as;

$$\theta_{cr} = \frac{|\tau_e|}{(\rho_{sed} - \rho_w) g d} \tag{2.14}$$

where τ_e [N/m^2] is the critical bed shear stress at the threshold of erosion, g [m/s^2] the gravitational force and d [m] the diameter of the sediment particles. Bed shear stress is the sum of skin friction and drag force. But in equation (2.14), only the skin friction part of the bed-shear stress causes erosion of sediment. Another significant parameter was also established by Shields, the so-called Reynolds-number. This parameter is defined as follows:

$$R_{e_*} = \frac{u_* d}{\upsilon_w} = \frac{\rho_w u_* d}{n_w} \tag{2.15}$$

where υ_w [m^2/s] is the kinematics viscosity of water, η_w [m^2/s] the dynamic viscosity of water and U_* [m/s] the friction velocity. The relation between θ_{cr} and R_{e_*} is shown in Figure 2.6. By knowing R_{e_*}, θ_{cr} can be determined and, subsequently, yields the critical shear stress of a sediment grain.

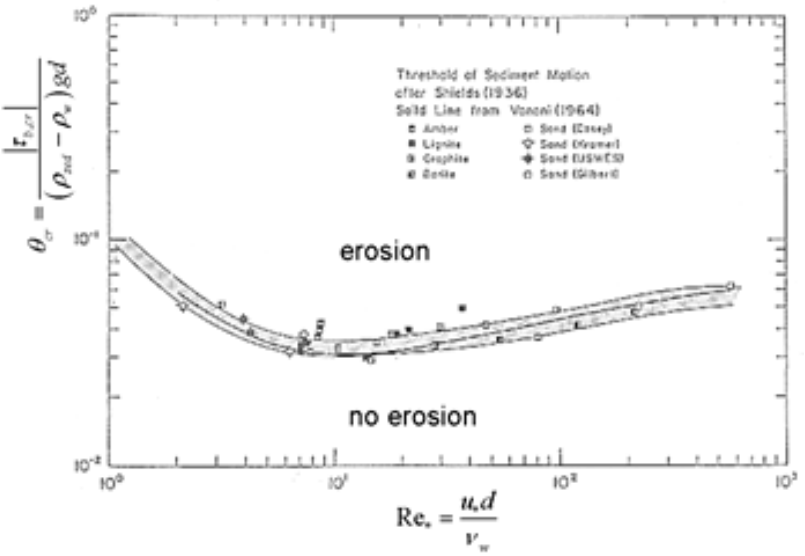

Figure 2.6: Shields diagram showing the erosion threshold for granular sediments (Shields, 1936).

The characteristic for the transport of eroded sand depends on the bed shear stress. For a relatively low bed shear stress, the transport of eroded sand is dominated by the so-called bed load transport regime. Sand particles are transported by means of rolling and jumping over the bed. Consequently, ripples occur when shear stresses are larger (10% - 20%) than the critical shear stress. For larger bed shear stress, the mode of eroded sand transport is changed into the so-called sheet flow regime. In this transport regime, sand particles are brought up in suspension as a result of the particle-particle interactions. Subsequently, bed forms no longer exist. In addition, in the sheet flow regime erodibility is not only determined by skeleton structure of sediments, but also permeability is important.

2.2.2 Erosion of mud

The major difference between the erosion of sand and mud lies in the fact that some of the resisting forces in cohesive soils are of an entirely different nature than those for cohesionless material, and, furthermore they are not constant in time (Partheniades, 1965). As a result of physico-chemical interactions between clay particles, cohesive beds form a coherent mass, which is one of the factors resisting erosion. Adhesion between clay and organic materials acts as a resisting force against erosion. Note that both forces can vary in time due to physico-chemical processes.

Various modes of erosion for cohesive sediment beds are entrainment, floc erosion, surface erosion and mass erosion. The occurrence of each mode depends on geotechnical properties of a sediment bed (i.e. permeability and shear strength). In brief, entrainment occurs when mud acts like a viscous fluid. The turbulence from water can entrain particles from the bed, resulting in erosion. Floc erosion occurs when flocs are disrupted from the bed by the induced-flow force. Surface erosion is similar to floc erosion in terms of sediment particles being disrupted from the bed. The main difference between these two modes is that for floc erosion, τ_b is in the same order of magnitude as the critical shear stress, while for surface erosion, τ_b is above this critical shear stress. Lastly, mass erosion refers to the condition when lumps of particles are eroded from the bed. Note that surface erosion is classified as a drained process as the removed particles can be replaced by water within the same time scale. For mass erosion, it is an un-drained process, which means that the time-scale of particles being removed is smaller than that of the water replacing it.

A typical erosion formula for cohesive sediments was proposed by Partheniades (1965). He combined several properties of the sediment bed in one single parameter, the so-called erosion parameter M [kg/m^2/s];

$$E = M \frac{(\tau_b - \tau_e)}{\tau_e}, \quad \tau_b > \tau_e \tag{2.16}$$

where E [kg/m^2/s] is the erosion rate, which is expressed as function of the excess bed shear stress $(\tau_b - \tau_e)$. The typical values for the erosion rate for cohesive sediments are $0.01*10^{-3} < E < 0.5*10^{-3}$ kg/m^2/s, and for the critical shear stress are 0.1 Pa $< \tau_e <$ 5 Pa (Jacobs, 2006). Equation (2.16) is applied for the case that the sediment bed is uniform and the bed shear strength does not change with depth (Parchure and Mehta, 1985; Zreik et al., 1998); the erosion rate is constant (Amos et al., 1992; Paterson and Black, 1999). For this reason, the suspended concentration of fines can be expected (see Figure 2.7) to increase linearly with time. In this respect, equation (2.16) is, therefore, defined as an equation of unlimited erosion (type I).

Contrary to the previous condition, depth limited or type II erosion varies with depth and time due to consolidation, physico-chemical effects or vertical stratification. In experiments, this condition usually occurs in the case of freshly-deposited beds as it displays strong gradients in strength. In this case, the erosion rate decreases with time and depth when the applied bed shear stress (τ_b) is reached by the critical shear stress (τ_e) at a

certain depth of the bed. Once, the shear stress is equal to the critical shear stress ($\tau_b = \tau_e$), erosion will stop (see Figure 2.8).

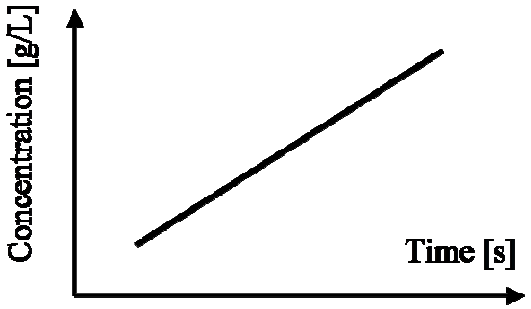

Figure 2.7: Unlimited erosion (type I): concentration of suspended fines as function of time showing a (rather) linearly increasing profile. This implies that the erosion rate is more or less constant.

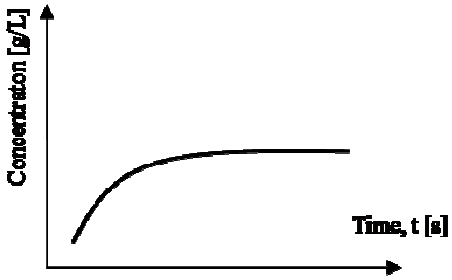

Figure 2.8: Depth limited erosion (type II): concentration of suspended fines as function of time showing a profile approaching a constant value after a certain time. This means that the erosion ceases at certain erosion depth.

Amos et al. (1992, 1997) conclude that a clear distinction is not necessary found between depth-limited and unlimited erosion. If the experimental duration is not sufficient for the condition of $\tau_b = \tau_e$, erosion will decrease in time but not yet reach zero. This condition is classified as type I/II erosion. It should be noted that if the given time is sufficient, erosion may cease completely and thus can be classified as type II erosion (Parchure and Mehta, 1985; Piedra- Cueva and Mory, 2001).

The formula in equation (2.16) is the most commonly used formula for the erosion of cohesive sediments due to its simplicity. However, as the formula was experimentally derived, it is empirical and has large variations of *M* because of some chemical, physical (i.e. clay content or mineralogy) and biological influences. For this reason, Winterwerp and Van Kesteren (2004) proposed a more physically founded erosion formula based on a geotechnical approach.

$$E = M_E(\tau_b - \tau_e)\rho_{dry}, \quad for\ \tau_b > \tau_e \tag{2.17}$$

$$M_E = \frac{c_v \phi_{sed}}{10 d_{50} c_u} \tag{2.18}$$

where the erosion parameter M_E [m/Pa.s] is a function of the consolidation coefficient (c_v) [m^2/s], the volume concentration of the sediment bed (ϕ_{sed}), the median floc size $(10d_{50})$ [m] and the undrained shear strength (c_u) [Pa].

3 Methods

Three sediment compositions were chosen to enable the study of the effect of the sediment structure and the cohesiveness on erosion behavior. These three compositions were first tested on a small-scale determining the optimum water content and the required duration for consolidation. After the optimum water contents were obtained, all samples were artificially generated using the mixer at GeoDelft. Afterward, the generated samples were placed in the annular flume, followed by the consolidation process to drain pore water out; thus the density increased. Different measuring devices were used to measure the concentration of eroded materials and the flow velocity. Bed shear stress was not measured, but calculated using the flow pattern as simulated by a large simulation model. During the erosion tests, by increasing the rotational speed step by step, the bed shear stresses increased, resulting in the increase of concentration. The important parameters such as erosion rate and erosion parameter are determined from the results of the erosion tests.

This chapter consists of three parts. First the composition and generation of the artificial sediment mixtures as applied in this study are considered. Next, an experimental set-up is discussed in which the placement and consolidation of the artificial samples is tested on a small-scale. Finally, the experimental set-up in which the erosion tests are executed is presented. Besides the general characteristics of the annular flume, the applied measurements techniques are presented together with the modeled hydrodynamics in the annular flume.

3.1 Artificial sediment mixtures

3.1.1 Sample compositions

The artificial sediment mixtures applied in this study exist of three sediment fractions (see Table 3.1). Each composition is different in terms of the sediment fraction by volume and water content. The variety of these sediment compositions enables us to study the effect of the different sediment network skeletons and cohesive properties on erosion behavior.

After a thorough analysis on the result of these annular flume tests, the results are expected to be compared with the result of erosion tests executed at Ifremer. Therefore, the sediment compositions are chosen in such a way that they resemble the samples applied for those tests. The term sandy sample refers to the high percentage of sand, while muddy refers to the high percentage of clay and silt. The term intermediate implies that this composition is a transition between the first two samples. The median floc size of sand (d_{50}) is about 170 μm. Kaolinite is the clay mineral used for all three compositions. The ratio between the clay and silt fractions is constant at 0.25. This particular ratio represents sediment mixtures commonly found in the Western Scheldt estuary.

The sand-silt-clay triangle (Jacobs, 2006) illustrates the three sample compositions (see Figure 3.1). In this figure, it should be noted that all three compositions are plotted on the same straight line, implying the constant ratio between the clay and silt fractions. Apart from the sand-silt-clay triangle, the porosity of sand-silt mixtures (Winterwerp and

Van Kesteren, 2004) is used to classify the sediment mixtures based on the sediment network skeletons, see Figure 3.2. In this figure, the sandy sample lies within the area of the sand-silt skeleton, which implies non-cohesive properties of the sediment mixture. Despite having higher percentage of clay, the intermediate sample's natural structure is also built by the sand-silt skeleton, and thus is non-cohesive sediment. With the highest percentage of clay, the muddy sample lies above the transition which separates the clay-water matrix from the sand-silt skeleton. This implies that this sediment sample will exhibit cohesive behavior.

Sample	ξ_{cl} [%]	ξ_{si} [%]	ξ_{sa} [%]	Mineral	ξ_{cl}/ξ_{si} [-]	W [-]	ρ_{wet} [kg/m^3]
1. Muddy	16	64	20	Kaolinite	0.25	0.4	1800
2 .Intermediate	6	24	70	Kaolinite	0.25	0.3	1900
3.Sandy	2	8	90	Kaolinite	0.25	0.23	2000

Table 3.1: Sediment compositions selected for the annular flume test

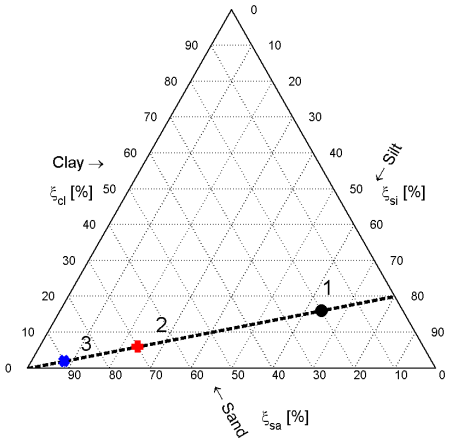

Figure 3.1: Sand-silt-clay triangle showing the three sediment compositions. 1 = muddy sample, 2 = intermediate sample, 3 = sandy sample. The dotted line indicates a constant ratio of the sediment fractions between clay and silt (~0.25).

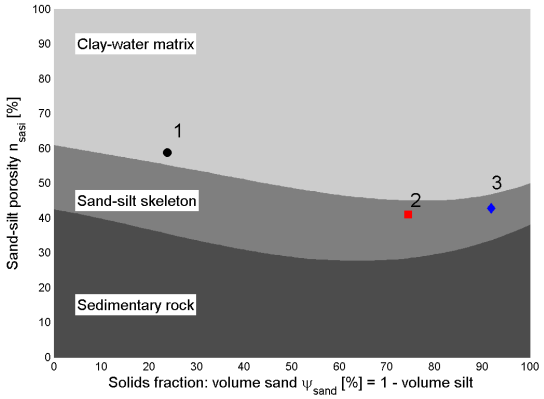

Figure 3.2: Granular porosity (n_{sasi}) as function of the volume fraction of sand in relation to the volume fraction of silt. The numbers indicate the samples as applied in this study. Sample '1' is located above the maximum porosity, indicating a dominant clay-water matrix. Samples '2' and '3' are located between the minimum and the maximum porosity, indicating a dominant sand-silt skeleton. The water contents to determine n_{sasi} is the average of the first 1 cm of the tested sediment beds (see Chapter 4).

3.1.2 Sample generation

Concerning the generation of the artificial sediment mixtures, the following requirements are proposed in order to obtain reproducible samples. The sediment sample should be fully saturated, as clay particles only exhibit cohesive behavior when wet. When a sample is only partly saturated, time-varying cohesive properties are expected. Next, the sediment samples should be homogenously mixed in order to avoid stratification and non-uniform erosion behavior. Besides reproducible, the sediment samples should be sufficiently plastic in order to pour them into the flume. This means that the sediment samples should be mixed with more water in comparison with the desired water content shown in Table 3.1. However, the erosion tests should be executed on sediment beds with higher densities. Therefore, after the placement of the sample, the mixture needed to be consolidated to decrease the water content and thus increase the density.

The facility used to generate the samples is a large-scale sediment mixer (see Figure 3.3) at GeoDelft. This mixer is used because it can mix the samples under vacuum. This eliminates the enclosement of air pockets and thus generates fully saturated mixtures. Another advantage of this mixer is the ability to generate large quantities of material (~400 kg or 200 liters).

The mixer in Figure 3.3 exists of a cone shaped tank with a rotating screw. The arm of this screw was slowly rotated around the tank. Before the mixing process, sediment was filled through the top opening hole. After mixing the sample is transferred through the bottom opening hole to a cylindrical batch.

In general, the mixing procedure executed for the sediment mixtures can be described as follows:

- Weigh all the dry sediment; sand, silt and clay, and then put them into the mixer
- Lower the pressure in the tank in order to de-air the dry mixture. Rotate the planetary screw in the upward direction. This pulls the dry powder up to allow all the air to be taken out completely
- Rotate the screw arm around the tank in order to break all the lump of the sediment powder. Maintain the pressure at approximately 25 mbar while mixing all the dry powder together
- Increase the pressure inside the tank prior to the filling with water (up to about 60 mbar), otherwise the water will evaporate. Fill in the desired quantity of water.
- Proceed the wet mixing by rotating the planetary screw downward. This allows the powder to be completely mixed with water. Continue the mixing for about 12 hours
- After the mixing, the mixtures are transferred to the batch connected at the bottom opening hole of the tank. Afterward, the batch is transported by a forklift to the annular flume (the distance between the mixer and the annular flume is approximately 500 m).

The quantity of the generated samples is:

- Sandy sample: the sediment mixture were generated with a 1st batch of 125 liter and a 2nd batch of 150 liters.

- Intermediate sample: the sediment mixtures were generated with 210 liters for both batches.
- Muddy sample: the sediment mixtures were generated with 210 liters for both batches.

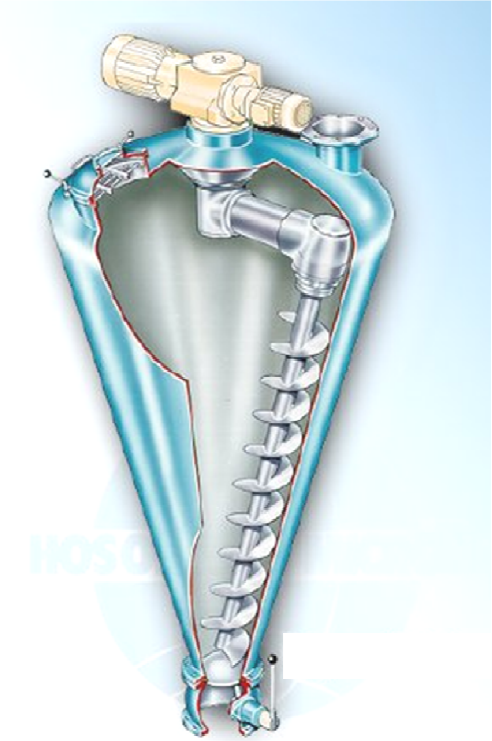

Figure 3.3: Schematic illustration of the sediment mixer. Both the screw and the arm which connects it to the motor are rotated during mixing

Figure 3.4: The yellow cylindrical container contains the sediment sample after the mixing procedure. The sample is transferred under gravity from the mixer into this container.

3.2 Small scale experiment

3.2.1 Introduction

The small-scale experiment is a preliminary test executed prior to the annular flume test. Regarding the requirements of the sample, it is essential that this small-scale experiment is executed to gain some insight into the placement of the sediment bed. In order to generate sediment samples that can be poured in the flume, the water content must be high enough. However, segregation is likely to occur if the water content is too high. In this respect, it is important to determine optimum water content. By varying the water content, we can visually investigate the sample condition, and justify the optimum water content.

Another main reason for the small-scale experiment is to see whether these liquid samples can be consolidated after they are placed within the flume. In this way the density of the sediment samples can be increased before the actual erosion test. Given the difference in sediment compositions, the time required for consolidating the samples needs to be determined for all three samples. Moreover, in order to implement the specific set-up for the consolidation process effectively, it is wise to test the set-up first on a small-scale. The samples for the small-scale experiment were generated using a concrete mixer. All three sediment compositions, according to Table 3.1, were generated and studied.

3.2.2 Experimental set-up and procedure

As the optimum water content for pouring the samples is higher than the desired water content, the mixtures need to be consolidated to reduce the water content and increase the density. Two different types of forcing are proposed to enhance this consolidation. The first one is the pressure as a result of a load of water, which is placed on top of the sediment samples. The second load is a negative water pressure applied under the sediment samples. The combined effect of the loading conditions is that the sample is compressed.

In Figure 3.5, bricks are laid at the bottom to provide a solid foundation for the sediment sample. On top of these bricks, a perforate plate and a filter fabric (kind of geotextile) are laid over the whole area. This fabric prevents small particles from being washed out by the draining pore water during consolidation.

The generated sediment sample was placed on top of the filter fabric. While placing the sample, outlet 1 (see Figure 3.6) was kept open in order to drain out any excess water from the sample. After the placement of the sample, a plastic foil was required to separate the sediment bed from the layer of water that will be placed on top. If water could flow through the sediment sample during consolidation, stratification of the density is expected to occur. During the filling of water, outlet 2 needed to remain open in order to drain out excess water.

Besides the pressure from the water on top, a negative water pressure was applied under the sample. In order to accommodate this application of negative water pressure, a specific set-up was required. Figure 3.6 shows three outlets equipped with valves and

connected to the container of the sediment sample. With a siphon, a water pressure gradient between the sample and the discharging outlet (3) was generated. Thus, the consolidation on the sample was enhanced.

To investigate if stratification did indeed not occur as well as to measure the density of the sediment sample, Conductivity concentration Meter probe (CCM) was applied. Although the mixtures were generated with fresh water, some salt was present in the (dry) clay. This salt has a significant effect on the conductivity of a sample. So, unfortunately, this CCM was not feasible to apply for this test. Another method to determine the density was required. After consolidation, sediment cores were taken at several locations in the sediment sample. After coring, the sample was sliced and dried in an oven for 24 hours. In this way a vertical profile of the water content could be determined. As a result, it was possible to determine if the bed was stratified due to the consolidation process by considering the uniformity of the water content over the depth.

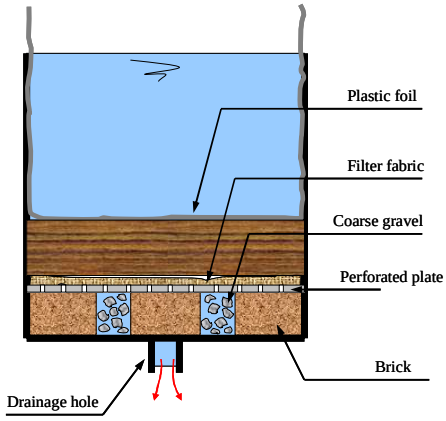

Figure 3.5: Cross section of the small-scale set-up. This set-up exists of a drainage layer, a sediment sample, a perforated plate, filter fabric, a plastic foil and water

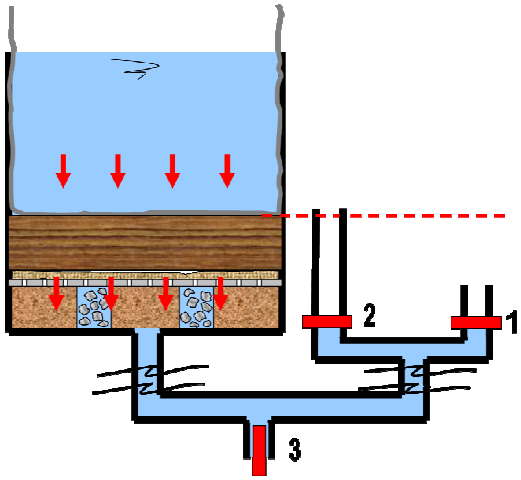

Figure 3.6: Cross section of the set-up connecting to the three outlets. By opening outlet 3 and closing outlet 1 and 2, a pressure gradient, which enhances the consolidation, is generated as indicated by the below arrows. Another load applied for the consolidation is subject to the water above a plastic foil. This water generates a pressure as indicated in the upper arrows.

3.2.3 Results and conclusions

The optimum water content for all three sediment compositions was determined following the two criteria; the water content should be sufficient to generate the sample that can be poured. On the other hand, the sediment sample with too much water might lead to stratification. After several mixing of the samples, the optimum water contents are 50 %, 25 % and 25 % for the muddy, intermediate and the sandy sample, respectively.

During the consolidation process, the settlement of the sediment beds was observed. The time span of this observation depends on the composition of the samples. For example, the consolidation period for the sandy sample was very short. It is, therefore, necessary to record the settlement with a high frequency, especially in the beginning. The

observation of the consolidation for all three samples is plotted as a function of time (see Figure 3.7). The time required for the consolidation can be determined by considering when the plot of the settling becomes constant. In summary, the muddy sample requires a consolidation time of approximately 27 hours. The intermediate and sandy sample require a much shorter period: 2-3 hours and 0.25 hour, respectively.

After consolidation, sediment cores were taken in order to check if the samples were not stratified. Four samples (from different locations) were taken for each sediment composition. The water contents were examined and plotted as a function of the depth, see Figure 3.8. The results show that the water content profiles can be assumed to be uniform over the depth. The water contents after consolidation are decreased as expected. In addition, the desired water contents (see Table 3.1) are compared with the water content after consolidation. It appears that for the sandy and muddy samples those values fairly agreed. For the intermediate sample, it should be noted that the optimum water content (25%) was lower than the desired water content (30%). The sample was still consolidated for the attempt in preventing entrapped air inside of the sediment grains. As a result, the water content after consolidation (20%) appeared even lower.

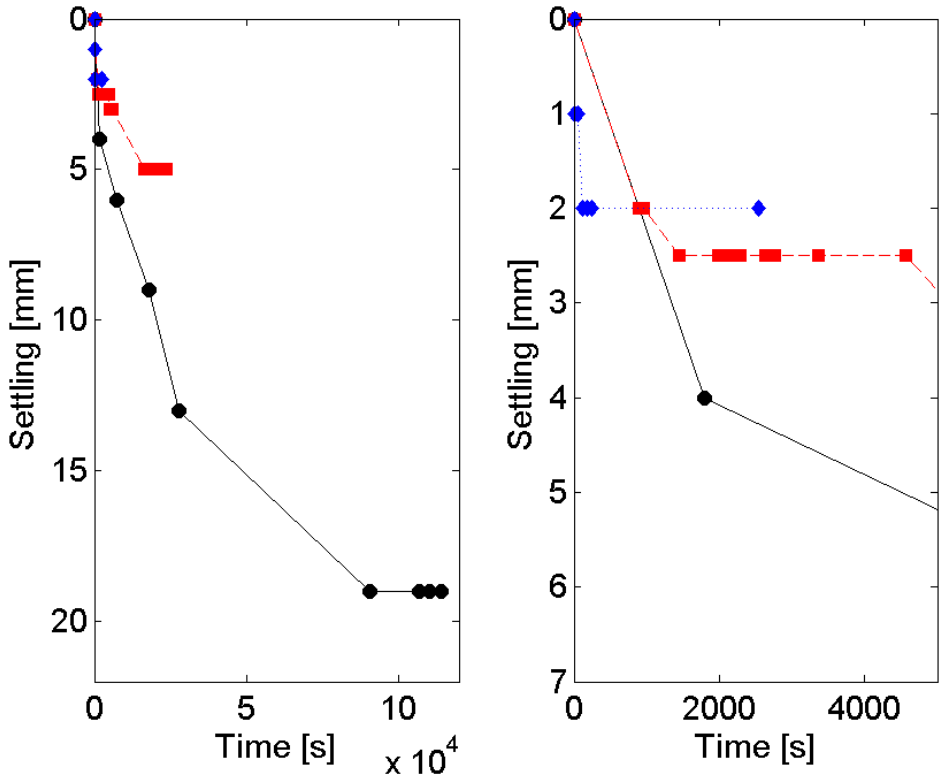

Figure 3.7: Settling as function of time for the three sediment mixtures as applied in this study. The circles, squares and diamonds indicate the profile of the muddy, intermediate and sandy sample, respectively. On the right, the figure displays the enlarged version for the settling of the intermediate and sandy sample.

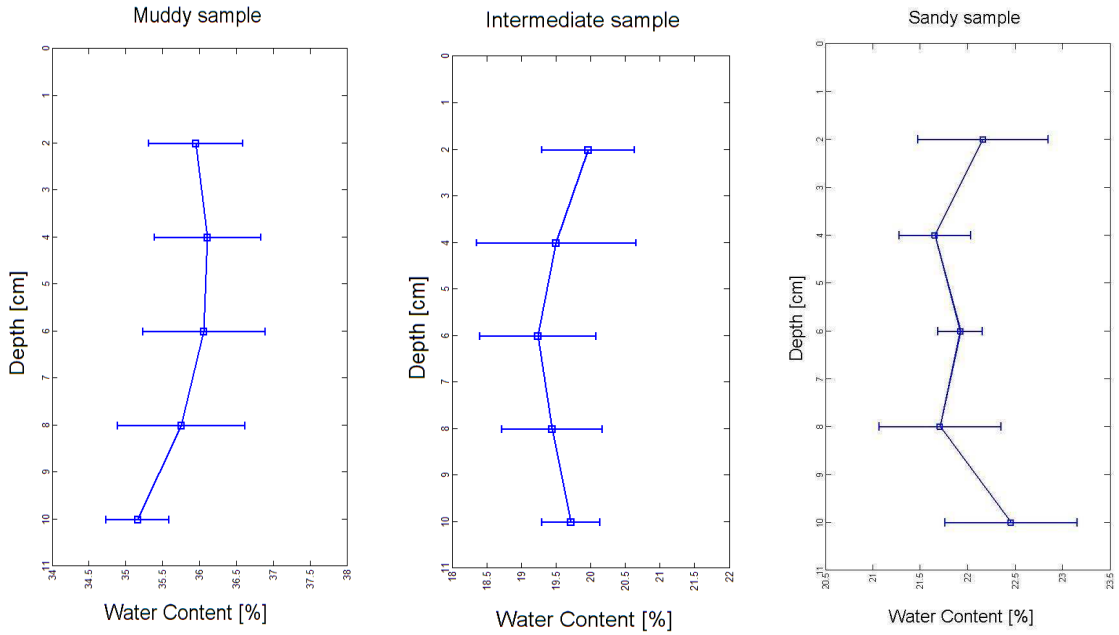

(a) (b) (c)

Figure 3.8: Error bars for the water contents of the sample cores as taken after consolidation plotted as function of depth for the three sediment samples: (a) muddy sample, (b) intermediate sample and (c) sandy sample

3.3 Annular flume

3.3.1 General characteristics

An annular flume is a typical ring shaped flume with two rotating elements, the top lid and the flume, which can be rotated independently. A uniform tangential flow velocity is generated by rotating the top-lid and the flume in opposite directions. This flow generates bed shear stresses at the sediment bed. The main advantage of using an annular flume for erosion tests is the infinite length of the sediment samples. This means that no boundary effects are occurring. This is a big problem in straight flumes, due to the transition between a smooth flume bottom and a rough surface of the sediment sample. The latter leads to scour at the upstream boundary and thus non-uniform erosion. Another advantage of an annular flume is the relatively large size of the bottom area of the flume. A sufficiently large surface area of the sediment bed enables a more accurate measurement of e.g. the erosion rate compared to experimental set-ups with much smaller sample surfaces. For the reasons as discussed, the annular flume is chosen for the erosion test in this study.

In this study, the annular flume of the laboratory of fluid mechanics at the TU Delft is applied (see Figure 3.9 and Figure 3.10). The flume has a rectangular cross-section with a width of 0.304 m and a height of 0.47 m. The mean diameter of the flume is 3.70 m. The walls of the flume are made of glass. The top lid, the bottom and the side-walls are considered as hydraulically smooth. The tangential velocity can be controlled over a range of 0.05 m/s – 2.0 m/s for the top lid, and of 0.05 m/s – 1.0 m/s for the flume. The power of the top lid motor is 0.55 kW, and that of the bottom motor 2.2 kW. Electrical power is supplied through a set of slip rings to power instruments such as a computer and measuring devices.

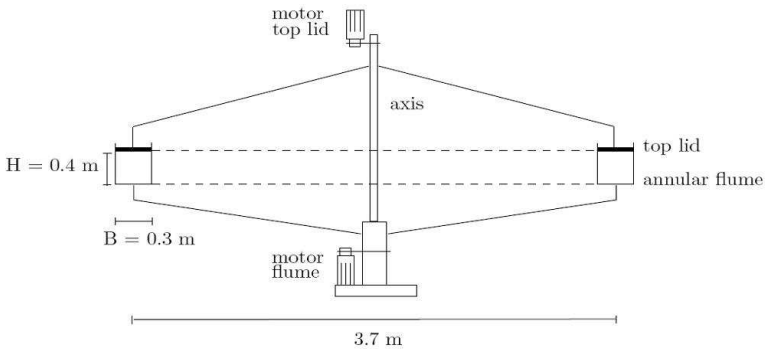

Figure 3.9: Schematic illustration of the annular flume of the laboratory of fluid mechanics of the TU Delft.

A disadvantage of annular flumes is the occurrence of secondary flows. When rotating the flume, different tangential flow directions along the top-lid and the bottom of the flume result in two secondary flow cells (see Figure 3.11). The vertical components of the secondary flow affect the turbulence structure. Therefore, this secondary flow should be considered in case of sedimentation or erosion studies. For this reason, Booij (1994) studied the characteristics of the secondary flows occurring in the same annular flume as

applied in this study. He determined an optimum ratio between the rotational speeds of the top-lid and flume, which minimizes the secondary flow (see more detail in 3.3.4).

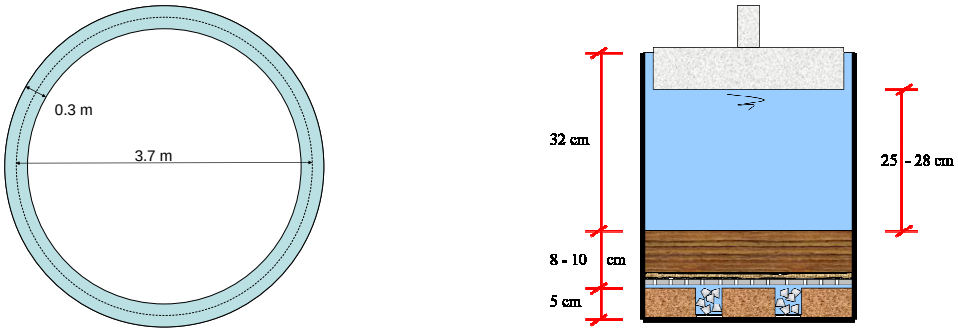

(a) (b)

Figure 3.10: Top view (a) and cross section (b) of the annular flume. The cross section of the annular flume set-up exists of a drainage layer, filter fabric, a sediment bed, water and the top lid. The scales indicate the sizes as commonly took place during the test.

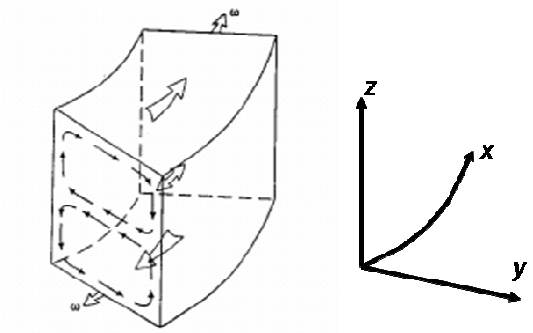

Figure 3.11: Schematized depiction (Sheng, 1989) of a part of an annular flume. It is shown that secondary flows generate two cells. The block arrows indicate the directions of the tangential flow; near the bottom the flow goes toward the reader, while near the top lid the flow goes away from the reader. The small arrows at the top and bottom indicate the rotational directions of the lid and the flume, respectively. At right, the axes as applied in this study are defined.

3.3.2 Placement of the samples

After mixing, the sediment samples are placed in the annular flume. Different approaches were applied for the placement, depending on the condition of the sediment samples. The muddy sample was liquid enough to pour under gravity. However, the intermediate and the sandy samples were too solid to pour. For this reason, these samples were manually placed with a shovel. After the placement, an investigation was made to determine if the sediment samples were placed equally in the entire flume. This was followed by leveling the surface of the sediment bed by means of a small shovel.

After the placement, the samples were consolidated for the periods as determined by the small-scale experiment (section 3.2.3) in order to decrease the water contents. Prior to the erosion test, the thickness of the sediment beds as well as the water depth were measured. In summary, the average thicknesses of the three samples are 8.7 cm, 9.1 cm, and 8.3 cm for the muddy, intermediate and the sandy sample, respectively. The water depths during the tests were 27.4 cm, 25.6 cm, and 26.47 cm for the muddy, intermediate, and the sandy sample, respectively.

(a) (b)

Figure 3.12: Placement of the samples through the top-lid opening hole of the flume with (a) a side view and (b) a top view

3.3.3 Measurement techniques and erosion test procedures

In this study, different measurement techniques were applied. Sub-samples were taken from the bed to determine the water content. Velocities in both main and vertical direction were measured by Electro Magnetic Flow Meters (EMS). During the erosion tests, the concentration of the suspended material was measured by Optical Silt Measuring Instruments (Oslim). The measurements of the Oslims were calibrated at two different stages, both before and after the erosion test. As the erosion rate is related to the bed shear stress, it is important to determine the bed shear stresses for each rotational step. However, the bed shear stress is not measured, but calculated by means of a numerical model (Booij, 2003). The measurements of both EMS devices can be used to verify the modeled flow pattern in the flume. When the measured and modeled velocities agree, it is assumed that the bed shear stresses are well simulated.

Determination of the water content

Sediment cores were collected from the sediment bed to examine the water content as well as the horizontal distribution of the water content. For each sediment sample this test was performed twice at two different stages: before and after the erosion test. The cores were taken using a PVC tube with a diameter of 3.5 cm and a length of 30 cm and a rubber part of a syringe. This method is commonly applied during field work. Samples were taken over the whole length of the placed sediment bed. By slicing the samples in segment of around 1 - 2 cm and drying them in an oven (24 hours, $105^{\circ}c$) subsequently, a vertical water content profile could be determined. The cored samples were taken from two opposite locations in the flume in order to examine also the uniformity of the sediment bed in the horizontal direction. The holes as a result of the coring were filled with coarse sand ($d_{50} \approx 1-2$ mm), which is assumed not to erode during the test.

Electro Magnetic Velocity Meter (EMS)

Flow velocities in both vertical (z) and main flow (x) direction were measured by a EMS device. This measurement is based on a magnetic field, which is produced by the flow through a small coil inside the body of the sensor. Two measuring devices were located at the same horizontal distance as the Oslim, except for being installed from the inner wall of the flume (see Figure 3.13, Figure 3.14 and Figure 3.15).

Optical Silt Measuring Instrument (Oslim)

Oslims are applied to measure the concentration of suspended material within the flume. The measurement is based on the attenuation of the intensity of a light beam by the absorption and scattering of light by suspended particles in a liquid. The output was presented as an analog voltage. The advantage of the Oslim is that its installation is fit with the annular flume, and that a wide range of concentrations is measurable.

Before the installation, the five Oslims were calibrated for a variety of sediment concentrations and suction speeds. First, the Oslims are calibrated for the three different proportions of silt and clay, as applied for samples 1, 2 and 3. Next, the Oslims are calibrated for the different suctions speeds at which water is extracted from the flume during the erosion tests. These suction speeds are varied in order to have more or less similar flow velocities both in the flume as in the Oslims. In this way representative samples are taken. To minimize the number of calibrations, three suction speeds were chosen that represented the whole range of the flow velocity: 0.183, 0.366 and 0.557 m/s (see Table 3.2). In addition, the five Oslims were tuned at two different ranges of concentration: 0-2 and 0-30 gram/liter. In this way it is possible to accurately measure the concentration, both at the beginning as at the end of the erosion test. The Oslim calibration is presented in Appendix. The 0-2 and 0-30 gram/liter Oslims were located at opposite sites of the flume (see Figure 3.13). By placing them at varying heights above the bed, it is possible to study the vertical concentration profiles. By multiplying the measured concentration by the total volume of water in the flume, the mass of eroded fines can be determined. During the erosion tests water samples are taken from the flume in order to calibrate the Oslims afterwards. At the end of each velocity step a sample was taken. The volumes of extracted water were replaced by clear water during the tests. Later on, the concentration of these water samples was determined by filtering. The results were used to verify the measurements of the Oslims.

Hydrodynamics in the flume

The maximum controllable rotational speed for the top-lid (ω_t) is approximately 2.0 m/s and for the flume (ω_f) approximately 1.0 m/s. It was decided that in total 13 rotational speeds were executed for the erosion test. The last column of Table 3.2 indicates the duration for each rotational step. For the 13 rotational steps, three different durations were applied. The first duration is relatively short, and increased for the next two groups. These durations are determined following the expected behavior of erosion. For each rotational step first erosion takes place, and then followed by sedimentation. In this way equilibrium is expected for each step. For larger rotational speeds longer periods are required to obtain this equilibrium concentration. For this reason the durations for higher rotational steps are longer.

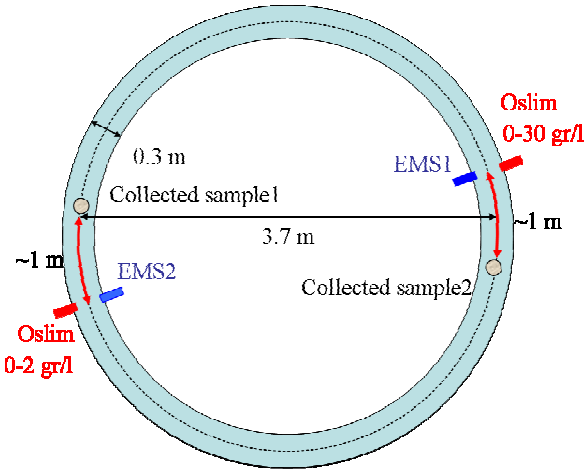

Figure 3.13: Schematic illustration of the top view of the annular flume with the location of the applied measuring devices and the locations at which bottom samples were taken. At two sides of the flume Oslims and EMSs are applied. Downstream from these locations sediment cores were taken.

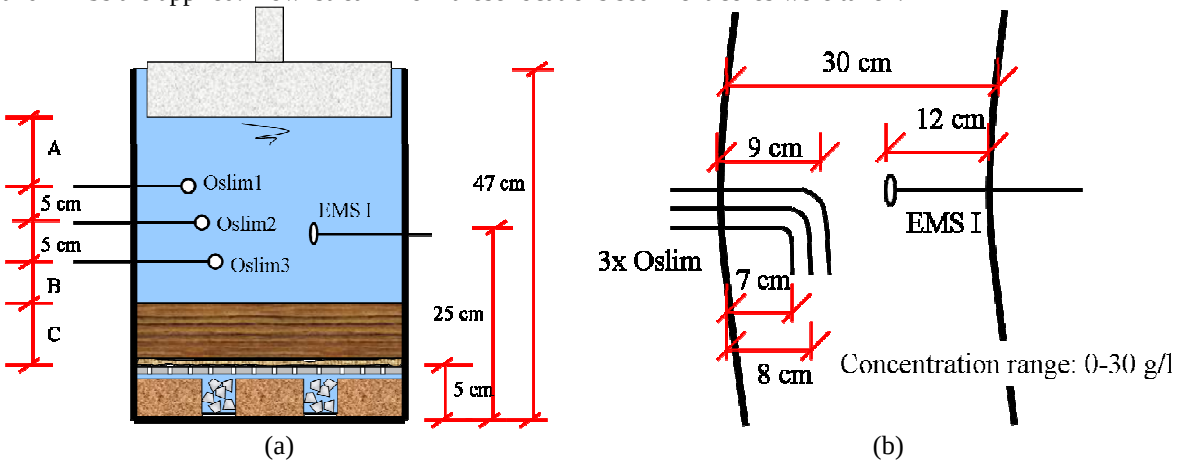

(a) (b)

Figure 3.14: Location of the EMS and Oslims (concentration range of 0-30 g/L) depicted in the cross-section of the flume.

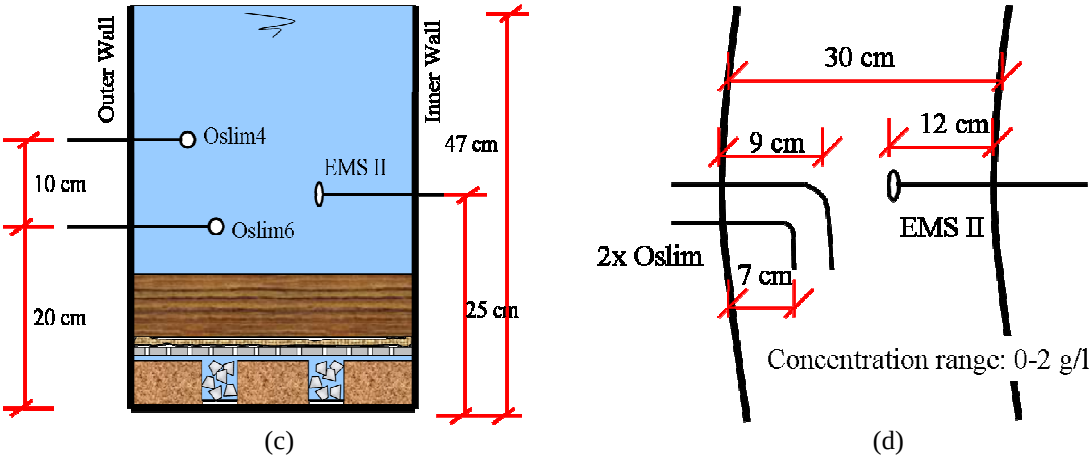

(c) (d)

Figure 3.15: Location of the EMS and Oslims (concentration range of 0-2 g/L) depicted in the cross-section of the flume.

.

(1) Step [-]	(2) ω_f [m/s]	(3) ω_t [m/s]	(4) ω_f [rpm]	(5) ω_t [rpm]	(6) Suction speed of Oslim [m/s]	(7) Duration [min]
1	-0.02	0.04	-0.103	0.10	0.18	7.5
2	-0.10	0.20	-0.516	1.02	0.18	7.5
3	-0.20	0.40	-1.032	2.04	0.18	7.5
4	-0.30	0.59	-1.549	3.06	0.18	7.5
5	-0.40	0.79	-2.065	4.08	0.37	10
6	-0.49	0.97	-2.529	4.99	0.37	10
7	-0.60	1.19	-3.097	6.12	0.56	10
8	-0.70	1.38	-3.613	7.14	0.56	10
9	-0.78	1.54	-4.026	7.95	0.56	12.5
10	-0.86	1.70	-4.439	8.77	0.56	12.5
11	-0.93	1.84	-4.800	9.48	0.56	12.5
12	-1.00	1.98	-5.162	10.19	0.56	12.5
13	-1.05	2.07	-5.420	10.70	0.56	12.5

Table 3.2: Conditions of the flume during the 13 different rotational steps: rotational speeds as applied for the erosion test (2), (3), (4) and (5), Oslim suction velocity (6) and duration for each velocity step (7).

3.3.4 Optimum ratio and bed shear stress determination

As mentioned before, Booij (1994) studied the secondary flow characteristics in an annular flume. An optimum ratio between the rotational speeds to reduce these secondary flows was found. He found that the optimum ratio strongly depends on the flow depth. This leads to the relation between the rotational speed and the aspect ratio (h/b) of the flume:

$$\frac{\omega_t}{\omega_f} + 1 = -1.17\frac{h}{b} \tag{3.1}$$

where ω_t [rpm] is the rotational speed of the top lid, ω_f [rpm] the rotational speed of the flume, b [m] the width and h [m] the height of the water column.

To determine the optimum ratio for this study, the width of the flume of 0.30 m and the flow depth of 0.27 m are substituted in equation (3.1), resulting in the optimum ratio of 1.975. This ratio is used to determine the rotational speeds for the lid and the bottom, as applied for all three erosion tests (see Table 3.2).

To determine the bed shear stress, an advanced turbulence model by means of a Large Eddy Simulation (LES), is applied (Booij, 2003). From this LES model, the full 3D hydrodynamics is obtained from which it is assumed that the bed is hydraulically smooth. This is not valid in our experiments where the flow is hydraulically transitional or rough due to the surface of sediment beds. However, as a first step we assume that the calculated bed shear stress is also valid for our experiments. We will discuss this in more detail in Chapter 5.

4 Results of the erosion tests

4.1 Measured hydrodynamics

During the erosion tests, 13 rotational speeds of the top lid and flume were applied, generating a flow within the annular flume. Two EMS devices were used to measure both the flow velocity in the main direction (*x*) as in the vertical direction (*z*). Typical results from an EMS-measurement are shown in Figure 4.1.

In Figure 4.1 (a) the flow velocity in the *x*-direction increases for each step. The vertical flow velocities are relatively small. The average flow velocity in the *z*-direction (see Figure 4.1 (b)) is about zero. Both figures indicate that for larger rotational speeds the level of turbulence increases. In the beginning of each rotational step the degree of turbulence as shown in fig 4.1a is similar to that at the end of the same step. This indicates that no effect of the spinning-up of the flume, after increasing the rotational speeds, is identified. In order to analyze the measurement more effectively, the average velocity over the duration of each rotational step is determined for both the main as the vertical flow (see Figure 4.2). The average velocity for the main flow (Figure 4.2 a, c and e) indicate that the two EMS-measurements are identical, except at the first few steps of the test on the sandy sample. The reason for this is that EMS1 was not working in the beginning of the test due to a problem with the connection of the measurement set-up. After it was fixed, the EMS1 operated properly.

In Figure 4.2 (b), (d), and (f) the average vertical velocities are not identical. However, the magnitudes of the three signals all occur in the same velocity-range. The velocities are within the range of -0.01 – 0.005 m/s, which is relatively small compared to the magnitude of the main flow velocity. These magnitudes are, however, large compared to sediment settling velocity. It should be noted that for the muddy and intermediate sample only the measurement from EMS2 is shown. The signal of the EMS1 is invalid due to a problem with the (horizontal) positioning of the sensor. For the sandy sample (last test), this problem was solved, and the EMS2 operated properly.

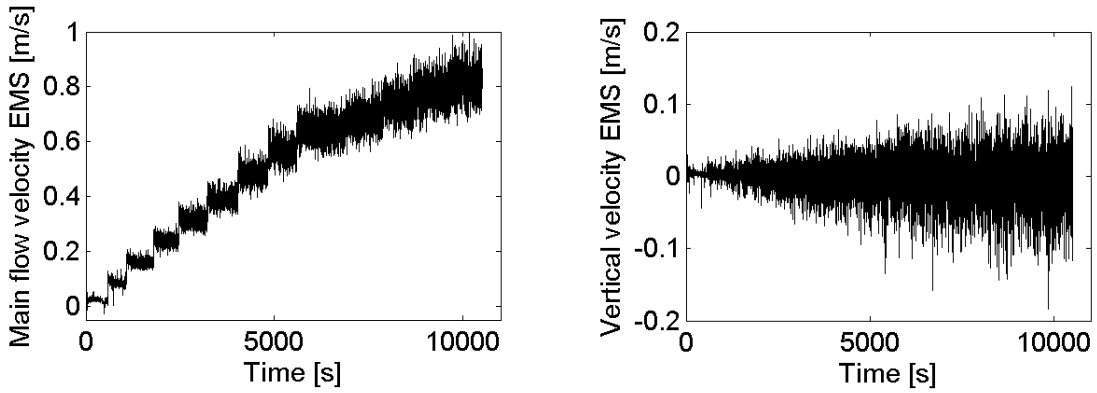

Figure 4.1: Typical output of EMS-measurement showing both the flow velocity in the *x*-direction (a) as in the *z*-direction (b).

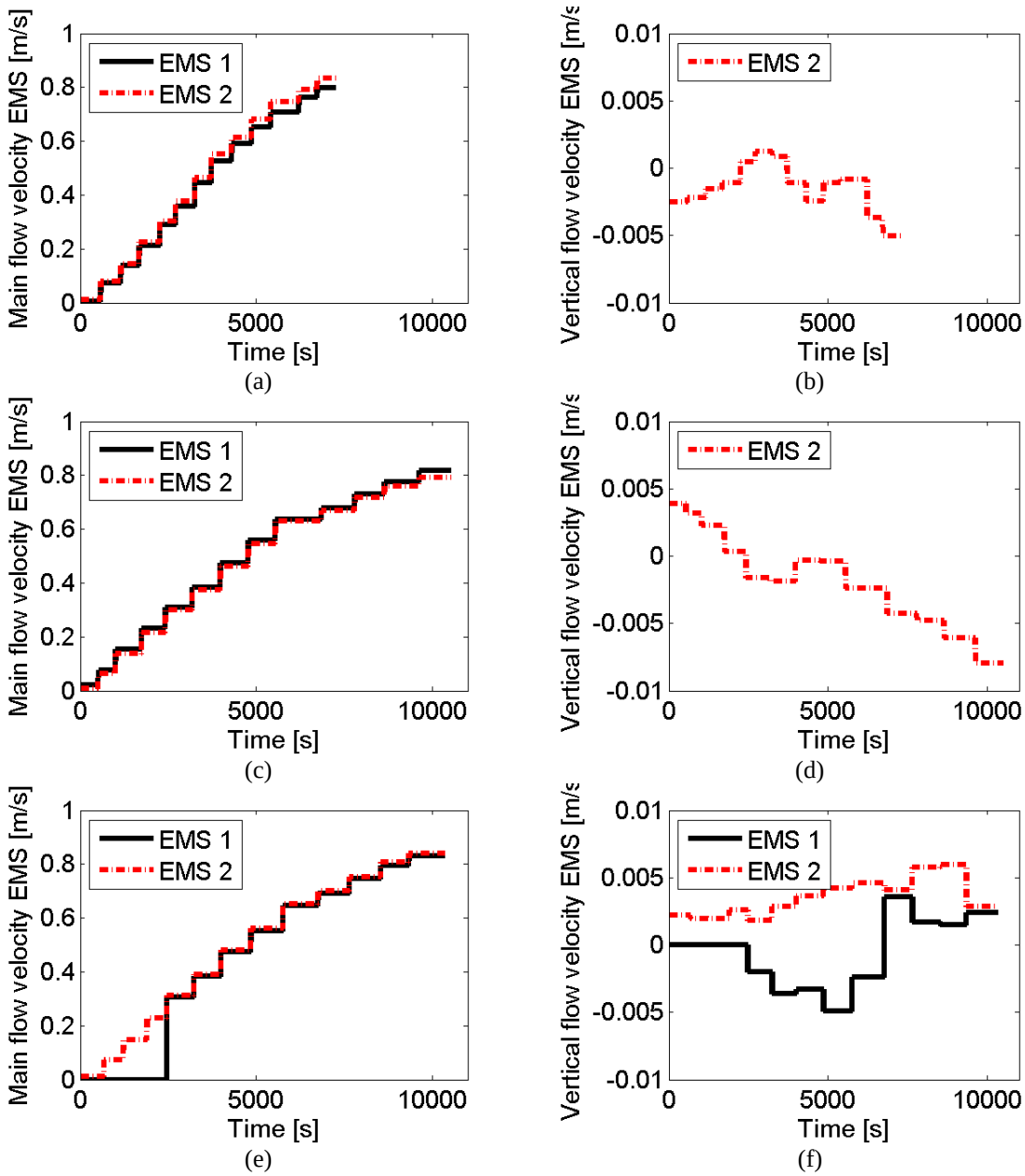

Figure 4.2: EMS-measurement for the test on the muddy (a, b), intermediate (c, d) and sandy sample (e, f). The average results of the two EMS are shown both for the main (left) and the vertical flow (right).

4.2 Simulated hydrodynamics

An advanced turbulence model in terms of a Large Eddy Simulation (Booij, 2003) is applied to determine the bed shear stresses. For given rotational speeds of the top lid and flume the flow pattern within the flume is reproduced. A detailed flow pattern concerning the tangential flow as well as the secondary flow is simulated for all rotational speeds as applied in Table 3.2. Here, an example of the simulated flow pattern is shown for a rotational speed of the flume (ω_b) of -3.097 rpm, an optimum ratio (ω_t / ω_b) of 1.97, and a water depth (h) of 0.27 m, Figure 4.3. In this figure the tangential flow velocity (a) appears reasonably uniform along the bed, but varying in upper layers. The flow near both sided-walls of the flume appears to be considerably influenced by the rotation of the flume. The numbers in the figure indicate that the tangential flow moves towards the reader for the flow at the near bottom, and moves away from the reader near the lid. For the current in a cross section of the flume (b), two secondary cells are observed. Both cells move towards the outer bend at the near bottom and near the lid.

Using the simulated 3D flow pattern, it is possible to derive the bed shear stress for all 13 rotational speeds. This is done by using the resultant of the frictional velocity in the *x*- and *y*-direction. Figure 4.4 shows the distribution of the bed shear stress over the width of the flume averaged over a certain time of xxx for each rotational step. The Figure 4.4 shows that for the first six steps the bed shear stresses are rather uniformly distributed over the width of the flume. The profiles become less uniform for higher bed shear stresses. The bed shear stresses close to the outer wall are larger than those along the inner wall.

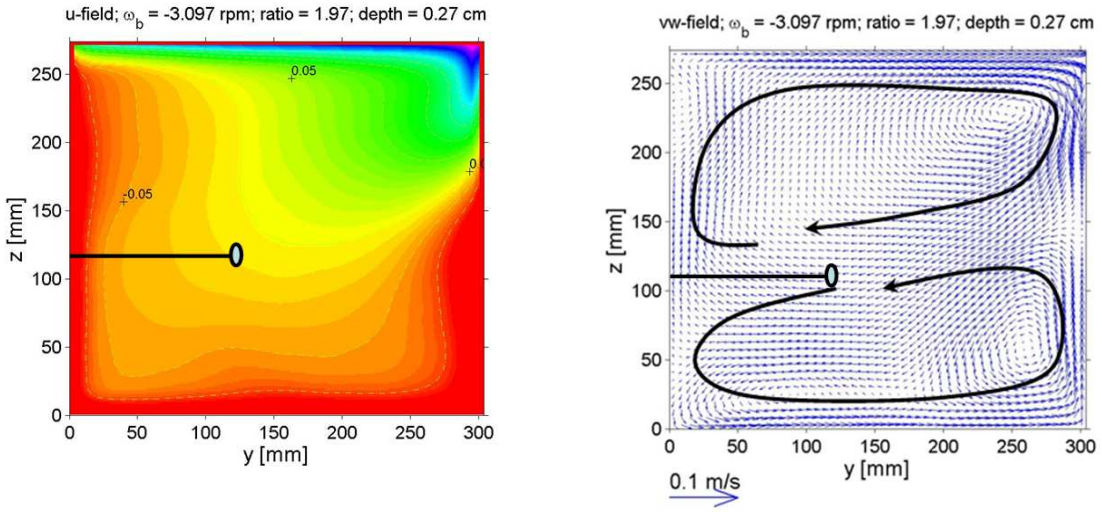

(a) (b)

Figure 4.3: Typical results of a LES simulation for both the (a) main flow and the currents in a cross-section of the flume (b) with the outer bend at right. The numbers (a) indicate the flow velocities [m/s] (as measured with respect to a fixed position out of the flume). The main flow appears uniform along the bed (towards the reader) and maximal along the lid (away from the reader), especially near the outer wall. For the flow in the cross-section two circulations cells are identified (b)

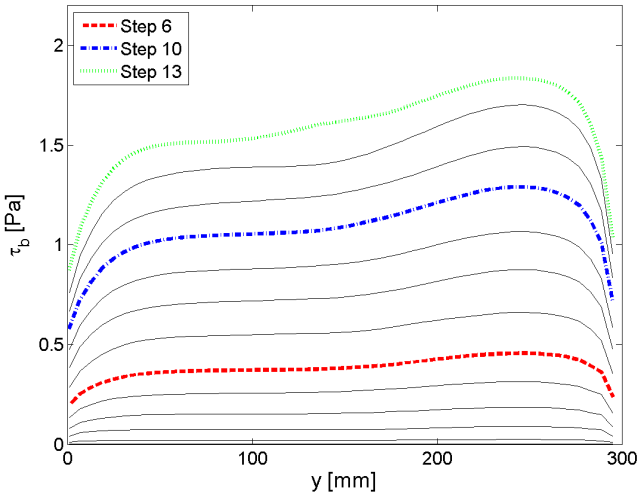

Figure 4.4: Distribution of the bed shear stress calculated over certain modeling durations which are in the same order of magnitude as the rotational steps. In this figure, all calculated profiles for the different rotational speeds for the test on the muddy sample are shown

4.3 Erosion test on the muddy sample

The composition of the muddy sample is shown in Table 4.1:

Condition	Clay [%]	Silt [%]	Sand [%]
Muddy	16	64	20
Intermediate	6	24	70
Sandy	2	8	90

Table 4.1: Compositions of the sediment samples as applied for the erosion test

This sediment sample was mixed with a water content of 50%, as discussed in section 3.2.3. The average thickness of the sample after placement was approximately 9.43 cm. The total settlement of the sediment bed measured before erosion was approximately 0.73 cm. During the consolidation process, the under-pressure, as mentioned in section 3.2.2, was applied to enhance consolidation. However, the pressure lasted shortly due to a leak in the bottom of the flume. From then on, only the load of water on top of the sample was compressing the sediment bed to consolidate. It appeared that due to wrinkles in the plastic foil in combination with the water on top a pattern of small ripples were generated (see Figure 4.5). The height of the print of these wrinkles was around 3 - 4 mm and its length scale around 10-20 cm. During the removal of the plastic foil a limited amount of fines was brought into suspension. This material settled before the erosion test started. So the erosion test started with clear water.

Cores were taken from the sediment bed to check if the bed exhibited a stratified density profile. Figure 4.6 shows the vertical profiles of the water content over the depth. The figure indicates that the water content decrease with increasing depth. This means that the bed has an increasing density at larger depth. It also appears that the water content at the surface for both locations is not varying much during the test. The water contents before and after the test are almost identical. However, the water contents at the surface of the two locations slightly differ. This implies a horizontal distribution of the water content over the surface of the bed. The average water content of the whole sediment bed is around 36.5% during the test. The average water content over the upper 1 cm of the bed is 39.9%. In addition, with reference to Figure 3.15 (a), the position of the Oslims can be indicated before erosion, as follows; A $\approx$10.3 cm, B$\approx$7.1 cm and C$\approx$8.7 cm.

The erosion behavior of the sediment bed was optically observed. For low rotational speeds ($\tau_b \approx 0-0.08$ Pa and $U \approx 0-0.15$ m/s) little erosion was observed. Only some material that settled after the removal of the plastic foil was re-suspended again. This especially took place from the top of the irregularities on the sediment bed. Considering the turbidity of the water, only fine particles (flocs) were eroded from step 4 (t = 1680 s, $\tau_b \approx 0.17$ Pa and $U \approx 0.2$ m/s) onward. No movement of sand was observed. From rotational step 6 (t = 2710 s, $\tau_b \approx 0.38$ Pa and $U \approx 0.36$ m/s) onward, the movement of aggregates of material and some sand was observed. From step 7 (t = 3252 s, $\tau_b \approx 0.56$ Pa and $U \approx 0.46$ m/s), also the movement of coarser sand was observed by rolling and jumping of sand particles. During step 12 (t = 6212 s, $\tau_b \approx 1.43$ Pa and $U \approx 0.76$ m/s) a

thin layer of sand was observed on top of the sediment bed along the outer bend of the flume. This sand was not collected after the tests to determine the mass of eroded sand, as its volume was too little to accurately collect it. After the test the water was extracted out and the bed surface was observed (Figure 4.7). The bed surface slightly differed from the initial condition. The irregular bed forms were still present, but their height decreased during the test due to erosion with around 50%.

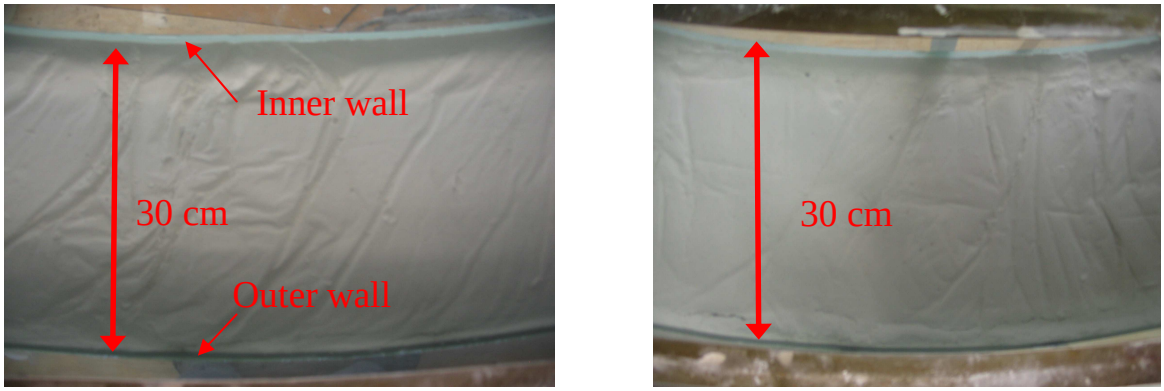

Figure 4.5. Top view of the bed surface of the muddy sample after removing the plastic foil. The pattern that resulted from the wrinkles in the foil is shown. This irregular surface was found for the entire bed. These two pictures are photographed at different locations of the bed surface.

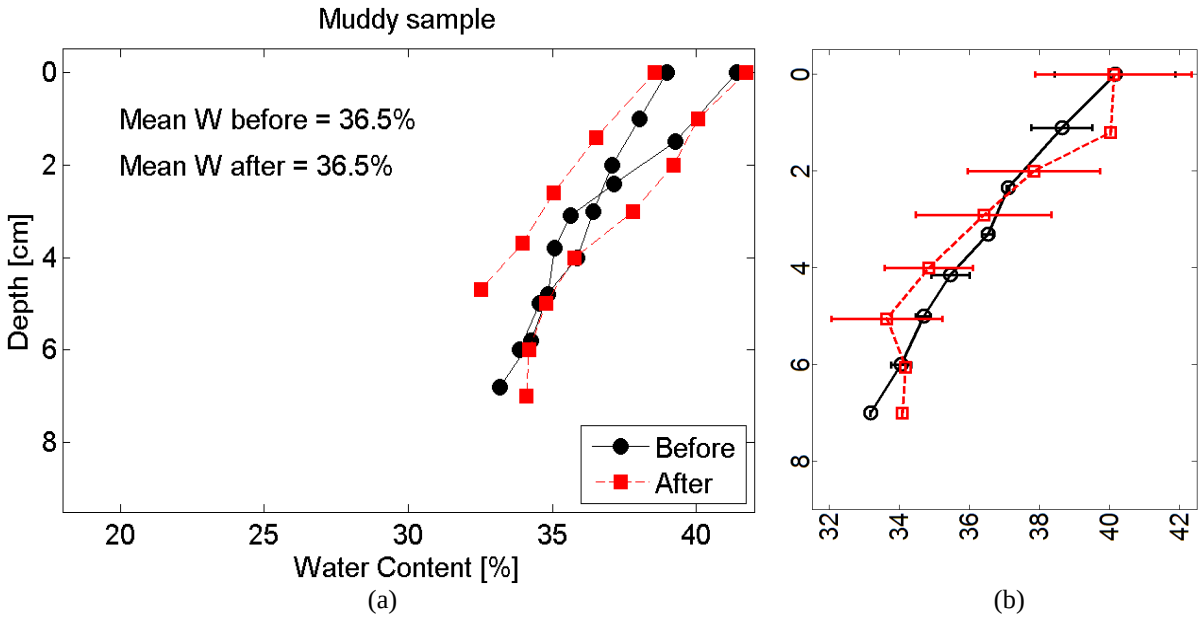

(a) (b)

Figure 4.6: Vertical profiles of the water content plotted over the depth (a) and the error bars (b) for the water contents of the sample cores as taken from the sediment bed before and after the erosion test. Also the average water contents are indicated.

Figure 4.7. Top views of the bed surfaces after the erosion test. It is shown that not much difference compared to the initial condition is identified, except that some bed forms were smoothened because of the erosion. These two pictures are photographed at different locations of the bed surface. Note that these two pictures are not the same place as the pictures of the bed surface before erosion.

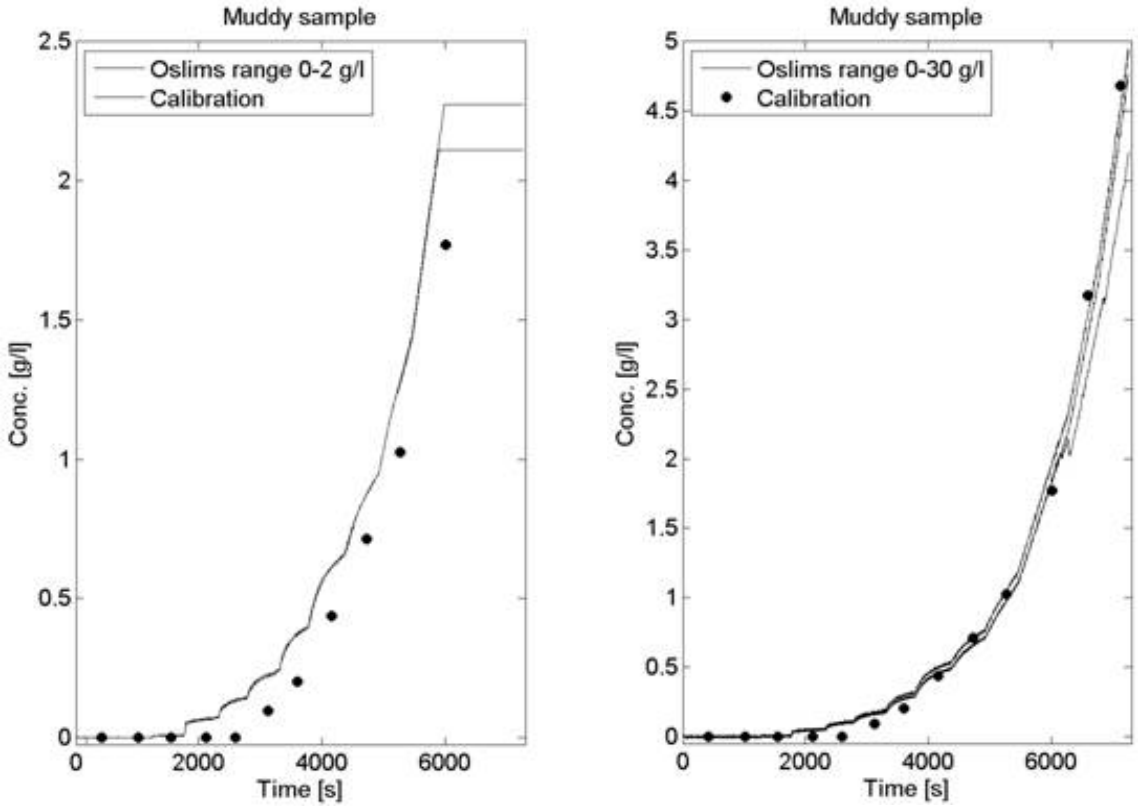

(a) (b)

Figure 4.8: Concentration as a function of time for the Oslims with the range of 0-2 g/L (a) and 0-30 g/L (b) for the muddy sample. The dots are the concentrations determined from the sampling of water samples. Each water sample was collected during the test.

During the erosion test, the concentration of eroded fines was measured using the five Oslims. The concentrations as a function of time are plotted in Figure 4.8. Both results of the Oslims of the 0 – 2 g/L range (a), as of the Oslims of the 0 – 30 g/L range (b) are shown. Also the result of the calibrated concentration is shown by the black dots. Figure 4.8 (a) and (b) indicate that the concentration measured by the Oslims increases in

a similar way as the calibration-concentrations. At the beginning of each rotational step the concentration increases rapidly. For low concentrations the concentrations reaches equilibrium. For higher concentration the equilibrium is not reached, although a similar tendency is observed. For the highest concentrations the increase in time is almost linear. For the Oslims with the range of 0-2 g/L, the calibration-concentration differs from the concentration of the Oslim. It appears that the dots of the calibration concentration are lower than the profile of the measured concentration. This difference also appears for lower concentrations measured by the 0-30 g/L Oslims. For higher concentrations, the calibrated and measured (0-30 g/L Oslims) concentrations are identical. It should be noted that the timing of the sample collection within each rotational step was not constant. It is assumed that the moment these samples are taken is at around 75% of the duration of a test.

4.4 Erosion test on the intermediate sample

The composition of the intermediate sample is shown in Table 4.2

Condition	Clay [%]	Silt [%]	Sand [%]
Muddy	16	64	20
Intermediate	6	24	70
Sandy	2	8	90

Table 4.2: Compositions of the sediment samples as applied for the erosion test

The water content as discussed in section 3.2.3 for the intermediate sample is 25%. However, the first batch of the sample was by mistake mixed to a water content of 50%. This resulted in a rather liquid sample, which enables the placement of the sample into the flume by gravity. Due to this high water content some segregation occurred during the placement. For the second batch, the sample was mixed to a water content of 25%. This resulted in a sample that was too plastic to pour by gravity. Therefore, the placement was done manually by means of a shovel. It is expected that any air that is entrapped during the placement is squeezed out during the consolidation. After the placement, the bed surface was smoothened. The average thickness of the sample before consolidation was approximately 9.9 cm.

During the consolidation process, only the load of water on top of the sample was applied. The negative water pressure as mentioned in section 3.2.2 was not applied because of the problem with the leak of the flume. After three hours of consolidation, the settlement of the sediment bed was almost finished. This duration corresponds to the required time for consolidation as determined in section 3.2.3. The settlement was 0.8 cm. Despite the quick rate of settlement, the plastic foil was remained for 22 hours before removing to assure the uniform condition of the sediment bed without any air entrapped inside. In addition, with reference to Figure 3.15 (a), the position of the Oslims in vertical can be indicated after measuring the thickness of the sediment bed; A $\approx$10.3 cm, B$\approx$5.3 cm and C$\approx$9.1 cm.

It appeared that much less wrinkles due to the plastic foil occurred. The bed surface was smoother than the surface of the muddy sample, as can be seen in Figure 4.9. The height of the ripples was around 2 – 3 mm, with a distance between them of around 10 – 20 cm. Sediment cores were taken from the sediment bed to check if a vertical stratification occurred. Figure 4.10 shows the vertical profiles of the water content over the depth. The figure indicates that the water contents slightly decrease with increasing depth. This means that the bed has an increasing density at larger depth. It appears that the water contents at the surface of the bed before and after the test differ slightly. Over depth, the water contents after erosion appear higher than the water content before erosion. The difference in water content before and after erosion is assumed as a result of the difference of the bed density in horizontal. The average water content of the whole sediment bed is around 21% during the test. The average water content over the first 1 cm is 22.8%.

During the erosion test, the erosion behavior of the sediment bed was optically observed. In the first three steps for low rotational speeds ($\tau_b \approx 0 - 0.08$ Pa

and $U \approx 0 - 0.15$ m/s) little erosion for fines was observed. From step 4 (t = 1750 s, $\tau_b \approx$ 0.17 Pa and $U \approx 0.24$ m/s) onward, fines were clearly eroded and dispersed into suspension. No movement of sand was observed. During step 7 (t = 3986 s, $\tau_b \approx 0.56$ Pa), the movement of aggregates of material and some sand was observed. Bed transport was occurring by means of rolling and jumping of sand particles. It was observed that sand was accumulating on top of the sediment bed along the outer bend of the flume.

From step 7, ripples were observed in the accumulated sand (see Figure 4.11). The ripples had an average length scale of ~7.5 cm and a height of ~0.5 cm. From step 9 (t = 5556 s, $\tau_b \approx 0.98$ Pa and $U \approx 0.64$ m/s) onward, all the ripples were suddenly eroded by the flow. The disappearance of these ripples indicates a transition in the transport mode of sand: from the bed load regime to the sheet flow regime. It was observed that more sand was suspended in the water column. From step 12 (t = 8653 s, $\tau_b \approx 1.47$ Pa and $U \approx 0.78$ m/s) onward, small scour holes were observed over the whole width of the bed, but especially along the inner bend (see Figure 4.12). The holes varied in size (between a diameter of 1 – 4 cm and a depth of 0.5 – 1 cm) and occurred without a clear pattern. .It appeared that the accumulated sand on the bed surface along the outer bend can be distinguished from the normal bed. This accumulated sand was collected to determine the total mass of eroded sand (see section 5.4). The accumulated sand formed an elongated triangle with a width of around 8 cm and a height of around 2.7 cm.

During the erosion test, the concentration of eroded fines was measured using the five Oslims. The concentrations as a function of time are plotted in Figure 4.14. Both results of the Oslims of the 0 – 2 g/L range (a), as of the Oslims of the 0 – 30 g/L range (b) are shown. From the water samples collected in each rotational step a calibration-concentration is determined, which is shown by the black dots. Figure 4.14 (a) and (b) indicate that the concentration measured by the Oslims increases in a similar way as the calibration-concentration.

As seen in the concentration profile of the muddy sample, the concentration is again reaching equilibrium for low rotational speeds. By increasing these velocities, the equilibrium is no longer reached, although the same tendency is still observed. For the highest velocities this tendency is hard to distinguish, and the concentration seems to linearly increase in time.

Figure 4.14 (a) and (b) show a comparison between the calibration-concentration and the concentration as measured by the Oslim. The difference between the compared concentrations is clearly identified for the Oslims of the 0 – 2 g/L range. For the Oslims of the 0 – 30 g/L range, the discrepancy occurred slightly for lower concentrations, while for higher concentrations the calibrated and measured (0 – 30 g/L) concentrations fairly agree. As same as the previous test on the muddy sample, the moment at which the water samples were collected is at around 75 % of the duration of a test. After the test, the accumulated sand along the outer bend was collected and, subsequently, oven-dried for 24 hrs at 105 $^\circ$C. The total mass of eroded sand is 21.26 kg.

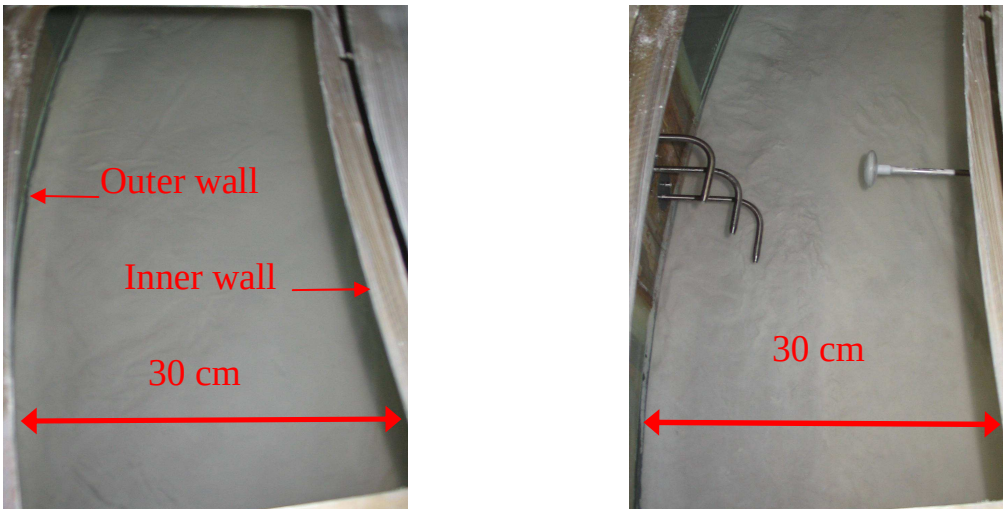

Figure 4.9. Top views of the bed surface of the intermediate sample after removing the plastic foil. No print as a result of the wrinkle of the plastic foil was observed. The bed exhibits a smooth and uniform surface.

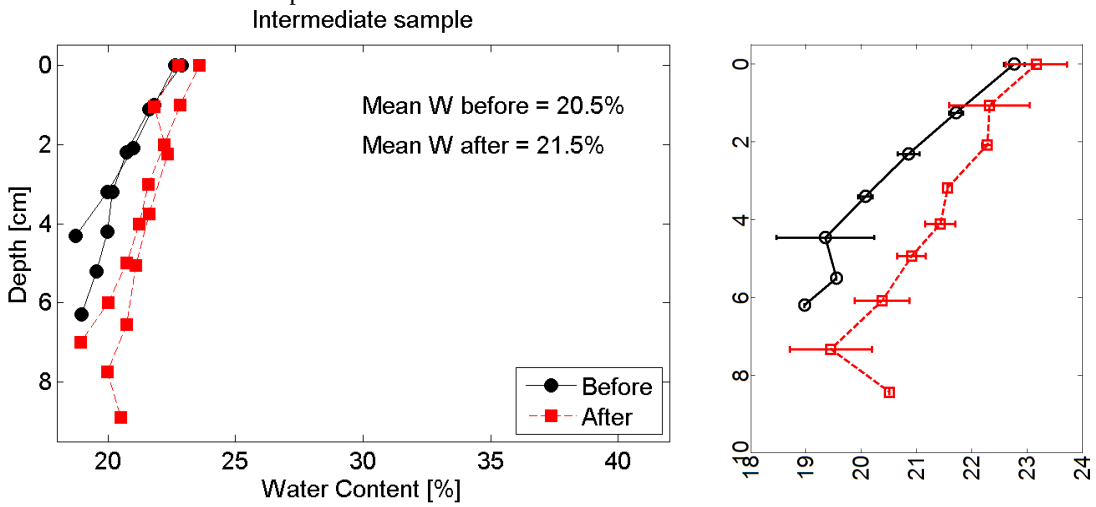

(a) (b)

Figure 4.10: Vertical profiles of the water content plotted over the depth (a) and the error bars (b) for the water contents of the sample cores as taken from the sediment bed before and after the erosion test. The average water contents are indicated.

Figure 4.11. Picture taken at the outer wall of the flume showing sand ripples within the layer of accumulated sand. The ripples indicate bed load transport of sand. The average size of these ripples is shown.

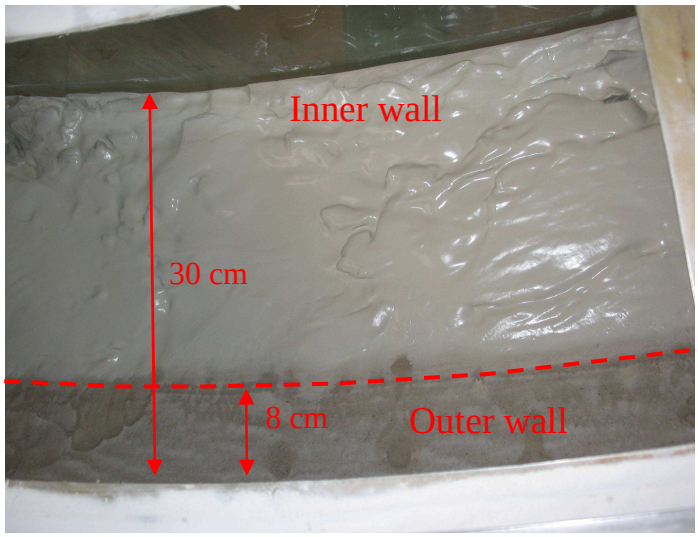

Figure 4.12: Top view of the bed surface after erosion. The accumulated sand along the outer wall is clearly visible. Also the holes in the sediment bed are shown.

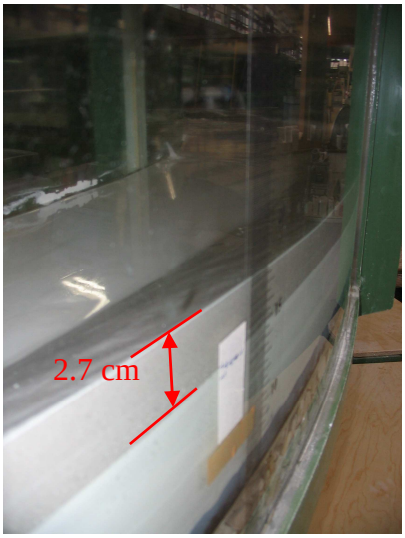

Figure 4.13: Picture taken at the outer wall after the test showing the sand accumulation on the bed surface in the corner along the outer wall. The height of the accumulated sand is shown.

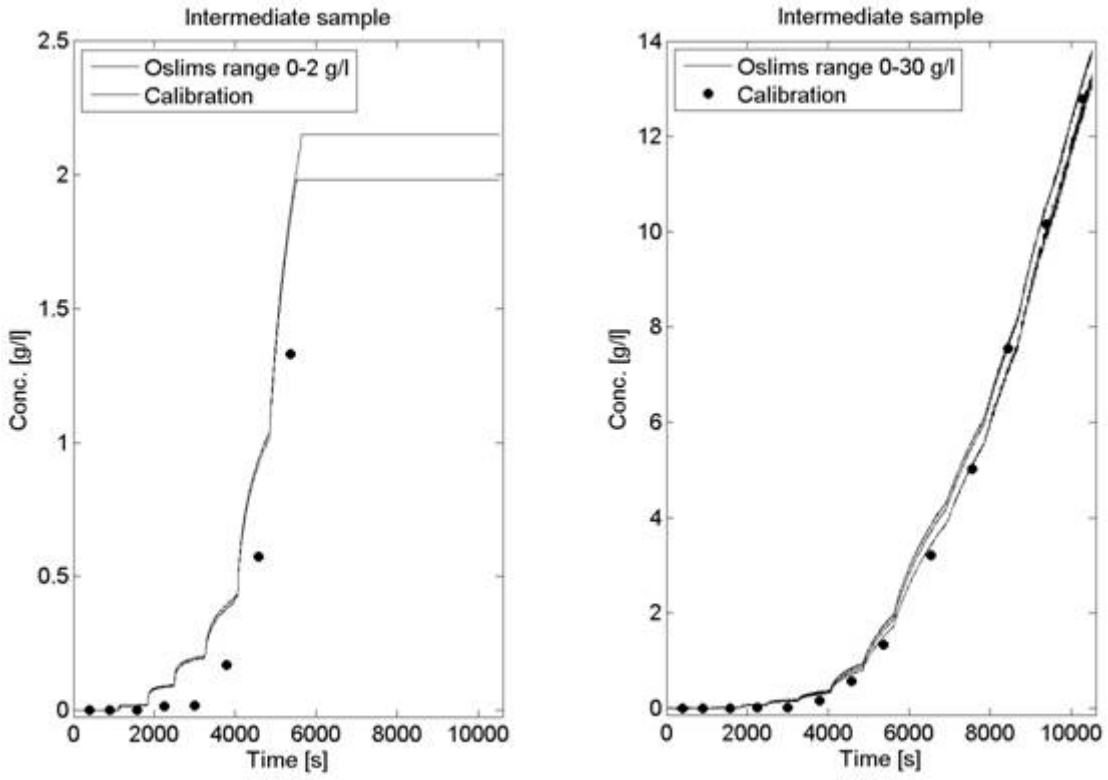

(a) (b)

Figure 4.14: Concentration as a function of time for the Oslims with the range of 0-2 g/L (a) and 0-30 g/L (b) for the intermediate sample. The dots are the calibration-concentrations of the Oslims. These concentrations are determined for the water samples collected during the test.

4.5 Erosion test on the sandy sample

The composition of the sandy sample is shown in Table 4.3.

Condition	Clay [%]	Silt [%]	Sand [%]
Muddy	16	64	20
Intermediate	6	24	70
Sandy	2	8	90

Table 4.3: Compositions of the sediment samples as applied for the erosion test

This sediment sample was mixed to a water content of 25%, as discussed in section 3.2.3. The mixture was rather solid and it was hard to pour it directly from the batch into the flume. The placement of the mixture was made using a shovel to scoop the mixture out. The thickness of the sample after placement was 8.5 cm. After 0.25 hours of consolidation, the settlement of the sediment bed was approximately 0.2 cm. During the consolidation process, only the load of water on top of the plastic foil was compressing the sediment bed. Again, the negative water pressure as mentioned in section 3.2.2 was not applied due to a leakage in the bottom of the flume. After removing the plastic foil, small ripples on the bed surface were found (see Figure 4.15). Their print was generated by wrinkles in the plastic foil in combination with the water on top. The height of the ripples was around 1-2 mm and its length scale was again around 10 20 cm.

Sediment cores were taken from the sediment bed to check if vertical stratification of the density occurred. Figure 4.16 shows the vertical profiles of the water content over the depth. It appears that the water contents decrease with increasing depth. This means that the bed has an increasing density at larger depth. All the profiles also differ slightly in horizontal. This implies a difference of the bed density in horizontal. The average water content of the whole sediment bed is around 26% during the test. The average water content over the first 1 cm is 27.3%. In addition, with reference to Figure 3.15 (a), the position of the Oslims in vertical can be indicated after measuring the thickness of the sediment bed; A $\approx$10.3 cm, B$\approx$6.2 cm and C$\approx$8.3 cm.

During the erosion test, the erosion behavior of the sediment bed was optically observed. It was observed that the fines, which settled after removing the plastic foil, were re-suspended during the first few steps (step 1 – 2). From step 3 (t = 1230 s, $\tau_b \approx$ 0.15 Pa and $U \approx 0.15$ m/s) onward, fines were clearly eroded and brought into suspension. Not much movement of aggregates or sand was observed along the surface of the bed. From step 5 (t = 2466 s, $\tau_b \approx 0.27$ Pa and $U \approx 0.3$ m/s) onward, the movement of aggregates and some sand was clearly observed. It appeared that sand was again slowly accumulating on top of the sediment bed along the outer bend of the flume.

During step 7 (t = 4002 s, $\tau_b \approx 0.56$ Pa and $U \approx 0.48$ m/s), rippled occurred in the layer of sand (see Figure 4.17). The same length scale occurred for the observed ripples as during the test on the previous samples: a length scale of ~7.5 cm and a height of ~0.5 cm. From step 8 (t = 4849 s, $\tau_b \approx 0.76$ Pa and $U \approx 0.58$ m/s) onward, these ripples were disappearing due to the larger flow velocities. This resulted in a flat layer of accumulated sand along the corner of the outer bend. This again indicates a sheet flow regime. From

step 11 (t = 7638 s, $\tau_b \approx 1.28$ Pa and $U \approx 0.76$ m/s) onward, it was observed that more sand was brought in suspension as the color of the turbidity occurred darker than observed in the beginning of the test. In the last two steps (step 12 and 13, $\tau_b \approx 1.45$ and 1.59 Pa, $U \approx 0.8$ m/s and 0.85 m/s) it appeared that sand was occurring in the suction tubes of the Oslims. After the test the water was drained out of the flume and the bed surface after erosion was observed (see Figure 4.18). It appeared that small scour holes were found over the whole width of the bed surface. The holes varied in size (between a diameter of 1 – 3 cm and a depth of 0.5 – 1 cm) and appeared without a clear pattern. In addition, the eroded sand, which was accumulated on the surface along the outer bend, was collected and, subsequently, oven-dried at 105 ° C. The total mass of the collected sand is 13.49 kg.

During the erosion test, the concentration of eroded fines was measured using the five Oslims. The concentrations as function of time are plotted in Figure 4.19. Both the results of the Oslims of the 0 – 2 g/L range (a), as of the Oslims of the 0 – 30 g/L range (b) are shown. The calibration-concentration determined from the water samples is shown by the black dots. Both Figure 4.19 (a) and (b) indicate the difference between the calibration-concentration and the concentration as measured by the Oslims. Also for this test, it appears that the calibration concentrations are lower than the measured profile for the lowest rotational steps (1 - 5). For steps 6 - 13, the dots are located above the profiles. Despite the difference, both calibration-concentration and the concentration as measured by the Oslim appear to increase in a similar way. In addition, both Figure 4.19 (a) and (b) indicate that at the beginning of each rotational step the concentration increases rapidly and tends towards equilibrium shortly afterward. This tendency is also observed for higher concentration, although the equilibrium is not reached. For the largest rotational steps the increase in time of the concentration is almost linear.

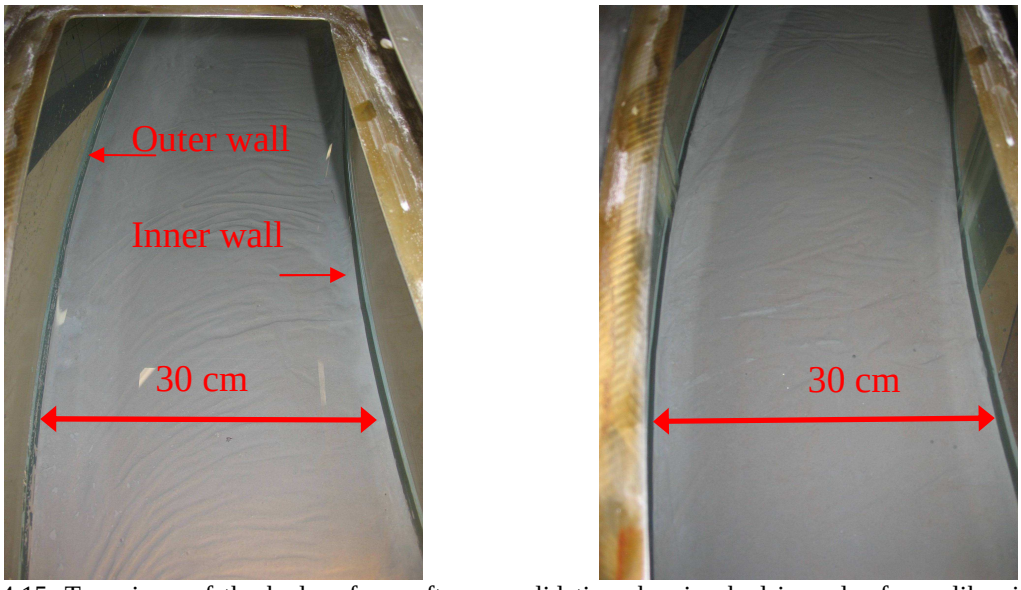

Figure 4.15. Top views of the bed surfaces after consolidation showing bed irregular forms like ripples. These ripples occurred due to the plastic foil. The ripples were small but appeared over the whole bed surface.

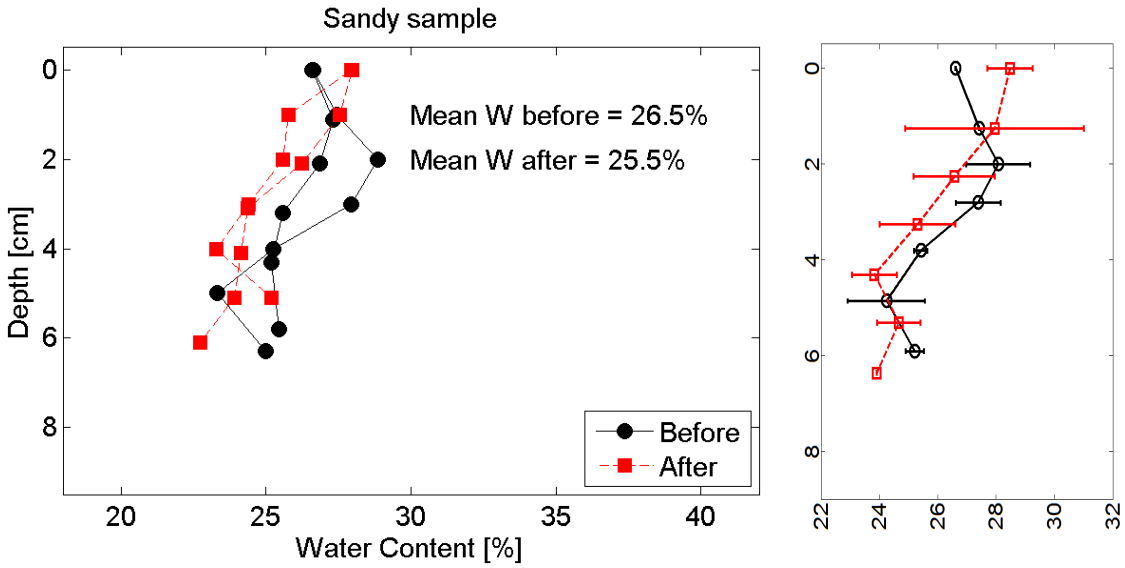

(a) (b)

Figure 4.16: Vertical profiles of the water content plotted over the depth (a) and the error bars (b) for the water contents of the sample cores as taken from the sediment bed before and after the erosion test. The average water contents are indicated.

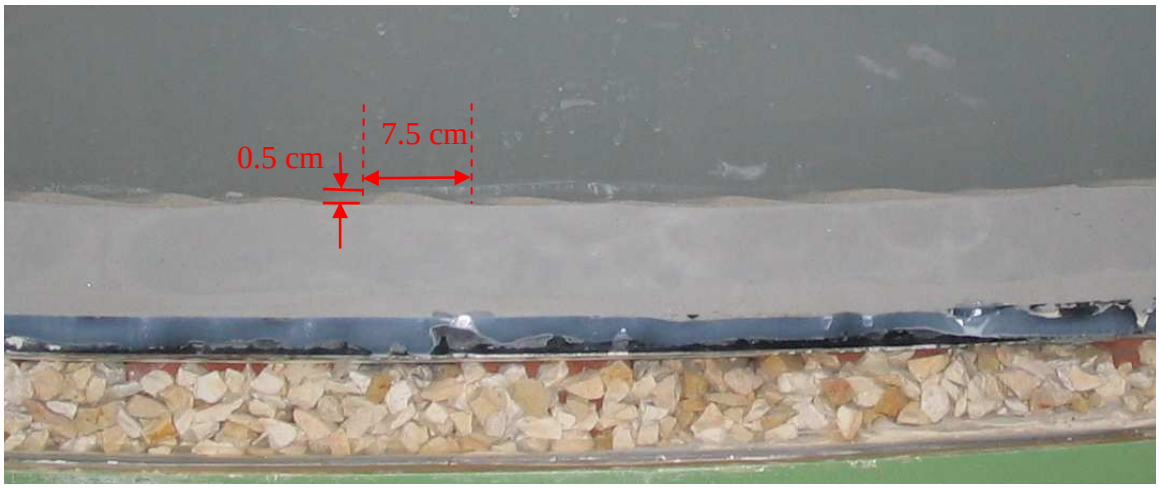

Figure 4.17: Picture taken at the outer wall of the flume showing sand ripples within the layer of accumulated sand for the sandy sample. The ripples indicate bed load transport of sand. The average size of these ripples is shown.

Figure 4.18: Top views of the bed surface after erosion of the sandy sample. The accumulated sand along the outer bend of the flume is shown along with the irregular pattern of holes. .

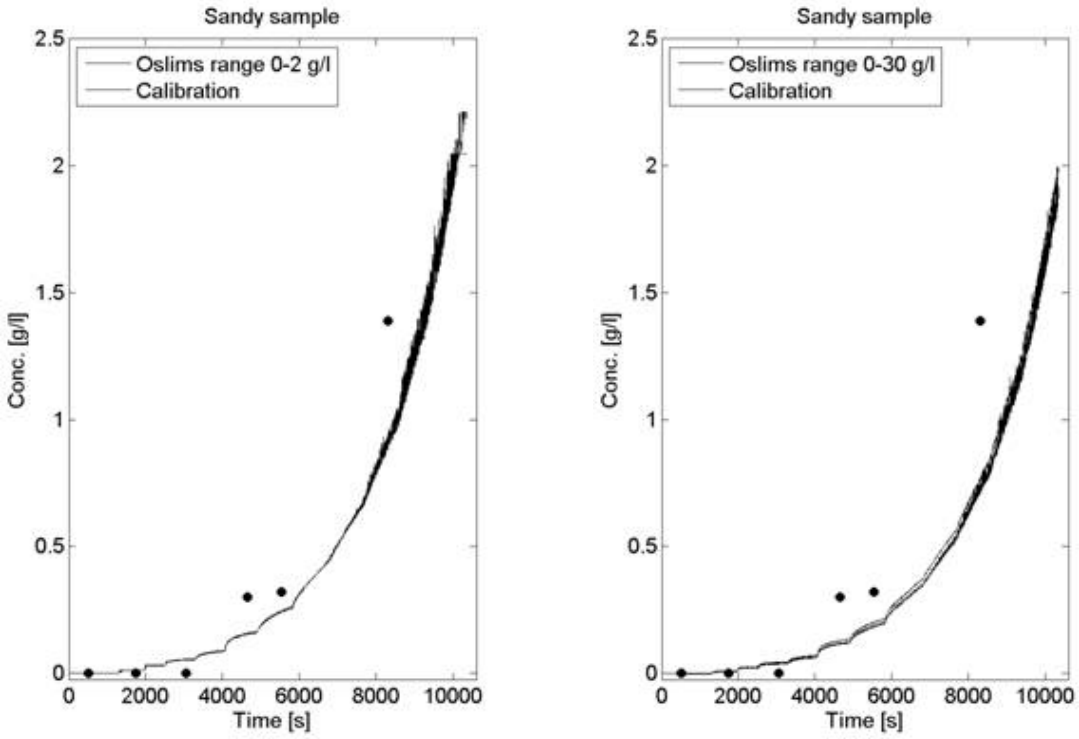

(a) (b)

Figure 4.19: Concentration as function of time for the Oslims with the range of 0 – 2 g/L (a) and 0 – 30 g/L (b) for the sandy sample. The dots are the calibration-concentrations of the Oslims. These concentrations are determined for the water samples collected during the test.

5 Discussion

5.1 Hydrodynamics

As discussed in section 4.2, the bed shear stresses are computed for all 13 rotational steps using a Large Eddy Simulation (LES) model. The bed shear stress will be used in combination with the erosion rate to determine the erosion threshold for both fines and sand. To validate the simulated bed shear stresses, the measured and simulated tangential and secondary flow patterns are compared. A good agreement between these two patterns implies that the bed shear stress as computed by the model can be used.

For each test the flow patterns of step 2, 5, 7 and 13 are compared. The simulated velocity can be determined from the flow patterns of the tangential flow (see Figure 5.1 (a), (c), (e) and (g)) and of the secondary flow (see Figure 5.1 (b), (d), (f) and (h)). First, the tangential flow velocity (u_{av}) is determined in the position where the EMS was measuring. To compare the velocity as indicated in Figure 5.1 with the measured velocity, the rotational speed of the flume (u_w) should be subtracted of the simulated velocity (u_{av}). In Table 5.1 the comparison of both simulated and measured velocities is shown.

Table 5.1 indicates that the simulated velocity as determined by the LES model is larger than the measured velocity from the EMS. The differences are all in the same range for all three samples; 23% for the muddy and intermediate sample and 20% for the sandy sample. The possible reason is that the simulated flow pattern is generated based on the assumption that the glass bottom of the flume is characterized as the hydraulically smooth flow. However, in this study the bed surfaces for all three samples were rougher due to the occurrence of ripples after the removal of the plastic foil. The influence of this rougher bed leads to a decrease of the actual velocity. As a result, the simulated velocity appear over-estimating to the measurement.

In these tests, the criterion of Nikuradse ($\nu_* k_s / \nu$), was used to characterize the bed roughness of the flow whether it is hydraulically smooth, rough or in the transitional zone. It is found that the flow condition for all three samples is characterized as a hydraulically transitional flow. As described in the previous paragraph, the effect of the rougher bed resulted in smaller flow velocity. It may seem that the decrease of velocity would also lead to the small value of the bed shear stress. This is not true, as the rougher bed surface contributed to the increase of the actual bed shear stress. This bed shear stress is determined taking into account the increase of the drag force due to the rougher bed surface. The bed shear stresses based on the rougher bed are compared with the bed shear stress as calculated by the LES model (see Table 5.2). The comparison shows both bed shear stresses are within the same range. Another possible measure to determine the bed shear stress, apart from the method following the roughness of the bed surface, is the so called energy balance of Darcy-Weisbach. Given all the friction coefficients for the top-lid and the wall are known as well as the velocity over the width of the flume, it is possible to determine the friction coefficient of the bed surface and thus the bed shear stress. However, it is complicated to obtain the vertical average-velocity along the wall as the flow velocities at the top and the bottom of the wall were not equal. This method can

be useful once proper measure is applied to determine the average-velocity near the wall. At this moment, this method is not considered any further.

Concerning the vertical flow pattern, the simulated flow velocity is determined from Figure 5.1 (b), (d), (f), and (h). The figures indicate that the arrows are almost horizontal in the measuring position of the EMS. This means that the simulated vertical flow velocities in the measuring position are very small (almost zero). During the test, the vertical flow velocity was measured by the EMS (see section 4.1). The measured velocities are approximately within the range of -0.01 – 0.005 m/s for all three samples. In this respect, it is concluded that the computed and measured flow velocities are in the same range.

In conclusion, despite a difference between the tangential flow velocity from the model and the measurements by the EMS, the bed shear stresses for both velocities are within the same range considering the contribution of the rougher bed surface as discussed above. It is then concluded that the model output is acceptable and that the calculation of the bed shear stress by the model is valid.

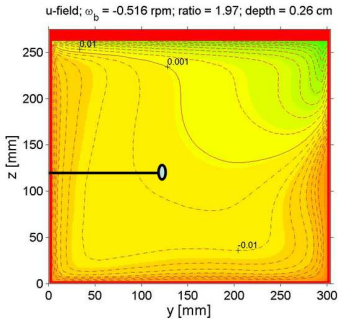

(a) Tangential flow velocity step 2

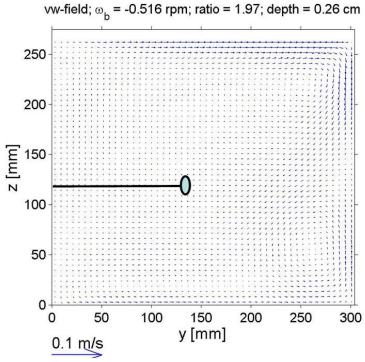

(b) Secondary flow velocity step 2

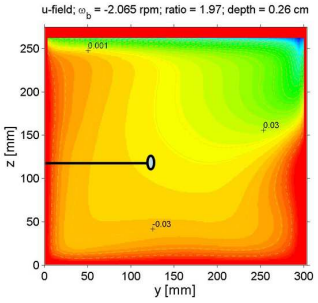

(c) Tangential flow velocity step 5

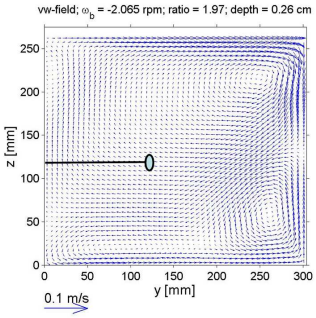

(d) Secondary flow velocity step 5

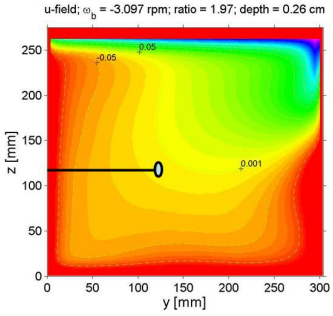

(e) Tangential flow velocity step 7

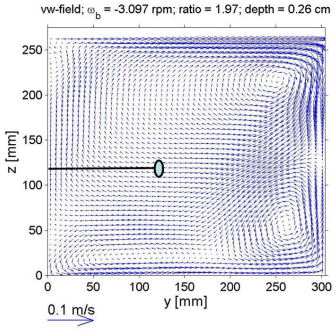

(f) Secondary flow velocity step 7

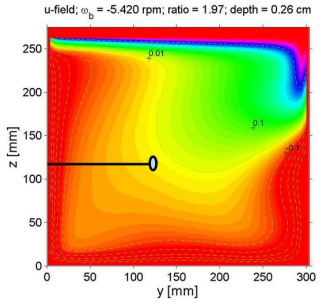

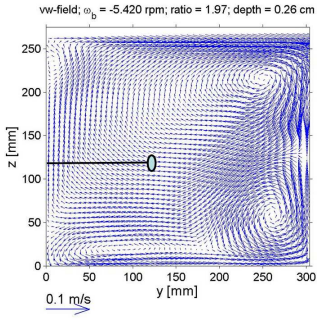

(g) Tangential flow velocity step 13 (h) Secondary flow velocity step 13

Figure 5.1: Typical results of LES simulation both for the tangential flow (a), (c), (e), and (g) and the secondary flow in a cross-section of the flume (b), (d), (f), and (h) with the outer bend at right. The numbers in those left figures indicate flow velocities [m/s]. In all figures the position of the EMS is indicated.

Sample	Rotational step	Computed Flow velocity u_{av}-$2\pi R\omega_b$ [m/s]	Measured flow velocity EMS [m/s]	Difference [%]
Muddy sample	2	0.095	0.076	+20
	5	0.401	0.296	+26
	7	0.590	0.454	+23
	13	1.050	0.816	+22
Intermediate sample	2	0.097	0.071	+27
	5	0.390	0.304	+22
	7	0.590	0.468	+21
	13	1.050	0.805	+23
Sandy sample	2	0.096	0.072	+25
	5	0.385	0.309	+20
	7	0.585	0.478	+18
	13	1.025	0.836	+18

Table 5.1: Comparison between the simulated flow velocities and the velocities measured by the EMS. For each sample, the velocities of 4 of the 13 rotational steps are compared. In the last column the difference between both considered velocities is shown.

Sample	Rotational step	Calculated τ_b LES model [Pa]	τ_b based on rougher bed [Pa]
Muddy sample	2	0.03	0.02
	5	0.27	0.25
	7	0.57	0.60
	13	1.59	1.93
Intermediate sample	2	0.03	0.01
	5	0.27	0.25
	7	0.57	0.59
	13	1.6	1.74
Sandy sample	2	0.03	0.01
	5	0.27	0.22
	7	0.57	0.53
	13	1.59	1.63

Table 5.2: Comparison between the calculated bed shear stress following the simulated flow and the bed shear stress based on the roughness of the bed surface. The results show that both bed shear stresses are within the same range for all three samples.

5.2 Erosion of fines

For all three tests the concentration is increasing in time in a similar way. At the beginning of each rotational step the concentration increases rapidly and almost linear in time. After this, the concentration tends to equilibrium. This is especially observed for the lower bed shear stresses. For larger bed shear stresses, the duration of the steps is apparently not sufficient to reach this equilibrium. These typical profiles are further discussed in section 5.5. Here it is discussed how the Oslim data are related to some calibration data. Next, the vertical concentration profiles as well as the accompanying mean concentrations are considered. With the derivative of the mean concentration as function of time (and the erosion surface) the erosion rate can be determined. In addition, using the maximum concentration, it is possible to derive the total mass of eroded fines.

For the muddy and intermediate samples (see Figure 4.8 and Figure 4.14), the measurements of the 0-30 g/L Oslims and the sampling concentration show a fair agreement for most rotational steps, except the step 4 – 7. The difference between concentrations within these steps appears considerable. For the measurements of the 0-2 g/L Oslims are larger than the sampling data. The difference between concentrations is possibly subject to the sensitivity of the method determining the sampling concentration. This explanation is, however, not clearly identified. The utilization of the measurements of the 0-2 g/L Oslims should be carefully made. Compared to the muddy and intermediate samples, the Oslim data of the sandy sample (see Figure 4.19) show different behavior. For both the 0-30 g/L Oslims as the 0-2 g/L Oslims the measured data are lower than the sampling concentrations. Probably this is due to the relatively large concentration of sand in the water samples extracted from the flume (sheet flow regime). As the Oslims were calibrated before the tests for the fines only, a mismatch is expected between the measured data (Oslim) and sampling data (by the water samples taken during the tests).

The sampling concentration is based on the weight of particles. This implies that the measurement is related to the volume of particles ($M = \rho v = \rho 4/3\pi r^3$). This means that the measurement with larger particles like sand can lead to a larger concentration compared with fine particles. This explains the large sampling concentration for the sandy sample as some sand particles were extracted into the water samples. The same effect of the sand particle does not occur with the Oslim concentration. In fact, large particle like sand can influence negatively on the measurement of the Oslim as, in principle, difficulty can be expected in the transmission of light by suspended particles. From the two abovementioned explanations, it is concluded that the difference between the sampling and the measured concentration is logical. Thus, the concentration as measured by the Oslims can be accepted. To determine the total concentration profile as function of time for the whole test, a combination of the measurements of both the 0-2 g/L Oslims and the 0-30 g/L Oslims is made; for lower concentrations the measurements of the 0-2 g/L Oslims are utilized, whilst for higher concentration the concentrations are taken from the 0-30 g/L Oslims.

To determine the total amount of eroded fines (M_{fines}) the total average concentration has to be multiplied by the volume of water in the flume. When the concentration is uniform over the vertical, the mean concentration as measured by the

Oslims can be used. However, in case of a non-uniform vertical concentration profile, a different approach is required to determine the mean concentration. Here it is discussed if a vertical concentration profile exists and how the average concentration can be determined.

As the Oslims are located in different vertical positions, it is possible to determine the differences between these measured concentrations. In this way a vertical profile of the concentration can be derived. The vertical positions of the different Oslims above the bed are indicated in Figure 5.2, Figure 5.3 and Figure 5.4 show the differences between Oslims 1 and 3, 2 and 3, 1 and 2 and 4 and 6. In the figures at right these differences are averaged over 500 s and plotted together. In this way the results can be compared. A positive difference means that the concentration measured by the lower Oslim has a larger concentration than the higher located Oslim. For a negative difference the higher Oslim has a larger concentration.

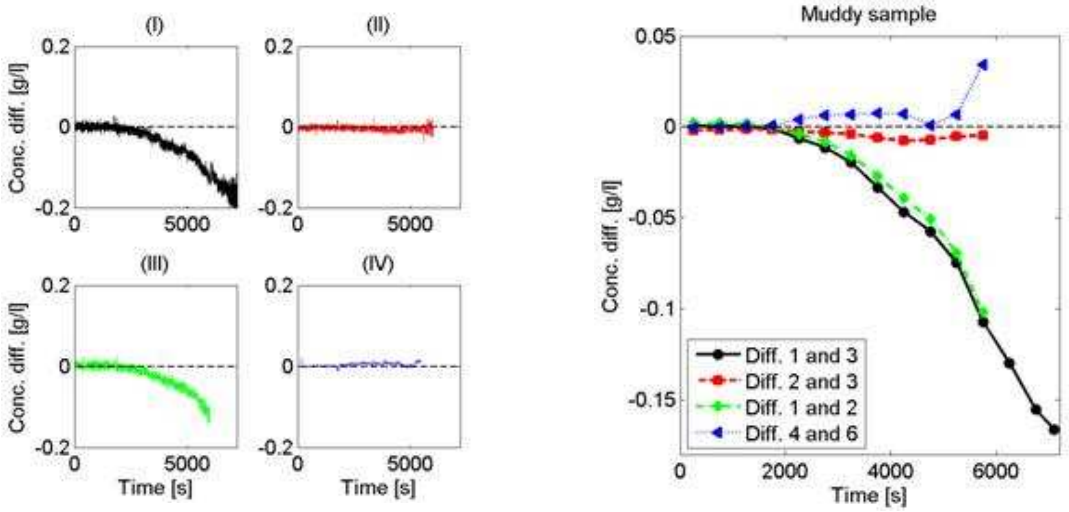

(a) (b)

Figure 5.2: Differences in concentration between differently located Oslims (see for their vertical positions (Figure 3.15) for the muddy sample. In (a) the differences between Oslims 1 and 3 (I), 2 and 3 (II), 1 and 2 (III) and 4 and 6 (IV) are shown. These differences are averaged over 500 s and plotted together in (b).

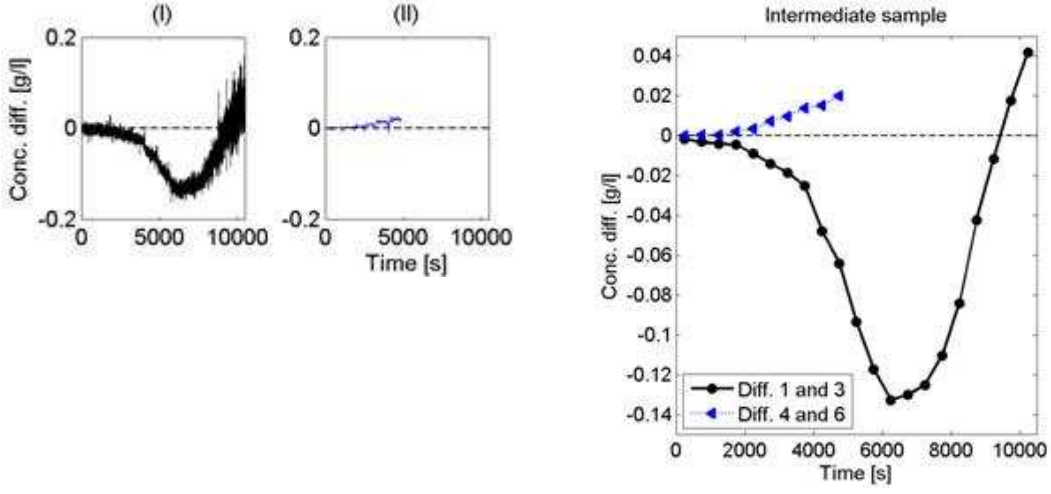

(a) (b)

Figure 5.3: Differences in concentration data between differently located Oslims (see for their vertical positions (Figure 3.15) for the intermediate sample. In (a) the differences between Oslims 1 and 3 (I), 4 and 6 (II) are shown. These differences are averaged over 500 s and plotted together in (b).

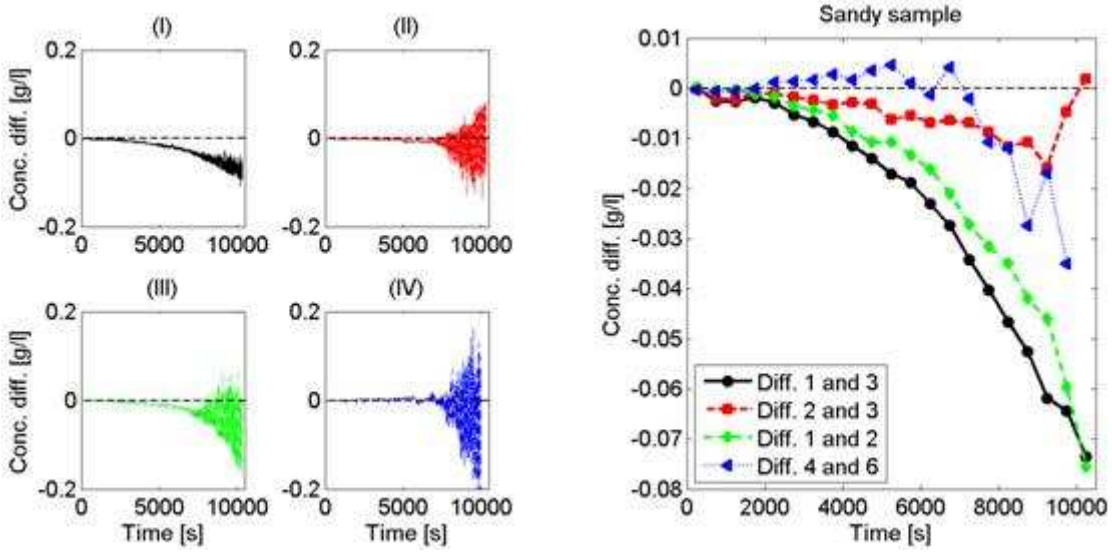

(a) (b)

Figure 5.4: Differences in concentration data between differently located Oslims (see for their different vertical positions Figure 3.15) for the sandy sample. In (a) the differences between Oslims 1 and 3 (I), 2 and 3 (II), 1 and 2 (III) and 4 and 6 (IV) are shown. These differences are averaged over 500 s and plotted together in (b)

For the muddy sample the difference between the measured concentration for Oslim 2 and 3 and 4 and 6 is small. The difference between Oslim 1- 3 is more or less equal to the difference between 1 and 2. In both cases the maximum difference is around 0.15 g/L, which is around 3% of the maximum measured concentration. However, it occurs that the concentration difference is negative, which indicates a larger concentration for the higher Oslim.

For the intermediate sample the data of Oslim 2 is not considered, as its values are lower than those of Oslim 1 and 3. This is in contradiction with the other two tests, where the data of Oslim 2, as expected, nicely fit in between the data of Oslim 1 and 3. This is probably due to the experimental set-up, as sometimes material accumulated in the tube through which water is pumped towards the Oslim. The difference between Oslim 4 and 6 is again small. The maximum difference between Oslim 1 and 3 for this test is again around 0.15 g/L. This comes down to approximately 1% of the maximum measured concentration. Furthermore, it occurs that for a concentration of 5 g/L and higher, the difference between Oslim 1 and 3 decreases and becomes positive.

For the sandy sample more or less similar differences are found as for the first two tests. Again small differences between Oslims 2 and 3 and 4 and 6 are found. The differences between 1 and 3 and 1 and 2 are larger, but the maximum difference is still only 4% of the maximum concentration. The only difference between this test and the other two is that more noise is occurring on the concentration as function of time (see Figure 4.19), which also occurs for the differences between the output of the Oslims

(Figure 5.4). Probably this is the effect of the relatively large concentration of sand during this test (sheet flow regime). The relatively large sand grains might cause oscillations in the measurement of the concentration as determined by the Oslim.

Considering the small differences between the concentrations as measured by the different Oslims, it is concluded that no vertical concentration profile can be identified. In fact it is possible that those small differences of the concentrations are due to the error during the calibration process of the Oslims. For the flow in a straight flume a vertical concentration profile is expected to occur. However, in case of an annular flume the occurring secondary currents are considerable. The occurring 3D turbulent flow pattern mixes the water column and eliminates the presence of a vertical concentration profile.

Additionally, Figure 5.5 (a) and (b) indicate that due to the two dominant secondary flows (the upper and bottom cells) the converging of concentrations was occurring near the measuring position of the highest Oslim. This might explain the negative differences as found. However, the differences between 1 and 3 at the one hand and 4 and 6 at the other hand are not the same. This is strange, as they are positioned at the same heights so identical concentrations are expected. This supports the statement that the differences can probably be subscribed to errors made during the calibration of the Oslims.

As no vertical concentration profile is identified, the mean concentration in time is determined by averaging the data of Oslims 4 and 6 for the concentrations between 0 and 2 g/L. For the larger concentrations the average of Oslims 1, 2 and 3 is applied. Only for the intermediate sample the data of the middle Oslim (2) is not considered for reasons as discussed.

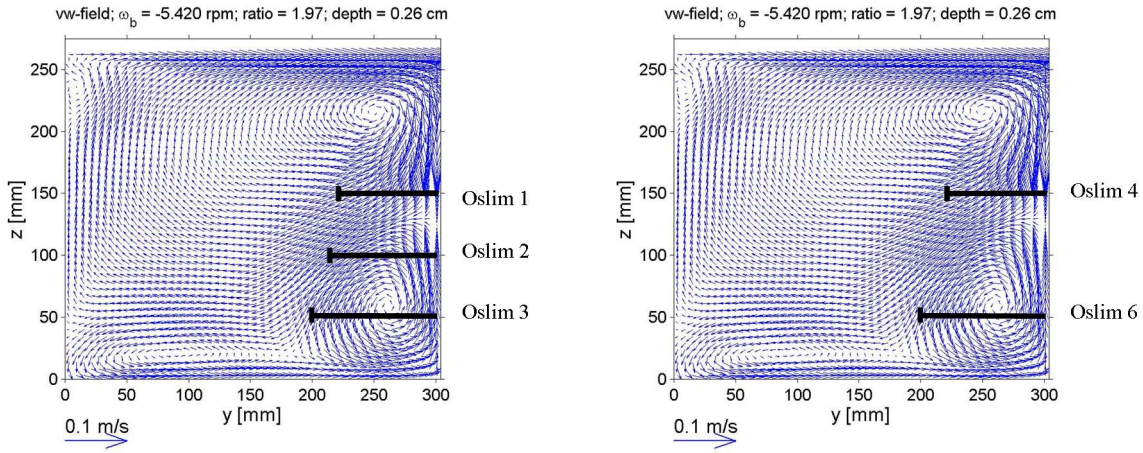

(a) (b)

Figure 5.5: Typical LES flow patterns in cross section of the annular flume with the outer bend at right. The three locations of the Oslims are indicated by the thick lines at the outer bend.

5.3 Erosion of sand

For all three tests some movement of sand was observed from rotational step 5 (τ_b = 0.3 Pa), as eroded sand was rolling and jumping along the surface of the sediment bed. The occurrence of this bed transport is checked with Shield's theorem of the initial motion of grains (see Figure 5.7). Shields' parameter is calculated for the bed shear stress as determined by the LES model (~ 0.3 Pa) and a median grain size (d_{50}) of 125 μm. this comes down to a value of approximately 0.15. This value is between 0.03 and 0.8, which indicates that bed transport is expected to occur.

During rotational step 7 (τ_b = 0.6 Pa), it was observed that eroded sand started to accumulate on the bed surface along the outer bend of the flume. This accumulation of sand was occurring in a similar way for the tests on the intermediate and sandy sample. This is explained by an influence of the secondary flow within the flume. The conceptual illustration in Figure 5.6 (a) shows the movement of eroded sand toward the outer bed. To explain how the secondary flow influences the movement of the sand, the secondary flow directions are shown in Figure 5.6 (b)). The arrow for the secondary flow along the bed indicates that sand can be transported towards the outer bend.

Around three minutes from the beginning of rotational step 7 ripples were developing in the layer of accumulated sand. For this rotational step (~ 0.7 Pa) the Shields' parameter is approximately 0.36. This value is relatively low, considering the value as found by Shields for the occurrence of the bed forms. The average height of the ripples was around 0.5 cm and the average length around 7.5 cm for both the test on the intermediate and sandy samples.

From rotational step 8 (τ_b = 0.95 Pa) onward, the ripples were washed out and the bed became plane again. Eroded sand was transported in a thin layer above the bed with a high concentration of sand. This indicates the sheet flow regime for the transport of sand. It was, therefore, concluded that rotational step 8 forms the transition of sand being transported in the bed load regime and in the sheet flow regime. For the calculated bed shear stress (~0.95 Pa), the Shields'parameter is approximately 0.48. This is still lower than the threshold for a sheet flow regime (θ > 0.8 by Dohmen-Janssen, 1999). The possible explanation for the difference between the Shields' parameters is that the actual bed shear stress as occurred might locally be higher, especially along the bed surface near the outer bend. It should be noted as well that the bed shear stress as determined by the LES is derived based on a smooth bed surface. With the larger roughness of the bed surface due to the bed forms compared with the smooth bed surface, it is logical to assume that apart from the normal shear force, a drag force also played a role for causing sand to move. For this reason, the bed shear stresses were enhanced with the normal stresses due to the drag force. As a result, Shield's parameters were larger than the parameters calculated based on the smooth bed surface. Another measure which confirms the occurrence of the sheet flow regime is a sediment concentration. At rotational step 8, Figure 5.12 indicates that 0.25 kg of fines and 1.70 kg of sand were being eroded. This means that 13% of sediments (by weight) were transported in the suspension layer and 87% in the sheet flow layer. This result agrees well with a criterion for the distinction between modes of erosion proposed by Dohmen-Janssen (1999).

Figure 4.19 indicates that from around t = 8000 s more noise was occurring in the profiles of the Oslim output. This can possibly be explained by the relatively large amounts of sand that were brought into suspension as a result of the sheet flow regime. The occurrence of the smallest sand particles in the inlet tubes for the Oslim could have caused noise in the output signal.

After the test, the accumulated sand on the bed surface along the outer wall was collected and, subsequently, oven-dried for 24 hours at $105^{\circ}C$ to determine the total mass of eroded sand. This mass is important as its value is used to compare with the estimated mass of eroded sand following from the mass balance. The masses of accumulated sand are approximately 21.26 kg and 13.49 kg for the intermediate and sandy sample, respectively. For the muddy sample no sand was collected because the accumulation of sand was very little. Therefore, it was impossible to accurately collect those eroded sand from the bed.

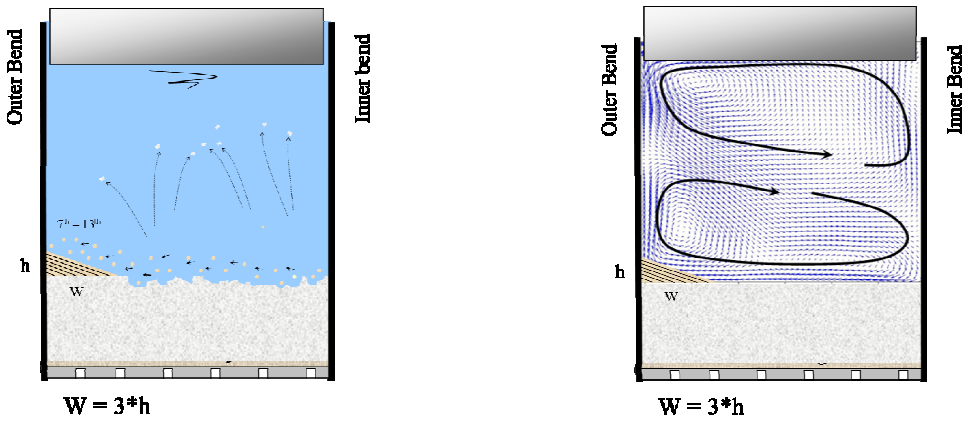

Figure 5.6: Schematic illustration of the cross section of the flume showing the sand accumulation on the bed surface along the outer bend (a). This accumulation of sand was a result of tangential bed transport in combination with the secondary flow. The arrows in (b) indicate that the secondary flow along the bed is directed towards the outer bend.

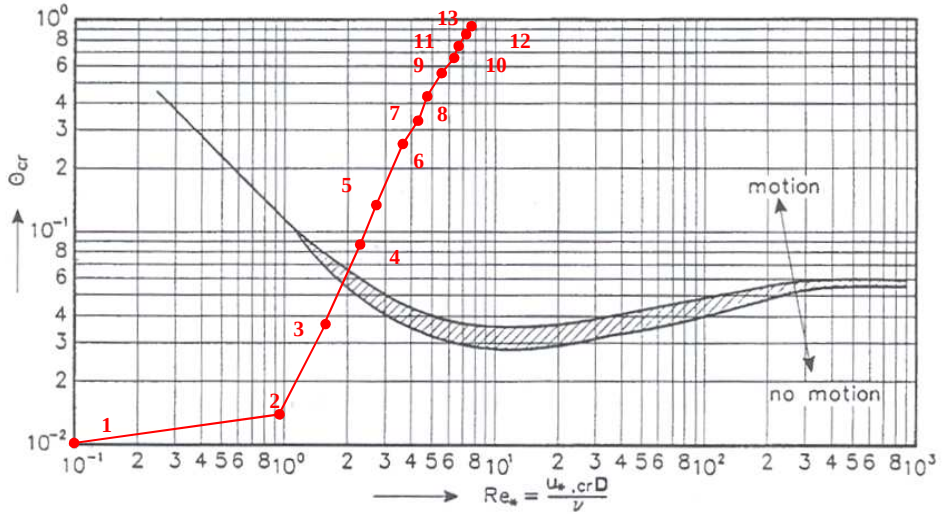

Figure 5.7: Shield's diagram illustrates that at rotational step 4 the shields parameter locates beyond the initiation of motion of the sand. This implies that sand particles started to move from this step onward.

5.4 Mass balance

In order to determine the erosion rates of both fines and sand, it is necessary to indicate the amount of eroded sand as function of time. However, for the annular flume as applied in this study there is no direct measurement to determine the mass of eroded sand during the tests. For this reason, a mass balance is applied. With this method, the mass of eroded sand can be determined using the concentration of eroded fines as function of time. To apply the mass balance concept, first the mass of eroded fines as function of time is determined by multiplying the volume of water in the flume by the mean concentration of eroded fines. This mass of eroded fines enables us to determine the mean erosion depth of the sediment bed. To do this, it is necessary to know the density of the sediment bed. For this reason, the assumption is made that the water content of the sediment bed during the test is an average of the water content over the erosion depth before and after the test. It is found (see Table 5.3 and Figure 5.9) that the erosion depth is less than 1 cm. Therefore, the average water content over the upper 1 cm of the bed during the test is used, which is 39.9%, 22.8% and 27.3% for the muddy, intermediate and sandy sample, respectively. This water content is applied to determine the dry density of the sediment bed. Considering the mass of eroded fines in a combination with the dry density of the sediment bed and the contents of fines and sand (see Table 3.1), the erosion depth is determined. Next, it is assumed that the sand within this layer is eroded simultaneously with the fines. In this way it is possible to determine the mass of eroded sand as function of time.

To verify the concept of the mass balance as described above, the mass of eroded sand following from the mass balance is compared with the mass of accumulated sand along the outer bend. The results of this comparison are presented in Table 5.3 as well as plotted in Figure 5.8. Table 5.3 shows that the mass balance overestimates the mass of eroded sand with around 25% compared to the mass as collected after the test. This difference can be explained as not all the eroded sand was transported towards the outer bend. Some sand is probably located on top of the sediment bed as it was transported along the bed in the tangential flow direction. Another reason is related to the occurrence of the sheet flow regime. Small fraction of sand was brought into suspension and afterward settled down uniformly over the bed. As the sand was collected merely from the area along the outer bend (the accumulated sand layer), sand over the remainder of the bed was excluded. As a result, the mass of eroded sand as collected appeared underestimating.

In conclusion, the difference between the mass of eroded sand as collected and the calculated mass from a mass balance can be explained qualitatively. Thus, it is assumed that the mass of eroded sand as function of time can be determined by considering the mass balance.

	Muddy sample	Intermediate sample	Sandy sample
Water content upper 1 cm of bed [%]	39.9	22.8	27.3
Mass of eroded fines [kg]	4.42	12.29	1.97
Erosion depth [mm]	1.2	7.2	3.7
Mass of eroded sand (from bed) [kg]	-	21.26	13.49
Mass of eroded sand (from mass balance) [kg]	1.11	28.67	17.70

Table 5.3: Erosion depth as determined following the mass balance. Water content and mass of eroded fines are required for its determination. The mass of eroded sand as collected and the calculated mass following the mass balance are also shown.

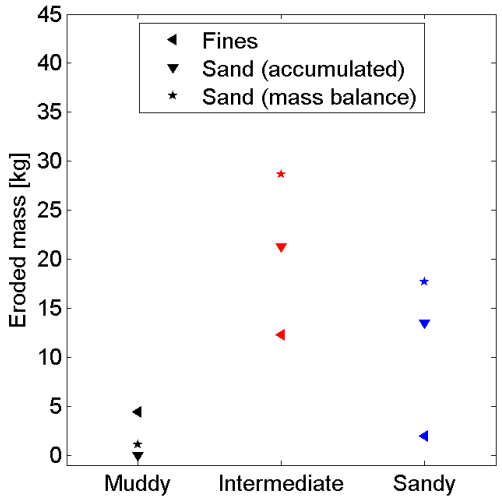

Figure 5.8: Masses of eroded fines and sand for the three different samples. Mass of eroded sand is also determined using the mass of eroded fines.

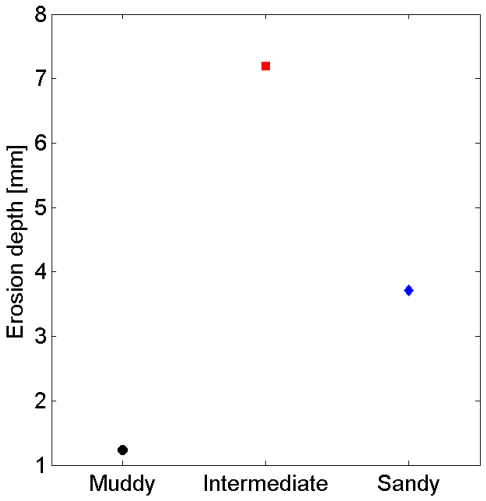

Figure 5.9: Erosion depths for the three different samples as determined by the mass balance.

As the eroded sand was accumulating on the bed surface along the outer bend, the total surface area of erosion was decreasing in time. To determine the erosion rate, this decrease of the surface area in time is required. By applying the mass balance approach the mass of eroded sand as function of time can be determined. In Table 5.3 it is found that the amount of accumulated sand is around 25% smaller than the mass based on the mass balance. Therefore, the amount of sand as accumulated along the outer wall can be determined as function of time by subtracting 25.5% (intermediate sample) and 23.8% (sandy sample) of the mass of eroded sand in time following the mass balance approach. For the muddy sample the average percentage of the two other tests (25%) is used to determine the amount of accumulated sand as function of time. The result is plotted for all three samples (see Figure 5.10, Figure 5.11 and Figure 5.12).

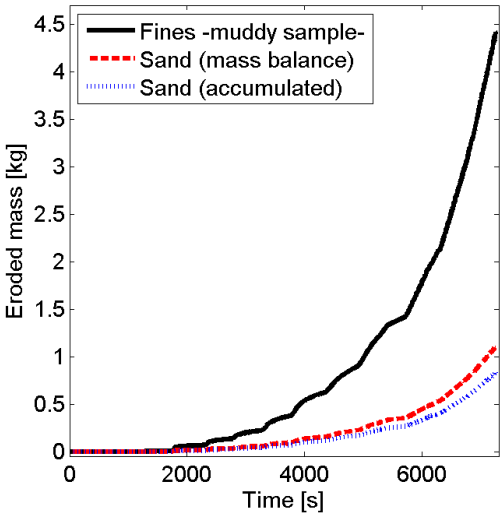

Figure 5.10: Mass of eroded fines, mass of eroded sand derived from the mass balance and mass of eroded accumulated sand as function of time for the muddy sample.

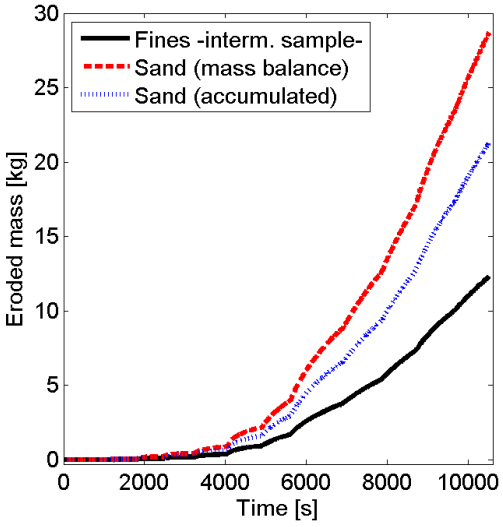

Figure 5.11: Mass of eroded fines, mass of eroded sand derived from the mass balance and mass of eroded accumulated sand as function of time for the intermediate sample.

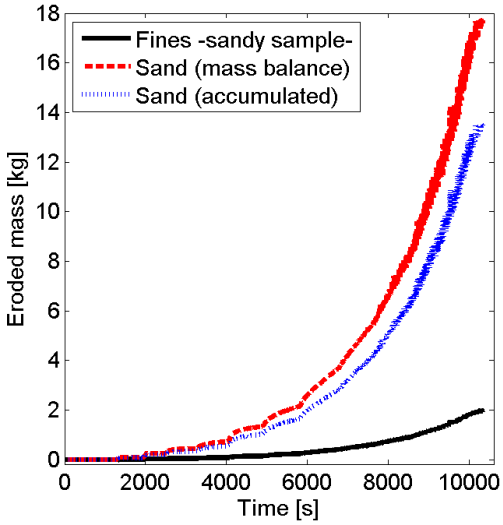

Figure 5.12: Mass of eroded fines, mass of eroded sand derived from the mass balance and mass of eroded accumulated sand as function of time for the sandy sample.

With this amount of accumulated eroded sand as function of time, it is possible to determine the decrease of the surface area for erosion in time. To verify this calculation, the results are compared with the final geometry, i.e. width and height of the accumulated sand as observed after the test. It is assumed that the porosity of the sand along the outer bend is around 45% (based on the porosity of a loosely packed sandy bed, see e.g. the min-max porosity plot in Figure 3.2). The volume of accumulated sand is defined as a function of the mass of eroded accumulated sand and the dry density:

$$V_{sand} = \frac{M}{\rho_{dry}} \tag{5.1}$$

where V_{sand} [m3] is the volume of accumulated sand, M [kg] the mass of accumulated sand and ρ_{dry} [kg/m3] the dry density of sand. Figure 5.13 illustrates the observed geometry of the accumulated sand. Using this geometry, the width of the accumulated sand is calculated. The results are shown in Table 5.4. It appears that the calculated widths and heights of the accumulated sand following the mass balance approach correspond to the observed geometry of the accumulated sand. This again confirms the applicability of the mass balance approach.

In conclusion, the width of accumulated sand in time can be determined as function of time using the mass balance approach. This means that also the decrease of the surface area in time can be calculated:

$$Area(t) = Area_{total} - (\pi R^2 - \pi(R - w(t))^2) \tag{5.2}$$

where $Area(t)$ [m^2] is the surface area as function of time, $Area_{total}$ [m^2] the total surface area of the bed surface, $w(t)$ [m] the width of the accumulated sand as function of time and R [m] the outer radius of the flume. Using equation (5.1) and (5.2) in combination with the observed geometry of the accumulated sand (see Figure 5.13), the decrease of the surface area as function of time can be determined for all three samples. The results are shown in Figure 5.14.

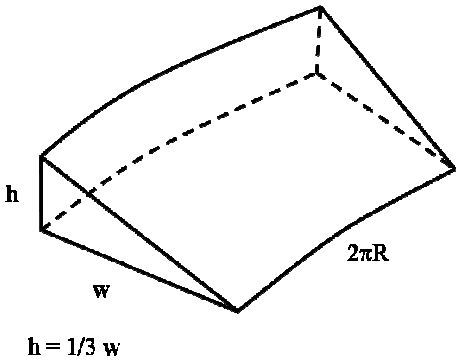

Figure 5.13: Schematic illustration of the eroded accumulated sand along the outer bend of the flume. The proportion between the height (h) and the width (w) is indicated.

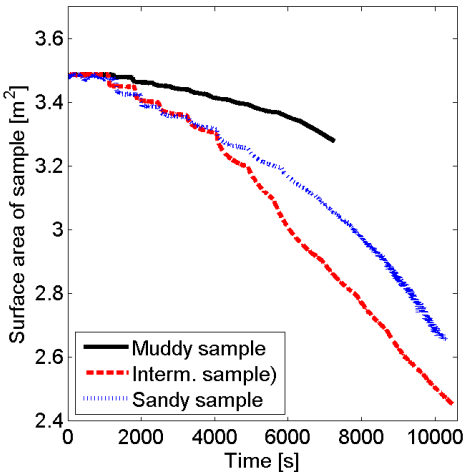

Figure 5.14: Surface area of the sediment sample as function of time for the three samples, assuming w = 3h, in the shape of Figure 5.15.

	Muddy	Intermediate	Sandy
Width of accumulated sand [cm]	1.7	8.4	6.7
Height of accumulated sand [cm]	0.6	2.8	2.2
Minimum surface area for erosion [m^2]	3.28	2.45	2.66

Table 5.4: Results for the width and height of the accumulated sand as determined by the mass balance approach. The minimum surface area is also given.

5.5 Erosion rates

Using the mass of eroded sand and fines as function of time, together with the erosion surface in time, erosion rates for all three samples are determined. The erosion rate is an important parameter to describe erosion behavior. By plotting the erosion rate as function of the bed shear stress it is possible to determine the erosion parameter (M_E) and the erosion threshold (τ_e).

First, the total eroded mass is determined by combining the mass of eroded sand and fines, both as function of time. Next, the derivative of the total eroded mass in time is determined. An example is shown in Figure 5.16. Combining this derivative with the surface area of the sediment bed, the erosion rate can be determined. However, as can be seen in the concentration profile as function of time for all three samples (Figure 4.8, Figure 4.14 and Figure 4.19), the concentration does not increase linearly for each rotational step. This explains why the derivative of the total eroded mass in time is large in the beginning of a rotational step, and decreases towards zero. Only for low concentrations equilibrium is reached, resulting in a zero derivative.

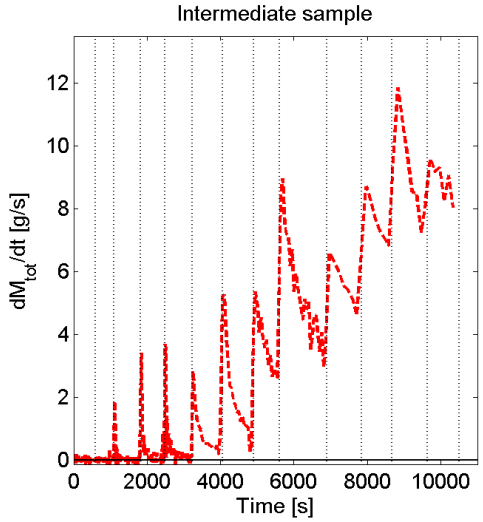

Figure 5.16: Derivative of the total eroded mass in time

To determine the derivative of the total eroded mass in time dM/dt should be independent of the duration of a rotational step. However, Figure 5.17 indicates that dM/dt varies for the different durations of a rotation step (*dt*). To solve this problem, dM/dt is determined over certain duration. The local rate of change of the averaged concentration is used to calculate the erosion rate. Results depend on the duration over which the original signal is averaged. For this reason, an optimum duration of a rotational step (*dt*) is required. By choosing too large *dt*, the initial increase of the concentration is averaged out. The duration of the initial increase depends on the concentration (see Figure 5.19 (b)). By taking $dt \leq 0.1T$, it is assumed that the sudden increase of concentration is well represented. On the other hand, by choosing too small *dt*, oscillations in the data output result in too large and/or negative derivatives, see example in Figure 5.19 (d). Therefore, the time-scale of these oscillations is the lower limit of *dt*.

During the tests for all three samples, T and the scale of the oscillation vary for different rotational steps. Therefore, three different dt are used to determined dM/dt as follows: 15 s, 50 s and 125 s for rotational step 1 – 5, 6 – 9 and 10 – 13, respectively.

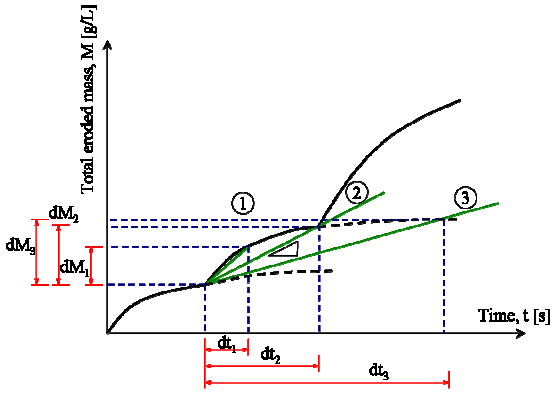

Figure 5.17: Schematic depiction of the total eroded mass in time. The duration for each rotational step was not long enough for the profile to reach equilibrium.

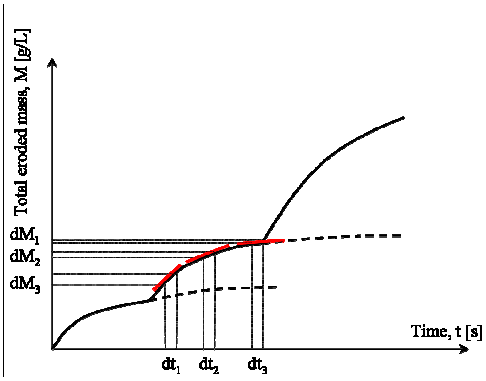

Figure 5.18. Schematic depiction of the total eroded mass in time. In order to represent the derivative correctly as it is determined locally.

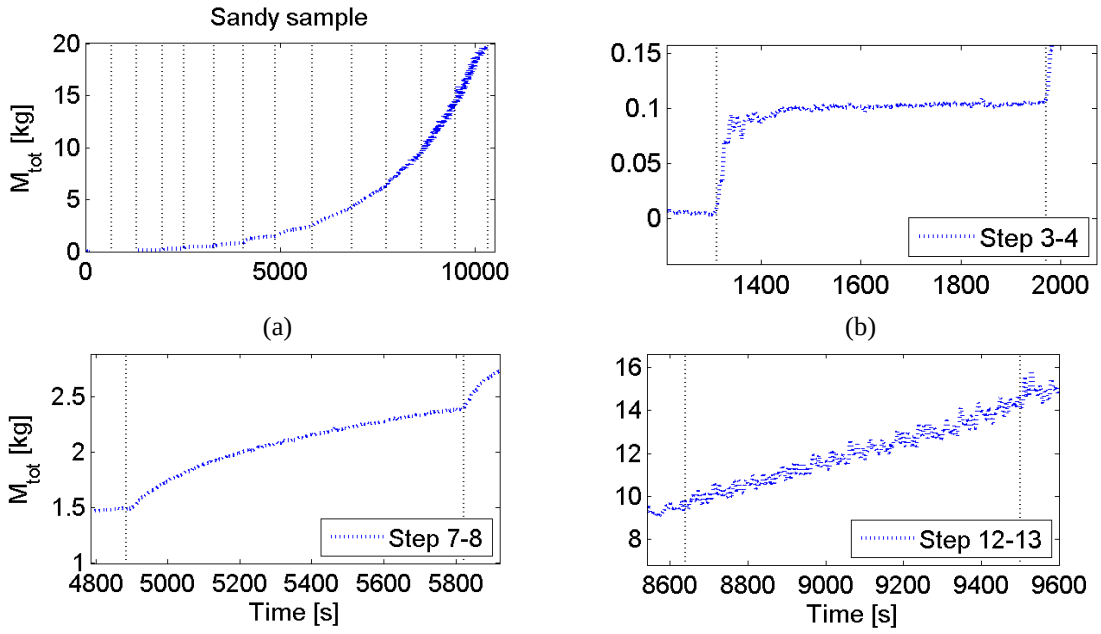

Figure 5.19: Result of the total eroded mass as function of time: the profile for the whole test (a), the sudden increase of the eroded mass in the enlarged profile for step 3 – 4 (b), the longer duration of the initial increase in the enlarged profile for step 7 – 8 (c) and the oscillation in the enlarged profile for step 12 – 13 (d).

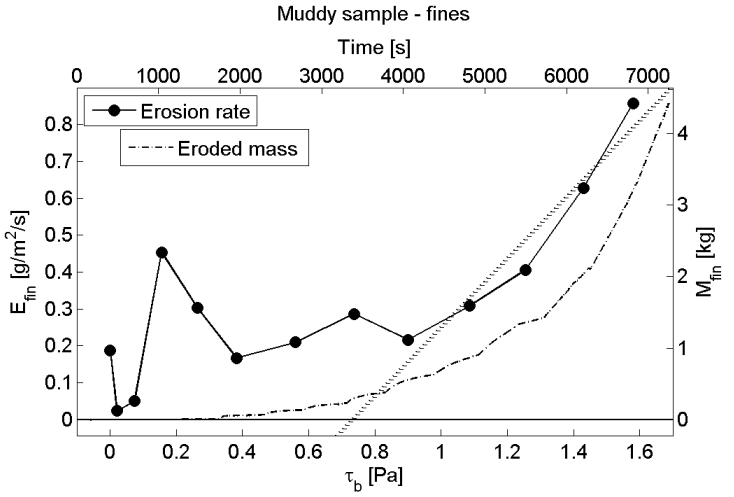
Muddy sample - fines
Time [s]
Erosion rate
Eroded mass
E_{fin} [g/m^2/s]
M_{fin} [kg]
τ_b [Pa]

(a)

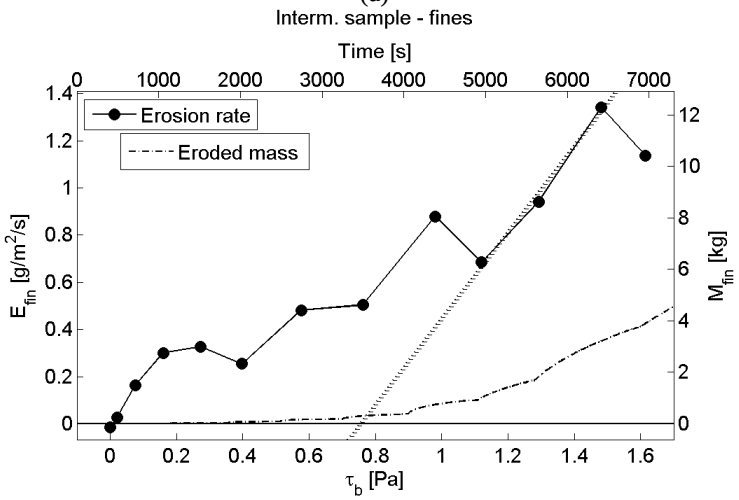
Interm. sample - fines
Time [s]
Erosion rate
Eroded mass
E_{fin} [g/m^2/s]
M_{fin} [kg]
τ_b [Pa]

(b)

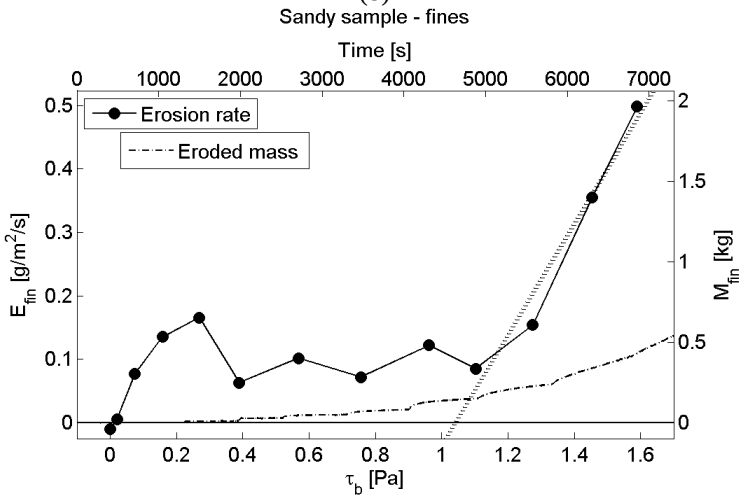
Sandy sample - fines
Time [s]
Erosion rate
Eroded mass
E_{fin} [g/m^2/s]
M_{fin} [kg]
τ_b [Pa]

(c)

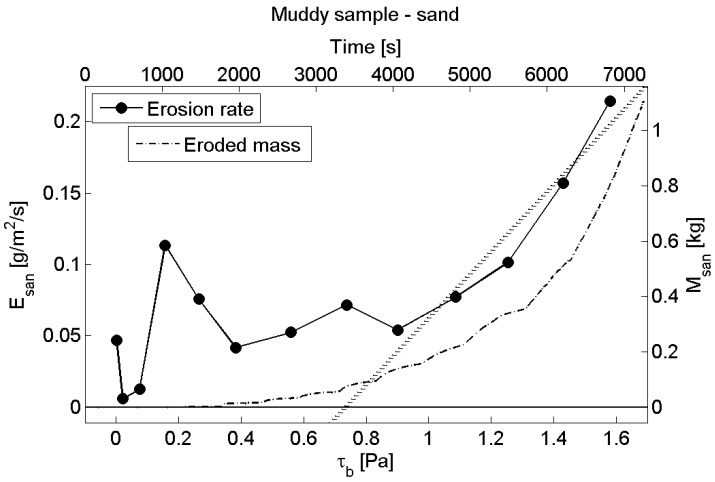

(d)

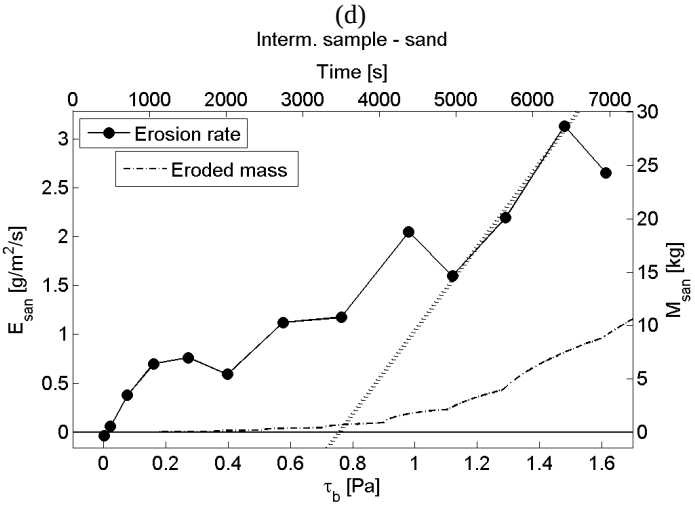

(e)

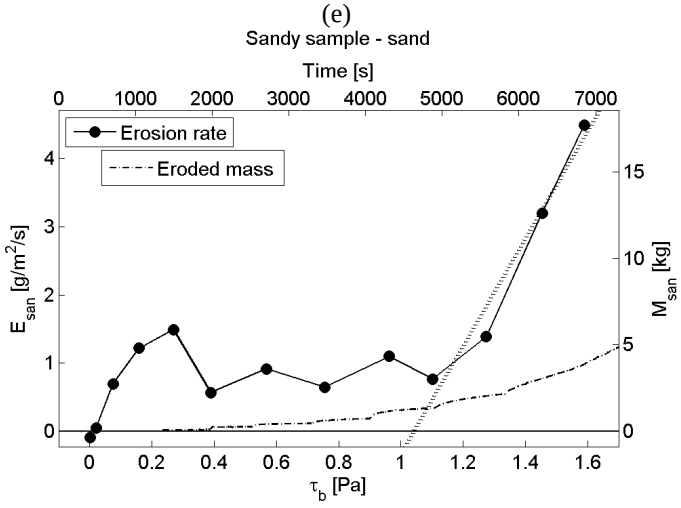

(f)

Figure 5.20: Erosion rates of fines (a, b and c) and sand (d, e, and f) as function of the bed shear stress. Also the mass of eroded fines and sand as function of time is shown. The fit lines of the erosion rates are extrapolated to the *x*-axis to indicate the erosion threshold.

Figure 5.20 shows erosion rates as function of the applied bed shear stress. It appears that for low τ_b relatively large erosion rates occur, which are indicated by the peaks in the erosion rate profiles. Despite those large erosion rates, the eroded masses are still small for those τ_b. This means that erosion did not really start.

For the tests with the intermediate and sandy sample three peaks occur before erosion really starts. For the muddy sample only two peaks are identified. It appears that the first peak occurs in all three cases for $\tau_b \approx 0.3$ Pa. As discussed before, the fines that were brought into suspension after removing the plastic foil were re-suspended for $\tau_b \approx 0.3$ Pa. This explains the occurrence of this erosion rate peak. Hence, bed erosion did not really start. The second peak occurs for $\tau_b \approx 0.6$ Pa. This corresponds with the bed shear stress at which ripples occurred on the accumulated sand. Also this peak seems to occur for constant τ_b, independent of the applied bed compositions. The final peak ($\tau_b \approx 0.9$) is related to the transition from bed load regime to sheet flow regime. For the muddy sample the second peak is found for $\tau_b \approx 0.7$ Pa.

From the erosion rates the erosion threshold (τ_e [Pa]) and erosion parameters (M [kg/(s·m^2·Pa)]) based on equation (2.17) are determined. The threshold is the intersection of the extrapolated fit line with the x-axis. The erosion parameter is the slope of the fit line. Figure 5.21 shows the erosion threshold (a,b), the erosion parameter for the fines (c,d) and for sand (e,f) as function of the plasticity index (a,c,e) and the relative water content (b,d,f).

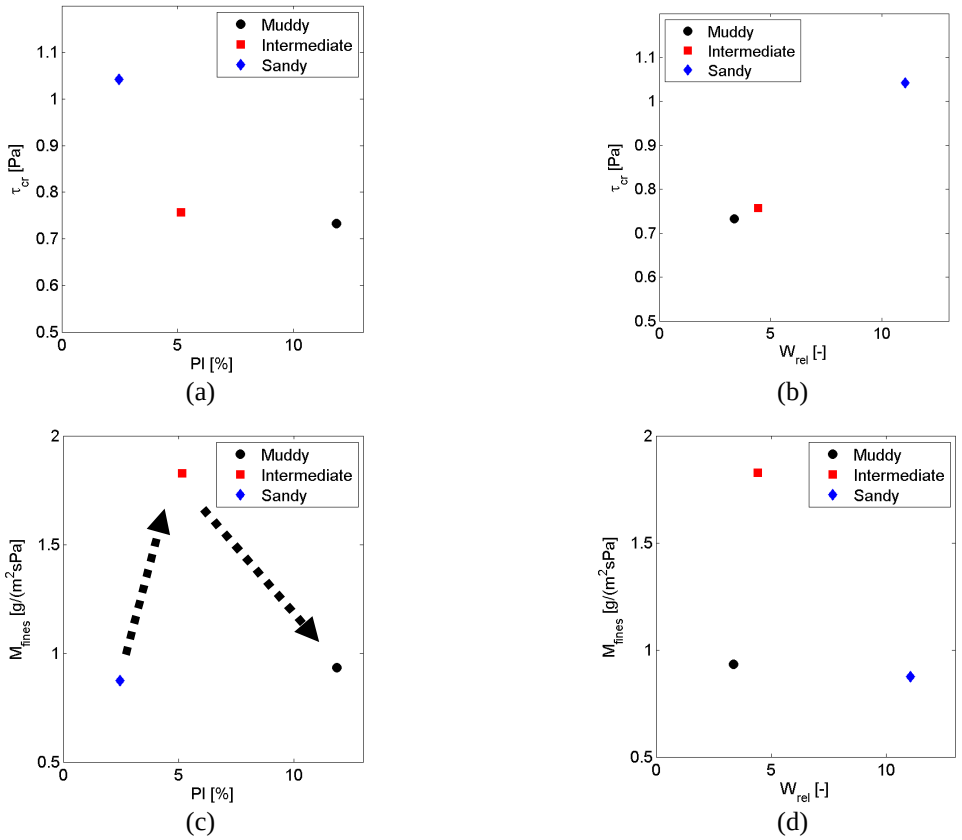

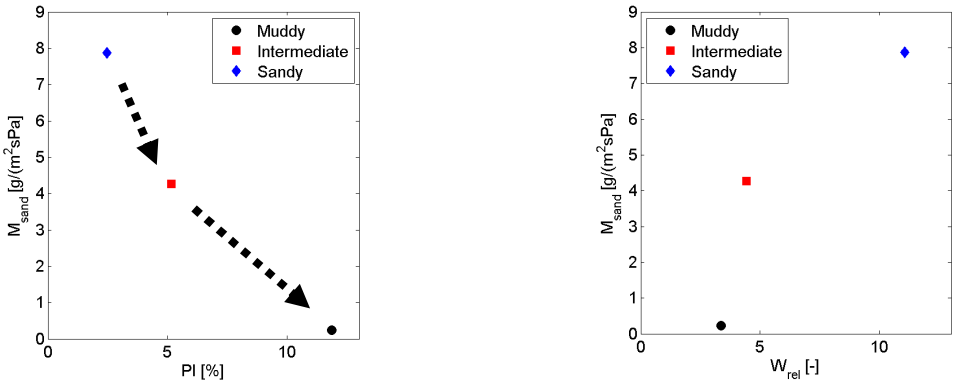

(e) (f)

Figure 5.21: Erosion threshold (a,b), the erosion parameter for fines (c,d) and sand (e,f) as function of the plasticity index (a,c,e) and the relative water content (b,d,f).

Figure 5.21 (a) and (b) show that the erosion threshold of the sandy sample is larger than the threshold of the intermediate and muddy sample. This means that the sandy sample has largest erosion resistance. Considering Figure 3.2, the locations of all three samples indicate that both the sandy and intermediate samples are dominated by a sand-silt sediment skeleton. Considering that the intermediate sample locates closer to the maximum porosity line in combination with its larger plasticity index, it implies that more clay fractions are located between the sediment particles of the intermediate sample. With a sand-silt skeleton dominating, the addition of the clay content results in the reduction of the bed shear strength (Jacobs, 2005). Thus, it can be concluded that the intermediate sample has smaller bed shear strength than the sandy sample. This explains the smaller erosion threshold of the intermediate sample. For the muddy sample, Figure 5.20 indicates that the sample is dominated by a clay-water matrix and thus, cohesive behavior is expected. Larger plasticity index also implies the large amount of clay for the muddy sample. With these conditions, large erosion threshold is expected for the muddy sample. Apparently, this is not happened as the threshold of the muddy sample is small. The only possible explanation can be that despite the presence of a clay-water matrix, the amount of clay content may not be sufficient to form a strong matrix surrounding those silt and sand particles. As a result, the sample still has small erosion resistance and thus the erosion threshold.

Figure 5.20 (c), (d), (e) and (f) implies that among the three samples, the sediment composition of the intermediate sample appears as a transition of the sediment behavior between non-cohesive and cohesive behavior. From Figure 5.20 (c) and (d), the erosion parameter, in other word, the erosion rate of fines is considered. With small amount of fines, it is logical that the erosion rate of fines for the sandy sample is small. With larger amount of fines in the intermediate sample, the erosion rate of fines is therefore increased provided that the sample still exhibits non-cohesive behavior. The trend of erosion rate changes for the muddy sample. The muddy sample, which exhibits cohesive behavior due to sufficient clay content, has small erosion rate. From Figure 5.20 (e) and (f), the erosion parameters or the erosion rates of sand is similar to fines. The only difference is the high erosion rate of the sandy sample. With large amount of the sand content, it is logical that the erosion rate of the sandy sample is large.

As mentioned in the previous paragraph, a transition of sediment behavior between non-cohesive and cohesive behavior is found. The plasticity index corresponding to this transition is about 7. This value agrees well with the plasticity index as commonly found in geotechnical studies. From which it states that for the sample with lower plasticity index than this critical value, non-cohesive behavior is exhibited, whereas for the sample with higher plasticity index, cohesive behavior is found.

5.6 Time-dependent increase of concentration

According to the requirements of the sample generation (see section 3.1), the sediment bed should be entirely homogenous and uniform. By applying a bed shear stress per rotational step, the concentration profile of eroded fines is expected to increase linearly for a given bed shear stress, provided that the shear stress is larger than the erosion threshold $(\tau_b > \tau_e)$. However, the concentration profiles (see Figure 4.8, Figure 4.14 and Figure 4.19) show a non-linear increase for the first rotational steps.

From the results, the profiles for lower concentration (rotational steps 1 – 5) show a non-linearly increase. After an initially steep increase, the profiles approach a constant value. For larger concentrations, the profiles increase almost linearly for a given bed shear stress. The concentration profiles within rotational steps 6 – 9 appear to increase non-linearly, as observed for the lower concentrations. However, it is not possible to predict a tendency for the latter part of the profiles due to the limited duration of the rotational steps. For this reason, two possibilities for the profiles can be expected. After a steep increase the profiles are assumed to either approach a constant value (see Figure 5.22 a) as found for lower concentration, or to increase linearly (see Figure 5.22 b) as found for higher concentration.

To explain the occurrence of the unexpected concentration profiles of eroded fines, the following explanations are considered as the possible causes:

- Occurrence of deposition
- Re-suspension of freshly deposited fines
- Variation of the critical bed shear stress with depth
- Ripples as a result of the plastic

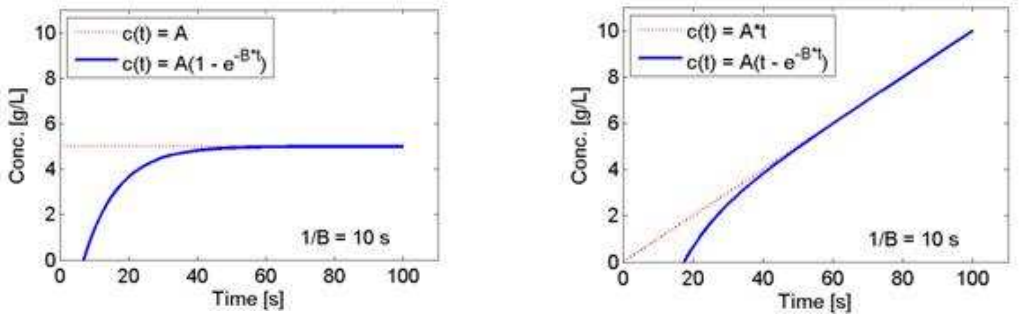

(a) (b)

Figure 5.22: Concentration profiles as function of time for constant equilibrium (a) and time-varying equilibrium (b). The red lines indicate the cases, for which both *E* and *D* are independent of time, the blue lines when both are a function of time.

1. **Occurrence of deposition**

Rate of change of concentration $h\partial c/\partial t$ [g/m^2/s] is in general expressed as:

$$h\partial c/\partial t = E - D \qquad \text{(Parchure and Mehta)} \qquad (5.3)$$

,where E [g/m^2/s] is the erosion rate and D [g/m^2/s] the rate of deposition at the sediment bed.

In principle, large concentrations yield a large deposition rate. If erosion rate (E) is constant, the increase of deposition rate will reduce $h\partial c/\partial t$ to zero. The deposition rate in general is expressed as $D = W_s c$, where W_s [m/s] is the settling velocity and c [g/m^3] the concentration of eroded fines. In Figure 5.23, the concentration increases (A) due to erosion. After mixing of suspended fines (B), deposition starts and increases (c) in time as well.

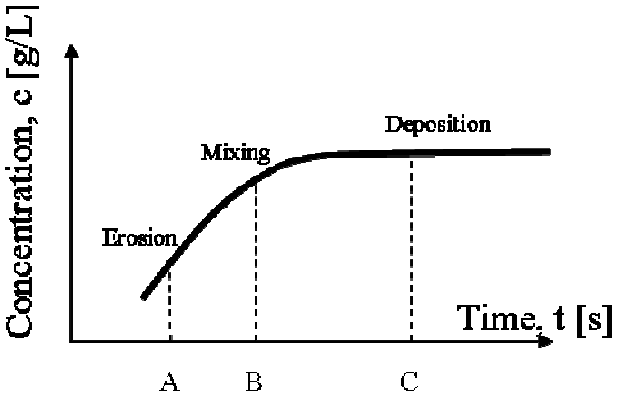

Figure 5.23: Concentration profile showing the non-linear increase. A, B and C indicate relations between E and D, starting from the bed being eroded, $E > 0$, $D = 0$ (A). After sometimes, concentration is mixing, $E > 0$, $D > 0$ and $E > D$ (B), and finally results in deposition, $E = D$ (C).

For instance, the concentrations of eroded fines at the beginning and the end of rotational step 7 for the intermediate sample are approximately 0.5 g/L and 0.7 g/L, respectively. This yields a deposition rate of 0.25 g/m^2/s and 0.35 g/m^2/s (Given a settling velocity, W_s, of 0.5 mm/s). By substituting these two deposition rates into equation (5.3), $h\partial c/\partial t$ is decreased provided that the erosion rate is constant ($E \approx 0.5$ g/m^2/s). Once the deposition rate is equal to the erosion rate ($D \to E$), $h\partial c/\partial t$ will approach zero.

This explanation corresponds well for the profiles as found in the middle range of concentration. The fact that the increase of the deposition rate causes $h\partial c/\partial t$ to approach zero explains why the concentration profiles tend towards a constant equilibrium value. However, for the lowest concentrations D is very small and much smaller than E. For example, at rotational step 4 of the intermediate sample $E \approx 0.4$ g/m^2/s and the deposition rates for the beginning and the end of the step are 0.025 and 0.05 g/m^2/s, respectively. The effect of these deposition rates is insignificant compared with the occurring erosion rate. D cannot affect E and, therefore, is not the reason for $\partial c/\partial t$ to approach zero.

2. Re-suspension of freshly deposited fines

Figure 4.8, Figure 4.14 and Figure 4.19 indicates that the profiles for lower concentration (from step 1 – 5) appear to have an initially steep increase at the beginning of the rotational step, and approach a constant value almost immediately afterward. This steep increase is in fact a result of the re-suspension of freshly deposited fines, which are brought in suspension during the removal of the plastic foil (after the consolidation process). The occurrence of the deposited fines corresponds well with the first concentration peak as shown in Figure 5.20 (a), (c) and (e) (see section 5.5). These re-suspended fines responded quickly to an eroding force, which explains the initially steep

increase of the profile. The 'fines peak' was observed for all three tests for identical bed shear stress ($\tau_b \approx 0.2$ Pa), and also the values of $h\partial c/\partial t$ are more or less the same.

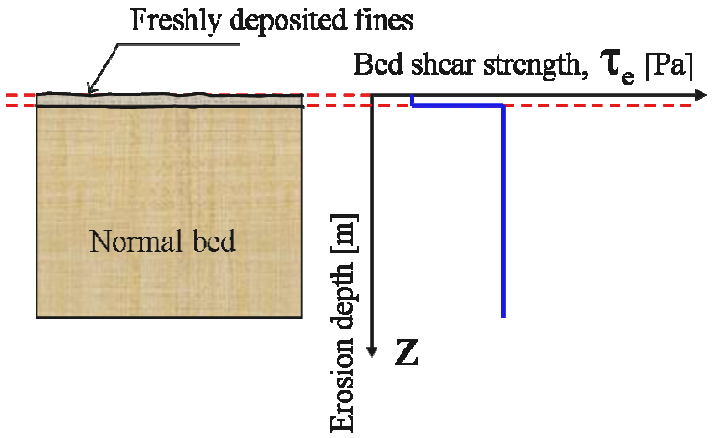

Figure 5.24: Schematic illustration showing the normal sediment bed with freshly deposited fines on top. These deposited fines are a result of the removal of the plastic foil after completion of the consolidation process. The right diagram indicates the vertical distribution of the critical shear stress for erosion (τ_e).

To relate the erosion behavior of these deposited fines to the profiles for lower concentration, Figure 5.25 is considered. In this figure, the probability density function (pdf of, i.e. τ_b of rotational step 1) exceeds some part of the pdf of the erosion threshold ($\tau_{e,layer1}$). This means that only a limited amount of fines can be eroded. This implies that a thin layer of loose fines erode for low τ_b. As the availability of these fines is limited, this can explain the time-dependent character of the concentration for the first few rotational steps.

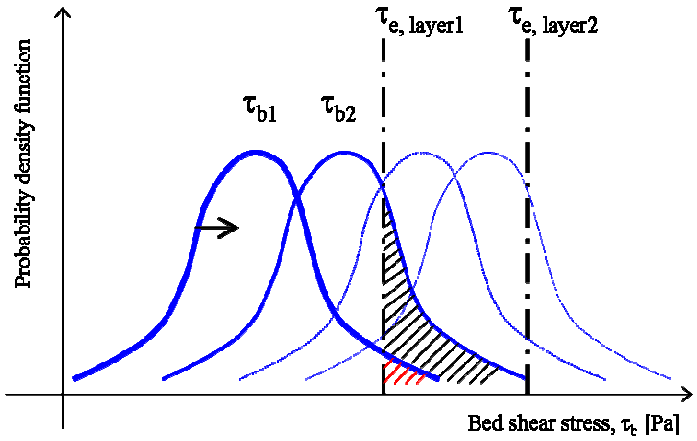

Figure 5.25: Schematic illustration of the probability density function of bed shear stress (τ_b) developing with increasing shear stresses. The highlighted area implies the limited amount of eroded fines with respect to the threshold of erosion for the freshly deposited fines ($\tau_e, layer\ 1$). The most right vertical line indicates the threshold of erosion for the normal bed ($\tau_e, layer\ 2$)

3. Variation of the critical shear stress for erosion on sediment beds

This explanation is often used to describe the non-linear increase of the concentration (Aberle, Kikora and Walters, 2004; Mehta and Partheniades, 1979 and Parchure and Mehta, 1985). With the increase of the bed density in lowering depth, the bed shear strength also increases. At certain point when the applied bed shear stress is equal to the bed shear strength ($\tau_e \rightarrow \tau_b$), erosion will stop ($E \approx 0$). Considering this condition with equation 5.3, together with the assumption that no deposition occurs (D = 0), the rate of change of the concentration then approaches zero ($h\partial c/\partial t \approx 0$). However, this behavior is only observed for erosion experiments using deposited cohesive beds (Parchure and Mehta, 1985). In this study, the possible explanation for the increase of the bed density in the upper layer can be that the sediment bed was disturbed during the placement process. As a result, the strength of the upper sediment layer decreased.

Regarding the previous assumptions, after the freshly deposited fines as well as the irregularities on the bed surface were all eroded, the actual bed surface began to erode (real erosion). Figure 5.26 indicates the non-uniform vertical distribution of the strength of the sediment bed. For a given shear stress, erosion occurs in the beginning when the shear stress (τ_b) is larger than the shear strength of the bed (τ_e). This erosion behavior corresponds well with the initially increasing profiles (see Figure 4.8, Figure 4.14 and Figure 4.19). As the erosion threshold increases with depth ($\tau_e \uparrow$), erosion is reduced. When $\tau_e = \tau_b$ erosion completely stops ($E = 0$). As a result, the rate of change of concentration approaches zero ($h\partial c/\partial t \approx 0$) provided no deposition occurs (D = 0). This explains why the profiles approach zero at the end of each rotational step. When the shear stress exceeds the erosion threshold of the bed at lower depth (see Figure 5.26), erosion occurs as a constant rate. This explains the linear increase for larger concentrations.

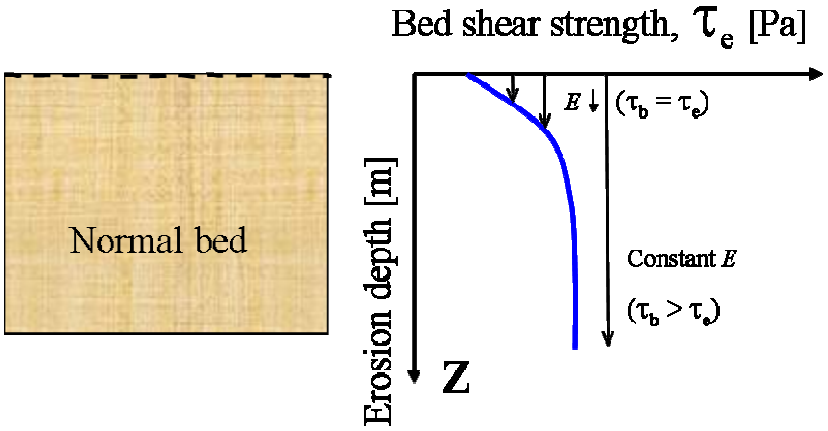

Figure 5.26: Schematic illustration showing the sediment bed after the freshly deposited fines are all eroded. The right diagram indicates the non-uniform vertical distribution of the strength of the bed. The shear strength of the bed becomes more uniform at lower depths.

4. Influence of the ripples as a result of the plastic

Another possibility for an explanation of the non-linear increase of the concentration profiles is that the eroding force on the occurring initial bed forms (ripples due to wrinkles) was in fact greater due to normal stresses acting on them (see Figure 5.27a). If the result of this normal stress and the shear stress is larger than the critical shear strength, erosion occurs (see Figure 5.27). Once these irregularities are smoothened, the eroding force is only a shear stress again ($\tau_b < \tau_e$). This means that erosion stops and thus, the concentration profile approaches a constant value (see Figure 5.27 b).

To explain the erosion behavior, Figure 5.20 (a, c and e) are considered once again. It appears that despite the applied bed shear stresses increasing beyond the shear stress at the first peak of the concentration rate, the rate of change of suspension concentration is still relatively small. This implies that the applied bed shear stresses are still smaller than the threshold of erosion. Once, the bed shear stress exceeds the erosion threshold ($\tau_b > \tau_e$), the erosion rate appears to increase linearly as expected.

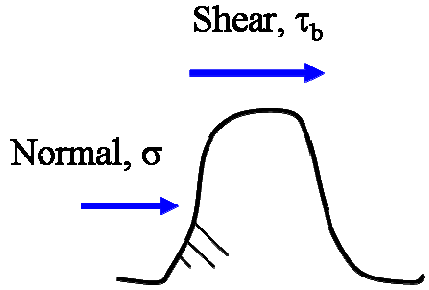

Erosion occurs

(a)

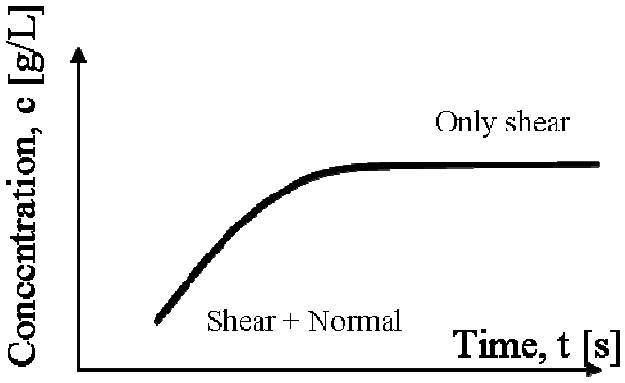

(b)

Figure 5.27: Schematic illustrations (a) the presence of the normal stress (σ) acting as an additional eroding force next to the shear stress (τ_b). Once, bed forms were all eroded, only the bed shear stress is active as the normal stress becomes zero. As a result, only the bed shear stress is not able to erode the sediment beds because $\tau_b < \tau_e$. therefore, the concentration profile approaches a constant value (b).

6 Conclusions and recommendations

6.1 Conclusions

In this study, erosion tests with an annular flume were executed on artificially generated sand-mud mixtures with three different compositions; a muddy, an intermediate and a sandy sample. The samples were homogeneously mixed and 100% saturated. During the tests, the bed shear stress was increased step-by-step. The concentration of suspended fines was measured at three vertical locations using Oslims. The horizontal and vertical flow velocities were measured by EMS devices. The flow-induced bed shear stresses were calculated by means of a large eddy simulation model. Erosion rates and erosion thresholds were studied.

Although there was a slight mismatch between calculations and measurements, it is concluded that the simulated bed shear stresses are a good representation of the occurring bed shear stresses. This implies that for a fairly smooth or transitional roughness of the sediment bed, such a model is a good alternative for complicated measurements of the bed shear stress.

The occurrence of both tangential as secondary currents in the annular flume had two advantages: 1) No vertical distribution of the concentration of suspended fines occurred. Therefore, the mean value of concentration was easily determined. 2) The accumulation of eroded sand on the bed surface along the outer wall of the flume occurred. By collecting and weighting this sand, the mass of eroded sand could be determined and consequently verified the estimation following the mass balance concept.

By setting up a simple mass balance it is, therefore, concluded that the amount of eroded fines can be used to determine the amount of eroded sand. The latter is a problem when applying annular flumes, as no sand trap can be applied. Afterward, the erosion rate for both mass of eroded fines and sand were determined as function of bed shear stress.

Concerning the concentration profile of eroded materials, for the first rotational steps an unexpected time-dependent behavior was observed in the concentration. Several explanations were studied. It is concluded that this behavior is a result of the placement of the sample and the subsequent process of consolidation. These experimental artifacts disturbed the upper layer (mm´s) of the sediment bed. In this layer the erosion threshold was varying both in vertical and horizontal direction, which caused the time dependency.

After the unexpected behavior in the first rotational steps, the concentration was increasing linearly for larger bed shear stress. This means that the applied bed shear stresses had exceeded the critical shear stress for erosion. As a result, erosion was significant and uniformly occurring from the whole surface of the bed.

From the results of the erosion threshold of all three samples, it can be concluded that for the sample exhibiting non-cohesive behavior, the addition of the clay content will result in smaller bed shear strength. As a result, the erosion threshold decreases. For the sample exhibiting cohesive behavior, the addition of the clay content has different influence on the bed shear strength. With added clay content, the bed shear strength will increase. As a result, the erosion threshold increases.

From the results of the erosion parameters of all three samples, it can be concluded that the effect of cohesive behavior is considerable to the erosion rate of the sample. This cohesive behavior makes it more difficult for both fine and sand particles in the sediment mixture to be eroded. On the contrary, a cohesionless behavior shows no influence on the erosion rate of the sample.

In addition, a transition of sediment behavior between cohesive and non-cohesive is found at the plasticity index 7. This agrees well with the transition as commonly found in geotechnical studies. This can draw the conclusion that the geotechnical approach can be used to define erosion behavior of mixed sediment very well.

6.2 Recommendations

It is recommended to extend the duration of a rotational step. This can enhance the distinction between depth limited and unlimited erosion. The distinctive type of erosion is important for an accurate determination of erosion rate. For this reason, the duration of around ½ - 1 hour per rotational step is recommended.

In this study special care was paid to the generation, placement and smoothening of the sediment bed. However, still some unexpected behavior was observed for the first rotational steps, such as the depositional fines due to the placement of the plastic and the non-uniform sediment density in the upper bed layer. This behavior should be further qualified and quantified, as it might be important for the results of other erosion studies using different or similar experimental setups.

In order to study the effect of the sediment composition on the erosion behavior further, it is recommended to execute more experiments. Also the effect of stratified beds and consolidated beds could be studied.

The results of this study should be compared with previous erosion tests in a straight flume on similar samples. In this way more conclusions can be drawn on the behavior of the erosion threshold and the erosion parameter as function of the plasticity index and the relative water content. These results should also be compared with the newly proposed formula.

References

Aberle, J., Nikora, V. and Waltets, R., 2004. Effects of bed material properties on cohesive sediment erosion. In: *Marine Geology*, Vol. 207, p. 83-93.

Amos, C.L., Daborn, G.R., Christian, H.A., Atkinson, A. and Robertson, A., 1992. In situ erosion measurements on fine-grained sediments from the Bay of Fundy. *Marine Geology*, 108: 175-196.

Booij, R., 1994. Measurements of the flow field in a rotating annular flume. *Communications on Hydraulic Geotechnical Engineering* (Delft: Delft University of Technology, faculty of Civil engineering). Report no. 2-94.

Booij, R., 2003. Measurements and large eddy simulations of the flows in some curved flumes. *Proceedings 5th International Symposium on Engineering Turbulence Modeling and measurements, Mallorca, 16-18 September 2002.* In: *Engineering Turbulence Modeling Measurements 5*, Elsevier Science, ISBN 0-08-044114-9, ed. W. Rodi and N. Fueyo.

Bosman, J.J. and Steetzel, H.J., 1988. Time and bed averaged concentrations under waves, Delft : Delft Hydraulics, WL Publications ISSN:0166-7521 385.

Bruens, A.W. 2003 Entraining mud suspensions. PhD thesis, Delft University of Technology, Faculty of Civil Engineering and Geosciences. *Communications on Hydraulic and Geotechnical Engineering*, Report 03-1, ISSN:0169-6548.

Chien, N. and Wan, Z., 1922-1986. Mechanics of sediment transport, Reston: ASCE, ISBN:0-7844-0400-3.

Dohmen-janssen, M., 1999. Grain size influence on sediment transport in oscillatory sheet flow/ phase lags and mobile-bed effects, Delft: Delft University of Technology, faculty of Civil engineering.

Jacobs, W., Van Kesteren, W.G.M. and Winterwerp, J.C., 2005. Strength of sediment mixtures as a function of sand content and clay mineralogy. *Special issue Marine Science*.

Jacobs, W., 2006. Eco-morphology of estuaries and tidal lagoons: Literature review and experiments on sand-mud mixtures (Delft: Delft University of Technology, faculty of Civil engineering). Report no. 1-06.

Panagiotopoulos, I., Voulgaris, G. and Collins, M.B., 1997. The influence of clay on the threshold of movement of fine sandy beds. Elsevier, *Coastal engineering*, Vol. 32 (1997), P. 19-43.

Parchure, T.M. and Mehta, A.J., 1985. Erosion of soft cohesive sediment deposits. U.S. Environmental Protection Agency, Washington, D.C., EPA/600/J-85/529.

Partheniades, E., 1965. Erosion and deposition of cohesive soils. In: *Journal of the Hydraulics division proceedings of the American Society of Civil Engineers*, P. 105-139.

Paterson, D.M., Black, K.S., 1999. Water flow, sediment dynamics and benthic biology. Advance in Ecological Research. 29: 155-193.

Raudkivi, A.J., 1990. Loose boundary hydraulics, 3rd Edition, Pergamon Press, Oxford, England.

Shields, A., 1936. Application of similarity principles and turbulence research to bed load movement. Mitteilunger der Preussischen Versuchsanstalt fur Wasserbau und Schiffbau 26: 5-24.

Van der Ham, R., 1996. A guide for carousel experiments on cohesive sediment. *Communications on Hydraulic Geotechnical Engineering* (Delft: Delft University of Technology, faculty of Civil engineering). Report no. 2-96.

Van Ledden, M., Van Kesteren, W.G.M. and Winterwerp, J.C., 2003. A conceptual framework for the erosion behavior of sand-mud mixtures. Elsevier, *Continental shelf research*, Vol. 24 (2004), P. 1-11.

Winterwerp, J.C. and Van Kesteren, W.G.M., 2004. Introduction to the physics of cohesive sediment in the marine environment. Elsevier, *Developments in sedimentology*, ISBN 0-4444-51553-4, ISSN 0070-4571.

Zreik, D., Krishnappan, B.G., Germaine, J.T., Madsen, O.S., and Ladd, C.C., 1998. Erosional and mechanical strengths of deposited cohesive sediments. ASCE Journal of Hydraulic Engineering.

Appendix: Calibration of Optical silt measuring instrument (Type OSLIM)

As mentioned in section 3.3.3 (the measurement techniques), five Oslims were calibrated for a variety of sediment concentrations and suction speeds. First, the Oslims were calibrated for concentrations using the different proportions of silt and clay of the three samples (see Table 3.1). Second, the Oslims were calibrated using the three suction speeds for the pumps. As the percentage in mass of silt and clay as obtained from the manufacturer is not the same as in volume, the actual composition is calculated using the following percentage of all sediment fractions:

	ξ_{cl} [-]	ξ_{si} [-]	ξ_{sa} [-]
clay from bag	0.312	0.688	0
silt from bag	0.039	0.786	0.175
sand from bag	0	0.006	0.994

As a result, the actual proportion in mass of silt and clay are:
Muddy sample: $M\_cl : M\_si = 1.1286 : 1$
Intermediate sample: $M\_cl : M\_si = 1.1736 : 1$
Sandy sample: $M\_cl : M\_si = 1.345 : 1$

Here, an example is given for the calculation of the mass of silt and clay. For a concentration of 1 g/L with water of 4 liters, using the proportion of clay and silt for the muddy sample as shown above the concentration requires a mass of clay of 2.1 g and a mass of silt of 1.9 g.

Besides, these three proportions of clay and silt, Oslims were also calibrated for the three suction speeds of the pumps; 0.183 m/s, 0.366 m/s and 0.557 m/s (see section 3.3.3)

Sediment	Concentration Range [g/L]	Oslim	Calibration plot	Pump
Sandy	0-2	9 (3x)	A1	3
	0-2	7 (3x)	A2	3
Intermediate	0-2	9 (3x)	B1	2
	0-2	7 (3x)	B2	2
Muddy	0-2	9 (3x)	C1	2
	0-2	7 (3x)	C2	2

Table A: Overview of the Oslim calibration for the concentration range 0-2 g/L

Sediment	Concentration Range [g/L]	Oslim	Calibration plot	Pump
Sandy	0-30	2 (3x)	D1	2
	0-30	8 (3x)	D2	2
	0-30	4 (3x)	D3	2
Intermediate	0-30	2 (3x)	E1	1
	0-30	8 (3x)	E2	1
	0-30	4 (3x)	E3	1
Muddy	0-30	2 (3x)	F1	1
	0-30	8 (3x)	F2	1
	0-30	4 (3x)	F3	1

Table B: Overview of the Oslim calibration for the concentration range 0-30 g/L

Note: The term (3x) in Table (A) and (B) indicates that the Oslims are calibrated for 3 times with different suction speeds of the pump.

Calibration of Oslims

Date: 7/28/2007

Range of concentration: 0-2 g/L

Composition: Sandy sample

Turbine speed = 250 rpm Clay/Silt ratio = 1.345

Condition: the pump is connected with the Oslims on 2 pumpheads. Each Oslim is calibrated for the specified concentraion, with a corresponding pump discharge

Oslim configurations:

switch/ Oslim no.	9	7
1	500	500
2	3	2
3	initally set	initally set
4	100	100

Pump#3

Voltage	Discharge [cm^3/s]
2.4	2.3
4.9	4.6
9.0	5.9

Concentration	Oslim no. 9			Oslim no. 7		
[unit]	2.3 cm^3/s	4.6 cm^3/s	7 cm^3/s	2.3 cm^3/s	4.6 cm^3/s	7 cm^3/s
0	-0.002	-0.004	-0.002	0.004	0.003	0.002
0.05	0.085	0.092	0.093	0.091	0.101	0.108
0.1	0.164	0.183	0.193	0.182	0.199	0.210
0.2	0.587	0.640	0.642	0.628	0.688	0.705
0.3	1.011	1.104	1.094	1.084	1.188	1.189
0.4	1.438	1.520	1.541	1.534	1.664	1.673
0.5	1.866	2.007	1.992	1.994	2.167	2.167
0.7	2.725	2.965	2.919	2.903	3.169	3.173
0.9	3.573	3.832	3.823	3.834	4.174	4.141
1	4.012	4.227	4.274	4.302	4.587	4.639
1.1	4.473	4.726	4.777	4.780	5.055	5.187
1.2	4.890	5.165	5.218	5.254	5.562	5.657
1.4	5.708	6.003	6.097	6.231	6.466	6.621
1.7	6.971	7.381	7.493	7.423	7.946	8.116
2	8.225	8.682	8.822	8.937	9.343	9.606

A1

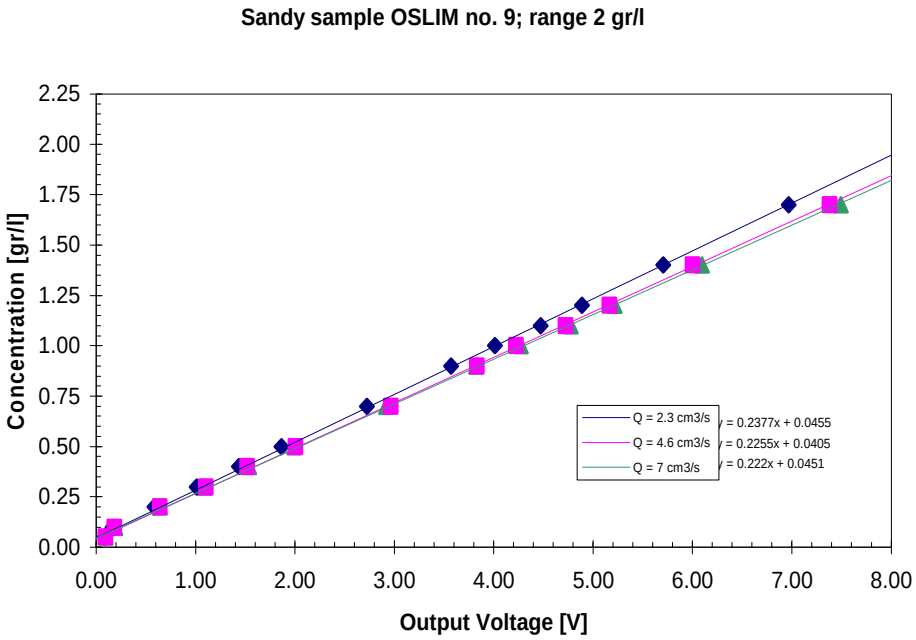
Sandy sample OSLIM no. 9; range 2 gr/l
Concentration [gr/l]
Output Voltage [V]
Q = 2.3 cm3/s
Q = 4.6 cm3/s
Q = 7 cm3/s
y = 0.2377x + 0.0455
y = 0.2255x + 0.0405
y = 0.222x + 0.0451

A2

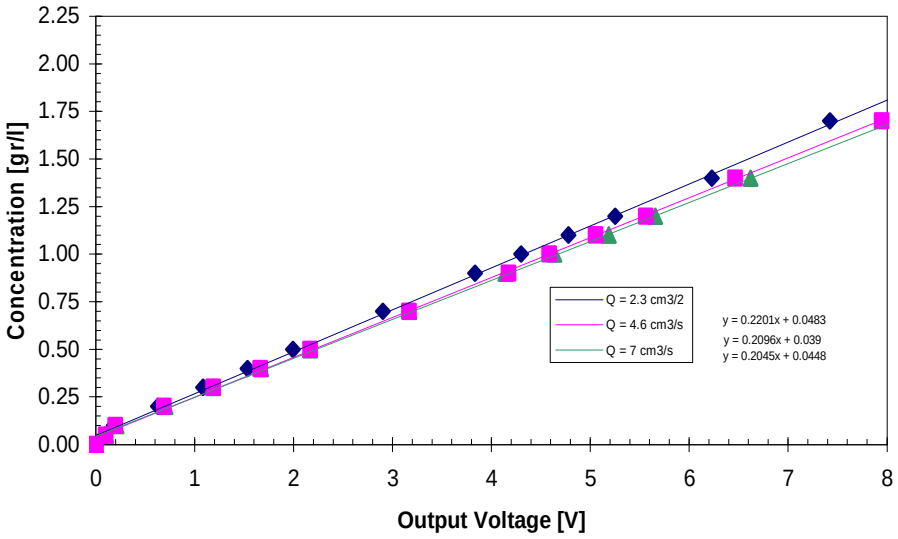
Sandy sample OSLIM no. 7; range 2 gr/l
Concentration [gr/l]
Output Voltage [V]
Q = 2.3 cm3/2
Q = 4.6 cm3/s
Q = 7 cm3/s
y = 0.2201x + 0.0483
y = 0.2096x + 0.039
y = 0.2045x + 0.0448

Calibration of Oslims

Date: 7/28/2007

Range of concentration: 0-2 g/L

Composition Intermediate sample

Turbine speed = 250 rpm Clay/Silt ratio = 1.1736

Condition: the pump is connected with the Oslims on all 2 pumpheads. Each Oslim is calibrated for the specified concentraion, with a corresponding pump discharge

Oslim configurations:

switch/ Oslim no.	9	7
1	500	500
2	3	2
3	initally set	initally set
4	100	100

Pump#2

Voltage	Discharge [cm^3/s]
2.2	2.3
3.8	4.6
8	7

Concentration	Oslim no. 9			Oslim no. 7		
[unit]	2.3 cm^3/s	4.6 cm^3/s	7 cm^3/s	2.3 cm^3/s	4.6 cm^3/s	7 cm^3/s
0	-0.011	-0.009	-0.011	-0.010	-0.009	-0.007
0.05	0.212	0.238	0.229	0.224	0.269	0.253
0.1	0.437	0.479	0.463	0.460	0.530	0.507
0.2	0.875	0.943	0.934	0.928	1.067	1.022
0.3	1.324	1.420	1.396	1.408	1.541	1.521
0.4	1.754	1.842	1.867	1.861	2.001	2.030
0.5	2.214	2.318	2.324	2.358	2.517	2.530
0.7	3.094	3.201	3.242	3.331	3.478	3.526
0.9	3.955	4.091	4.144	4.273	4.432	4.508
1	4.379	4.548	4.614	4.691	4.920	5.017
1.2	5.243	5.445	5.492	5.709	5.869	5.983
1.6	6.893	7.183	7.317	7.520	7.745	7.946
2	8.567	8.961	9.225	9.258	9.663	10.000

B1

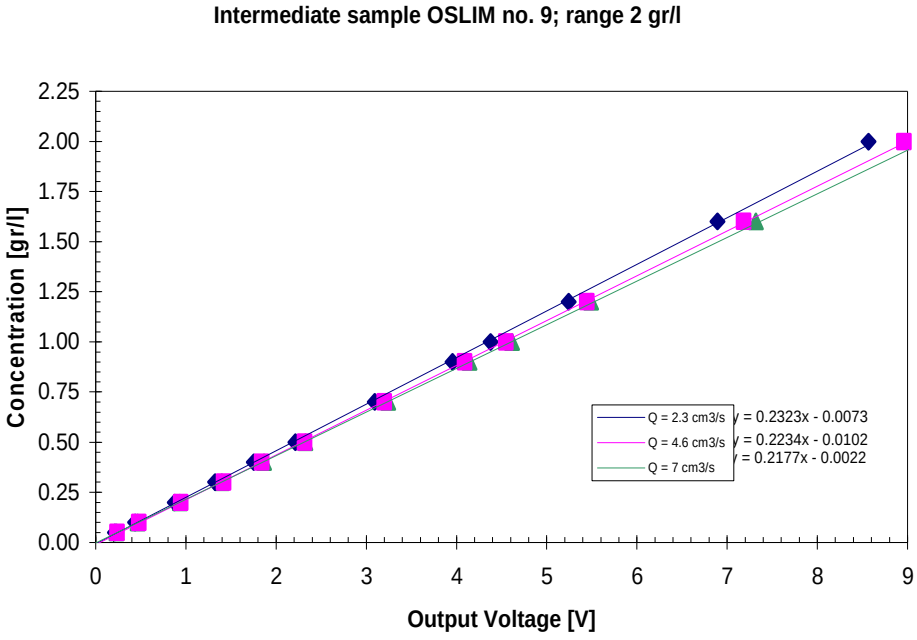

B2

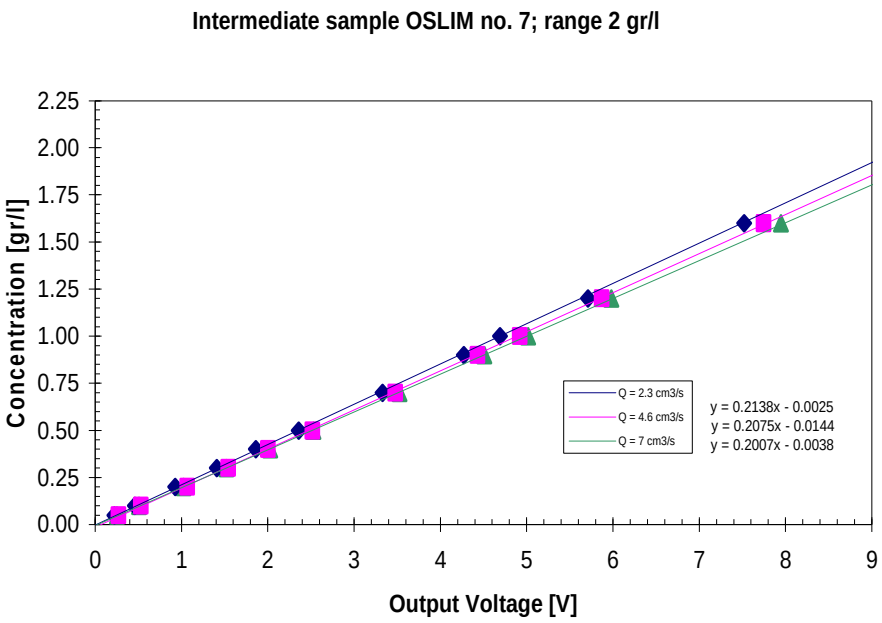

Calibration of Oslims

Date: 7/30/2007

Range of concentration: 0-2 g/L

Composition: Muddy sample

Turbine speed = 250 rpm Clay/Silt ratio = 1.1286

Condition: the pump is connected with the Oslims on all 2 pumpheads. Each Oslim is calibrated for the specified concentraion, with a corresponding pump discharge

Oslim configurations:			**Pump#2**	
switch/ Oslim no.	9	7	Voltage	Discharge [cm^3/s]
1	500	500	2.2	2.3
2	3	2	3.8	4.6
3	initally set	initally set	8	7
4	100	100		

Concentration	Oslim no. 9			Oslim no. 7		
[unit]	2.3 cm3/s	4.6 cm3/s	7 cm3/s	2.3 cm3/s	4.6 cm3/s	7 cm3/s
0	-0.045	-0.046	-0.047	-0.019	-0.018	-0.019
0.05	0.159	0.178	0.180	0.197	0.211	0.225
0.1	0.373	0.410	0.407	0.421	0.460	0.463
0.2	0.784	0.852	0.847	0.860	0.926	0.939
0.3	1.209	1.289	1.292	1.305	1.377	1.410
0.4	1.619	1.716	1.729	1.746	1.854	1.882
0.5	2.034	2.137	2.137	2.198	2.323	2.323
0.7	2.863	3.006	3.031	3.070	3.214	3.289
0.9	3.703	3.849	3.895	3.960	4.109	4.210
1	4.115	4.318	4.351	4.403	4.605	4.708
1.2	4.968	5.254	5.298	5.306	5.613	5.730
1.6	6.593	6.927	7.003	7.053	7.424	7.552
2	8.191	8.624	8.740	8.779	9.176	9.426

C1

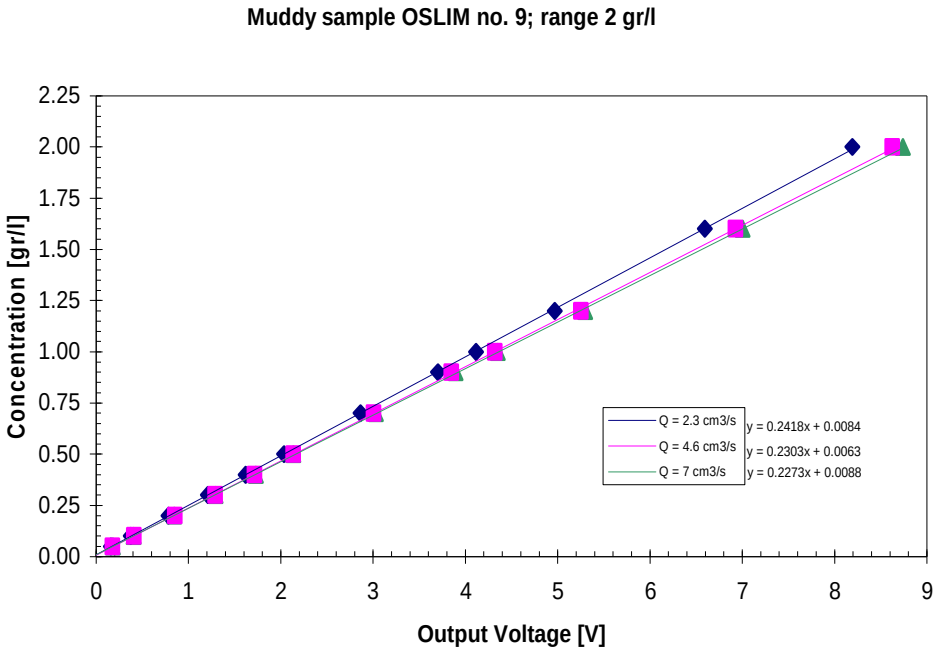
Muddy sample OSLIM no. 9; range 2 gr/l
Concentration [gr/l]
Output Voltage [V]
Q = 2.3 cm3/s
Q = 4.6 cm3/s
Q = 7 cm3/s
y = 0.2418x + 0.0084
y = 0.2303x + 0.0063
y = 0.2273x + 0.0088

C2

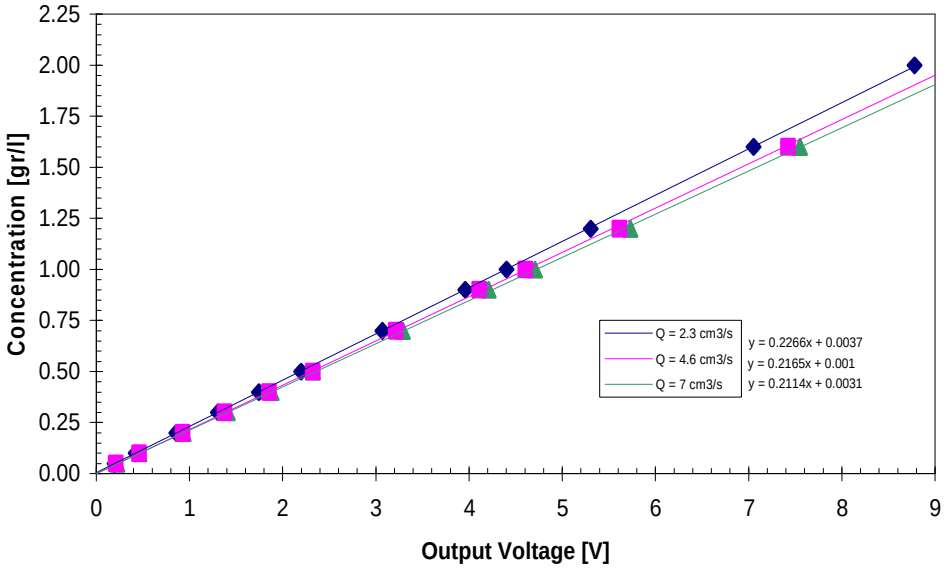
Muddy sample OSLIM no. 7; range 2 gr/l
Concentration [gr/l]
Output Voltage [V]
Q = 2.3 cm3/s
Q = 4.6 cm3/s
Q = 7 cm3/s
y = 0.2266x + 0.0037
y = 0.2165x + 0.001
y = 0.2114x + 0.0031

Calibration of Oslims

Date: 07/082007

Range of concentration: 0-30 g/L

Composition: Sandy sample

Turbine speed = 250 rpm Clay/Silt ratio = 1.345

Condition: the pump is connected with the Oslims on all 3 pumpheads. Each Oslim is calibrated for the specified concentraion, with corresponding pump discharges

Oslim configurations:

switch/ Oslim no.	2	8	4
1	500	500	500
2	2	3	3
3	initally set	initally set	initally set
4	10	10	10

Pump#2

Voltage	Discharge [cm^3/s]
2.2	2.3
3.8	4.6
8	7

Concentration		Oslim no. 2			Oslim no. 8			Oslim no. 4	
[unit]	2.3 cm^3/s	4.6 cm^3/s	7 cm^3/s	2.3 cm^3/s	4.6 cm^3/s	7 cm^3/s	2.3 cm^3/s	4.6 cm^3/s	7 cm^3/s
0	-0.071	-0.070	-0.071	0.071	0.071	0.071	-0.005	-0.004	-0.004
1	0.354	0.396	0.385	0.513	0.537	0.537	0.414	0.454	0.468
2	0.758	0.781	0.818	0.939	0.979	0.986	0.835	0.784	0.885
3	1.153	1.202	1.242	1.343	1.403	1.419	1.230	1.205	1.309
4	1.535	1.585	1.685	1.730	1.811	1.835	1.612	1.588	1.752
5	1.908	1.980	2.103	2.113	2.183	2.239	1.985	1.983	2.170
7	2.616	2.768	2.874	2.846	2.961	3.133	2.693	2.771	2.962
9	3.123	3.480	3.586	3.477	3.679	3.875	3.200	3.483	3.653
12	4.108	4.466	4.698	4.391	4.649	4.756	4.053	4.431	4.678
15	4.959	5.400	5.632	5.240	5.523	5.668	4.904	5.367	5.613
20	6.277	6.807	6.925	6.542	6.911	6.915	6.135	6.643	6.855
25	7.524	7.987	8.192	7.399	7.841	7.976	7.292	7.748	7.999

D1

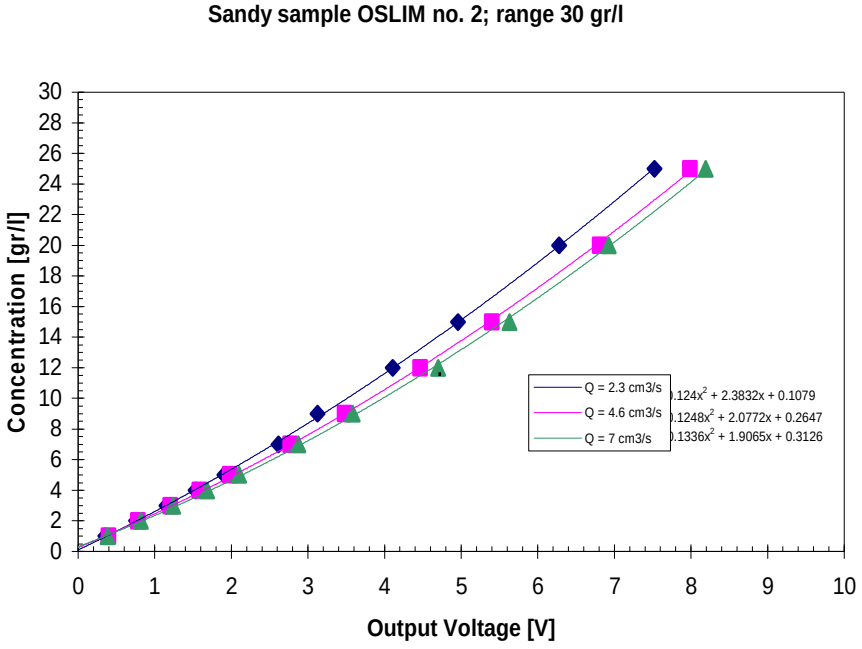

D2

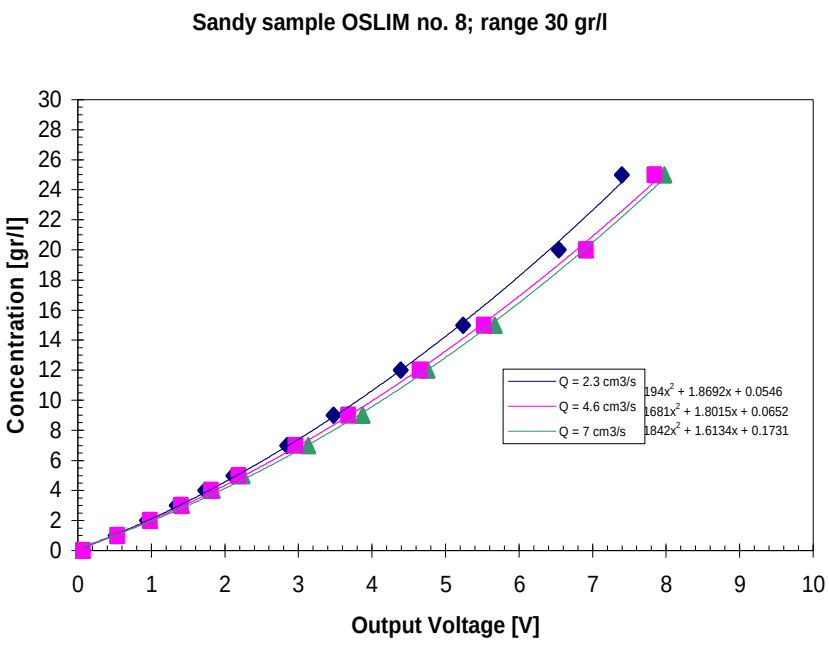
Sandy sample OSLIM no. 8; range 30 gr/l
Concentration [gr/l]
Output Voltage [V]
Q = 2.3 cm3/s
Q = 4.6 cm3/s
Q = 7 cm3/s
194x2 + 1.8692x + 0.0546
1681x2 + 1.8015x + 0.0652
1842x2 + 1.6134x + 0.1731

D3

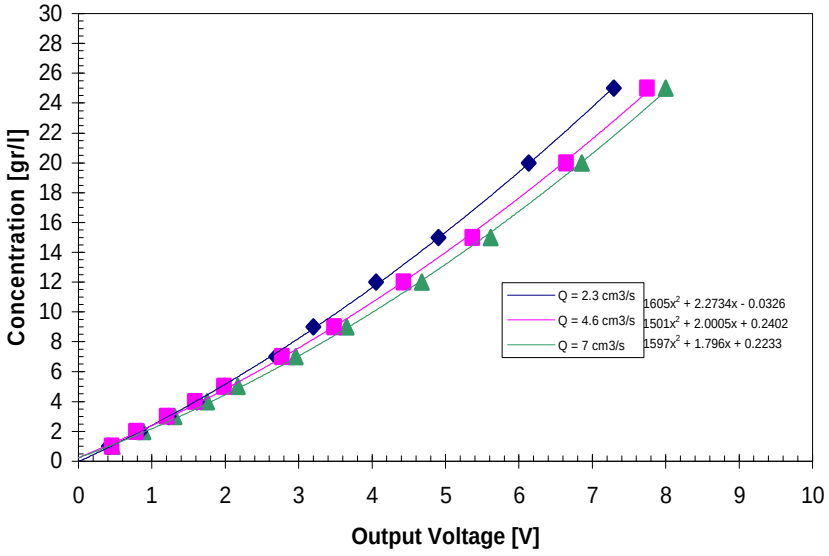
Sandy sample OSLIM no. 4; range 30 gr/l
Concentration [gr/l]
Output Voltage [V]
Q = 2.3 cm3/s
Q = 4.6 cm3/s
Q = 7 cm3/s
1605x2 + 2.2734x - 0.0326
1501x2 + 2.0005x + 0.2402
1597x2 + 1.796x + 0.2233

Calibration of Oslims

Date: 07/082007

Range of concentration: 0-30 g/L

Composition no. Intermediate sample

Turbine speed = 250 rpm Clay/Silt ratio = 1.1736

Condition: the pump is connected with the Oslims on all 3 pumpheads. Each Oslim is calibrated for the specified concentraion, with corresponding pump discharges

Oslim configurations:

switch/ Oslim no.	2	8	4
1	500	500	500
2	2	3	3
3	initally set	initally set	initally set
4	10	10	10

Pump#1

Voltage	Discharge [cm^3/s]
1.55	2.3
3.3	4.6
8	7

Concentration		Oslim no. 2			Oslim no. 8			Oslim no. 4	
[unit]	2.3 cm^3/s	4.6 cm^3/s	7 cm^3/s	2.3 cm^3/s	4.6 cm^3/s	7 cm^3/s	2.3 cm^3/s	4.6 cm^3/s	7 cm^3/s
0	-0.056	-0.055	-0.055	0.052	0.054	0.053	0.004	0.004	0.005
1	0.339	0.366	0.382	0.477	0.505	0.509	0.396	0.436	0.435
2	0.694	0.720	0.776	0.841	0.874	0.907	0.757	0.814	0.851
3	1.041	1.077	1.172	1.210	1.300	1.304	1.110	1.330	1.258
4	1.408	1.443	1.570	1.545	1.627	1.693	1.446	1.600	1.649
5	1.759	1.821	1.945	1.936	2.040	2.089	1.809	1.951	2.059
7	2.483	2.538	2.703	2.645	2.831	2.852	2.505	2.697	2.789
9	3.143	3.269	3.432	3.309	3.463	3.561	3.175	3.363	3.697
12	4.156	4.263	4.470	4.263	4.427	4.563	4.206	4.407	4.582
15	5.080	5.230	5.442	5.119	5.352	5.448	5.114	5.364	5.529
20	6.418	6.665	6.834	6.385	6.547	6.701	6.372	6.669	6.887
25	7.599	7.779	8.038	7.387	7.639	7.748	7.432	7.801	7.925
30	8.648	8.775	9.035	8.246	8.487	8.612	8.384	8.694	8.790

E1

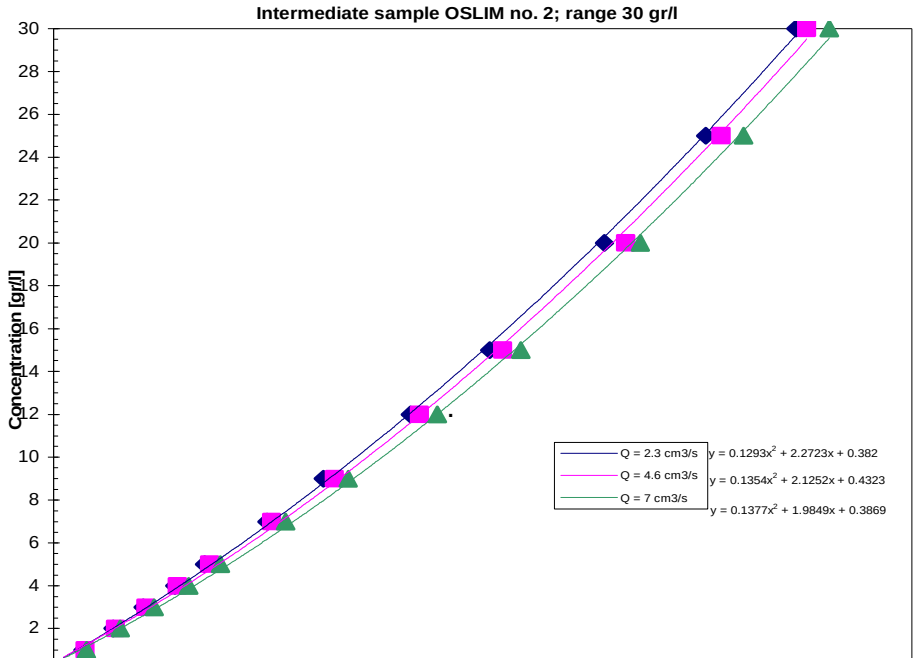

E2

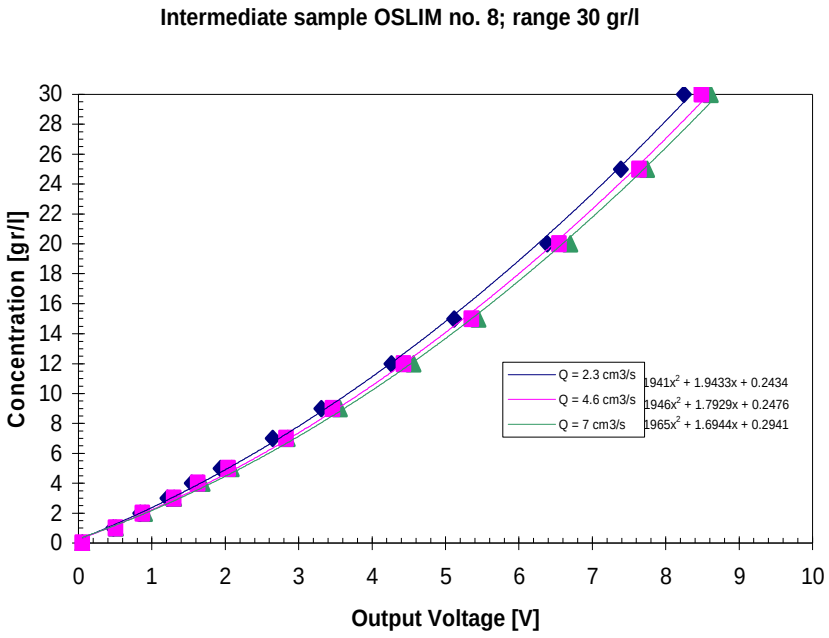
Intermediate sample OSLIM no. 8; range 30 gr/l
Concentration [gr/l]
Output Voltage [V]
Q = 2.3 cm3/s
Q = 4.6 cm3/s
Q = 7 cm3/s
1941x2 + 1.9433x + 0.2434
1946x2 + 1.7929x + 0.2476
1965x2 + 1.6944x + 0.2941

E3

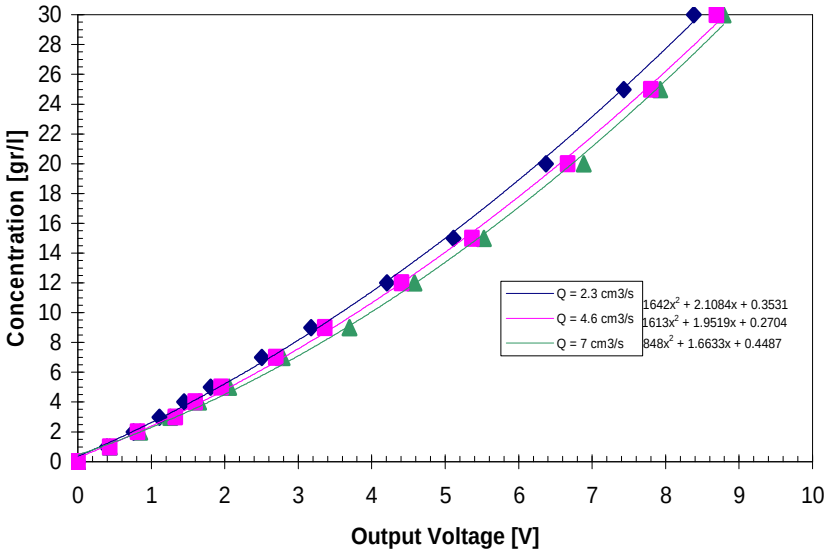
Intermediate sample OSLIM no. 4; range 30 gr/l
Concentration [gr/l]
Output Voltage [V]
Q = 2.3 cm3/s
Q = 4.6 cm3/s
Q = 7 cm3/s
1642x2 + 2.1084x + 0.3531
1613x2 + 1.9519x + 0.2704
848x2 + 1.6633x + 0.4487

Calibration of Oslims

Date: 30/072007

Range of concentration: 0-30 g/L

Composition no. Muddy sample

Turbine speed = 250 rpm Clay/Silt ratio = 1.1286

Condition: the pump is connected with the Oslims on all 3 pumpheads. Each Oslim is calibrated for the specified concentraion, with a corresponding pump discharge

Oslim configurations:

switch/ Oslim no.	2	8	4
1	500	500	500
2	2	3	3
3	initally set	initally set	initally set
4	10	10	10

Pump#1

Voltage	Discharge [cm^3/s]
1.55	2.3
3.3	4.6
8	7

Concentration		Oslim no. 2			Oslim no. 8			Oslim no. 4	
[unit]	2.3 cm^3/s	4.6 cm^3/s	7 cm^3/s	2.3 cm^3/s	4.6 cm^3/s	7 cm^3/s	2.3 cm^3/s	4.6 cm^3/s	7 cm^3/s
0	0.002	0.002	0.001	0.002	0.002	0.002	0.005	0.005	0.005
1	0.375	0.406	0.417	0.419	0.438	0.440	0.388	0.397	0.421
2	0.727	0.786	0.794	0.794	0.823	0.851	0.739	0.755	0.815
3	1.088	1.160	1.181	1.163	1.243	1.260	1.092	1.130	1.230
4	1.460	1.540	1.578	1.549	1.635	1.670	1.466	1.507	1.598
5	1.827	1.976	2.003	1.966	2.067	2.102	1.864	1.909	2.006
7	2.540	2.800	2.752	2.644	2.799	2.852	2.587	2.659	2.807
9	3.258	3.510	3.539	3.371	3.543	3.620	3.239	3.360	3.537
12	4.247	4.535	4.550	4.334	4.498	4.633	4.203	4.369	4.576
15	5.176	5.481	5.548	5.207	5.434	5.533	5.084	5.271	5.575
20	6.100	6.890	6.934	6.224	6.716	6.828	6.141	6.609	6.924
25	7.639	8.068	8.112	7.443	7.717	7.847	7.496	7.712	7.965
30	8.672	9.002	9.075	8.344	8.580	8.715	8.384	8.584	8.877

F1

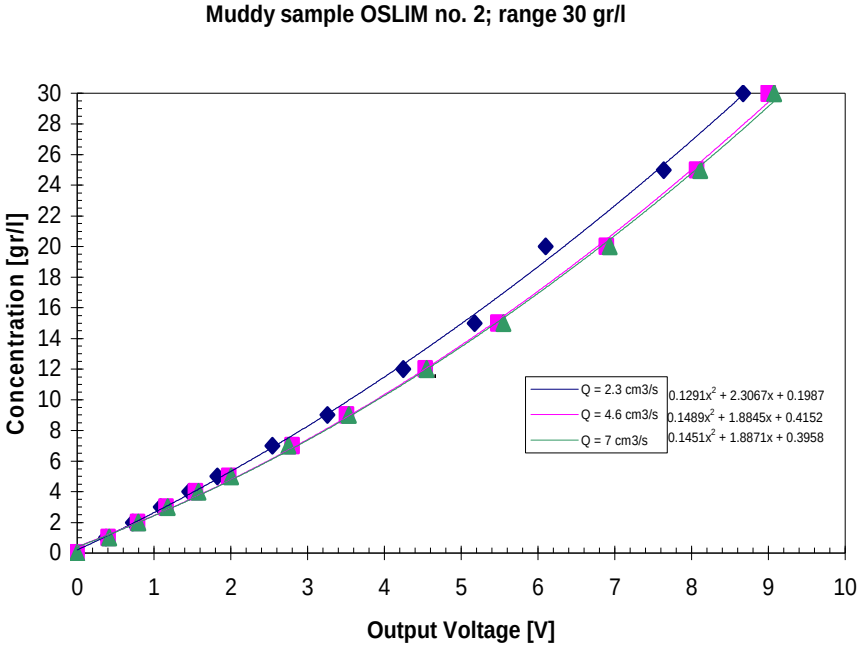

F2

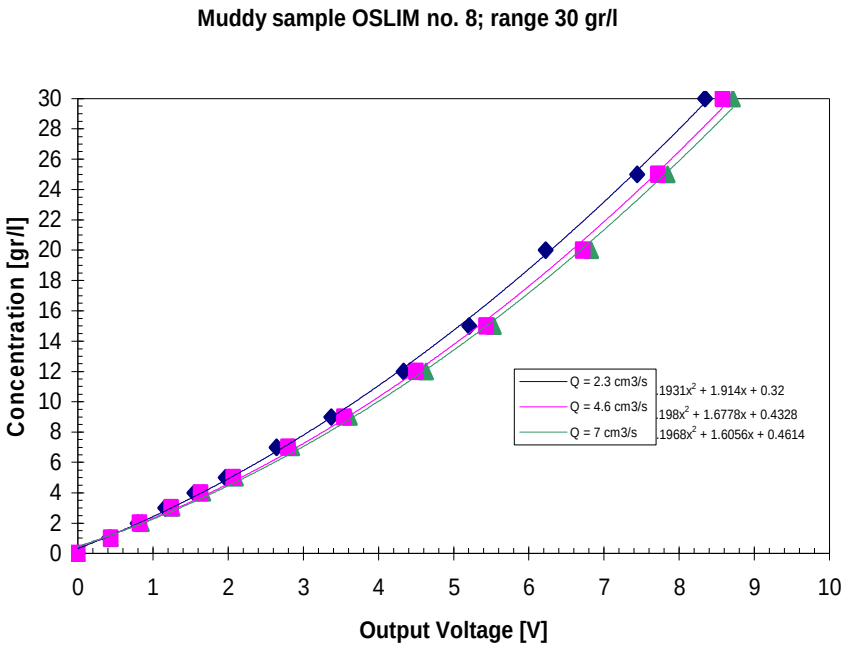
Muddy sample OSLIM no. 8; range 30 gr/l
Concentration [gr/l]
Output Voltage [V]
Q = 2.3 cm3/s
Q = 4.6 cm3/s
Q = 7 cm3/s
.1931x² + 1.914x + 0.32
.198x² + 1.6778x + 0.4328
.1968x² + 1.6056x + 0.4614

F3

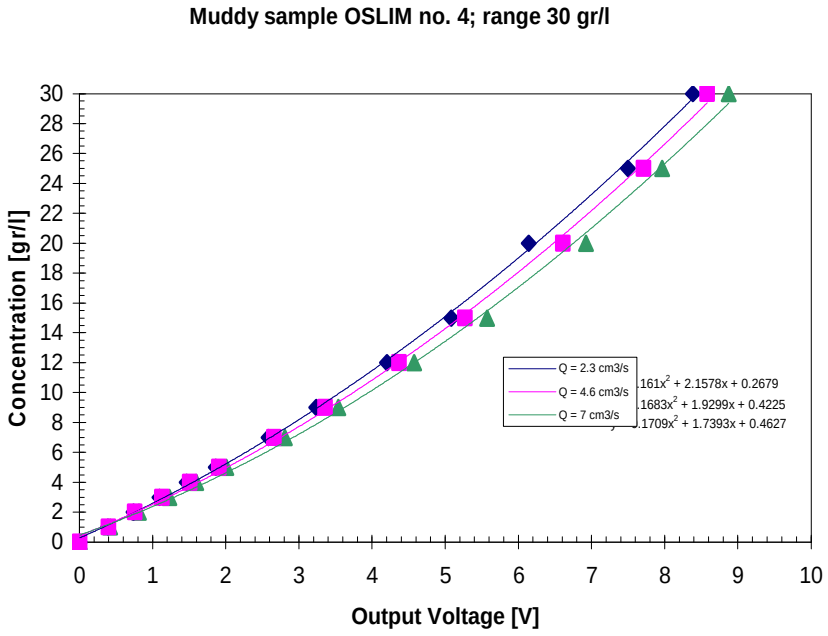
Muddy sample OSLIM no. 4; range 30 gr/l
Concentration [gr/l]
Output Voltage [V]
Q = 2.3 cm3/s
Q = 4.6 cm3/s
Q = 7 cm3/s
.161x² + 2.1578x + 0.2679
.1683x² + 1.9299x + 0.4225
.1709x² + 1.7393x + 0.4627